Panayiotis Romanos

Thermal Model Predictive Control for Demand Side Management Cooling Strategies

kassel university press

This work has been accepted by the faculty of electrical engineering / computer science of the University of Kassel as a thesis for acquiring the academic degree of Doktor der Ingenieurwissenschaften (Dr.-Ing.).

Supervisor:	Prof. Dr.-Ing. J. Schmid
Co-Supervisor:	Prof. Dr.-Ing. habil. I. Stadler

Defense day 27th July 2007

Bibliographic information published by Deutsche Nationalbibliothek
Die Deutsche Nationalbibliothek lists this publication in the Deutsche Nationalbibliografie; detailed bibliographic data is available in the Internet at http://dnb.ddb.de

Zugl.: Kassel, Univ., Diss. 2007
ISBN: 978-3-89958-405-9
URN: urn:nbn:de:0002-4054

Cover layout: Grafik Design Jörg Batschi, Kassel
Printed by: Unidruckerei, University of Kassel
Printed in Germany

Zusammenfassung

Diese Abhandlung zielt darauf ab, die Entwicklung, die Auslegung und die Analyse eines Steuerungskonzepts darzustellen, der „Thermal Model Predictive Control for Demand Side Management Cooling Strategies" genannt wird. Die Steuerung ist auf einem Gebäude in Athen eingeführt worden, dessen thermisches Modell mit der Differenzen-Verfahren-Methode berechnet wurde. Die Entwicklung und die Prüfung des thermischen Modells wurden online durchgeführt, während die Steuerung für Kühlungs-Strategien durch Simulationsergebnisse analysiert wurde. Die Vorteile des Entwurfs, einschließlich der Fähigkeit der Steuerung, die Benutzer über Energie- und Kosteneinsparungen während des Höchstnachfrage-Zeitintervalls in einer annehmbaren Weise zu beraten, werden in dieser Arbeit beschrieben.

Dieser Bericht beabsichtigt, die Theorie und die Implementierung der „Thermal Model Predictive Control for Demand Side Management Cooling Strategies" zu entwickeln.

Kassel, Juni 2007 Panayiotis Romanos

Abstract

This dissertation aims to present the development, design and analysis of a control scheme named Thermal Model Predictive Control for Demand Side Management Cooling Strategies. The control is implemented on a building in Athens whose thermal model is derived using the Finite Difference Calculation Method. The development and testing of the thermal model is implemented on-line while the predictive controller for cooling strategies is analysed through simulation results. The advantages of the scheme are described, including the ability of the predictive controller to consult the users for energy and cost savings during the peak demand, in an acceptable way by them regarding the thermal comfort issue.

The report intends to develop the theory and implementation of Predictive Control for Demand Side Management Cooling Strategies.

Kassel, June 2007 Panayiotis Romanos

Acknowledgements

I would like to thank particularly my supervisor Prof. Dr.-Ing. Jürgen Schmid for giving me the scientific knowledge and way of thinking and acting. I would also like to thank for his valuable supervision, constantly help, support and encouragement for completing my research work and dissertation. His way of thinking and the guidelines that he gave me on research have considerably influenced me.

I wish to express my thanks to Prof. Dr.-Ing. habil. Ingo Stadler for his significant support in many crucial phases of my PhD work and to be co-supervisor in my thesis.

I also want to thank my colleague and friend Dr.-Ing. Efstratios Tapanlis for his support in starting PhD in Universität Kassel and for his comments during my research work.

I would like to express my thanks to the secretary of the Department of Efficient Energy Conversion in Universität Kassel, Lady Claudia Erdt for her friendly support during my all PhD work.

I am grateful to my colleagues in Universität Kassel, Department of Efficient Energy Conversion, Aleksandra Sasa Bukvic-Schäfer, Dr.-Ing. Sergio Daher, Bjorn Eide, Giovanni Mattarolo, Thilo Bocklish, Ümit Cali, Ingo Hahn, Dr.-Ing. Martin Staffhorst and Thorsten Hodapp as well as Prof. Dr.-Ing. Bernd Weidemann who benefited my research during the latest stages of the project.

I am also grateful to ISET staffs, Prof. Dr.-Ing. Peter Zacharias, Michael Durstewitz, Dr.-Ing. Cornel Ensslin, Randolf Geipel and Yves-Marie Saint-Drenan for their support and collaboration for this study.

I would like to express my thanks to my parents, Spyridoula and Gerasimos Romanos, for teaching me how to choose a profession without only thinking the financial perspectives but taking also into consideration that I am very fond of it, as well as my brother Elisseos Romanos for his technical support during the KNX/EIB installation.

I would like also to thank my personal friends in Greece, Panayiotis Gaitanaros, Aggeliki Markolefa, Betty Nikolopoulou, Andreas Tsorvadelis and Stergios Vrekos for their encouragement, aid and support to continue my research in Germany.

I would like to thank my colleague and friend in Greece, aeronautic engineer Vassilios La Rocca, partner of National Instruments for the information and support he gave me on relative products.

I also want to thank my teacher in Sivitanidios School, Greece, Kostas Tsinaris, for inspiring me to continue my studies in electronics.

I would like to thank my supervisor during my MSc in University of Sheffield, Prof. S. A. Billings, who believed in the quality of my research work and convinced me to start my PhD work.

I would like to express my thanks to Prof. Gianfranco Rizzo, in University of Palermo, for his constructive comments when he visited the thesis building in Athens, in July 2005.

I would like to thank the owners of the building in Athens where the Thermal Model Predictive Controller is implemented, Mrs Helena Georgiadis and Mr. Antonios Georgiadis as well as their colleague Mr. Nikitas Sigalas, for their appreciation and investment in the thesis project.

Last but not least, I would like to thank my friend Lady Fotini Tsitoura for her suggestions as far as the improvements on the presentation of the text are concerned.

Kassel, June 2007 Panayiotis Romanos

TABLE OF CONTENTS

LIST OF FIGURES

LIST OF TABLES

Nomenclature

Symbol	Units	Description
a	m^2/s	Thermal diffusivity
A	m^2	Area
A_i	-	Anisotropy index
Bi	-	Biot number
c	J/KgK	Specific heat
c_p	J/KgK	Specific heat at constant pressure
c_v	J/KgK	Specific heat at constant volume
E	J, minutes	Energy, equation of time
$\dot{E}$	W	Rate of energy
$\dot{E}_g$	W	Rate of energy generation
$\dot{E}_{in}$	W	Rate of energy transfer into a control volume
$\dot{E}_{out}$	W	Rate of energy transfer out of a control volume
$\dot{E}_{st}$	W	Rate of increase of energy stored within a control volume
f	-	Modulating factor
Fo	-	Fourier number
F_{i-j}	-	Diffuse energy leaving surface *i* that is incident on surface *j* without reflection/diffuse energy leaving surface *i* (view factor)
G_{sc}	W/m^2	Solar constant
G	W/m^2	Irradiance
I	W/m^2	Hourly irradiation
k_T	-	Hourly clearness index
KE	J or Wh	Kinetic energy
L	degrees, m	Longitude, length
m	Kg	Mass
N	hours	Day length
p	N/m^2	Pressure

PE	J or Wh	Potential energy, prediction error
Q	J or Wh	Heat transfer
$\dot{Q}$	W	Heat transfer rate
$\dot{q}$	W/m^3	Rate of energy generation per unit volume
q''	W/m^2	Heat flux
R	K/W	Ratio of total radiation on a tilted plane to that on the plane of measurement (usually horizontal), heat transfer resistance
R_b	-	Ratio of beam radiation on a tilted plane to that on the plane of measurement (usually horizontal)
R_d	-	Ratio of diffuse radiation on a tilted plane to that on the plane of measurement (usually horizontal)
t	s	Time
T	K	Temperature
u	J/Kg	Internal energy per unit of mass
U	W/m^2K, J	Overall heat transfer coefficient, internal energy
w	-	Weighting factor
W	J or Wh	Work
$\dot{W}$	W	Rate of work, or power
x,y,z	m	Rectangular coordinates

Greek

α	%, W/m^2K	Absorptance, heat transfer coefficient including convection and radiation
β	degrees	Slope
γ	degrees	Surface azimuth angle
γ_s	degrees	Solar azimuth angle
δ	degrees	Declination
Δ	-	Change = final minus initial

θ	degrees	Angle (defined locally), angle between surface normal and incident radiation
θ_z	degrees	Zenith angle
λ	W/mK	Thermal conductivity
ρ	Kg/m^3, %	Density, reflectance
τ	%	Transmittance
φ	degrees	Latitude, angle (defined locally)
ω	degrees	Hour angle
ω_s	degrees	Sunset (or sunrise) hour angle

1 Introduction

Demand Side Management (DSM) is a measure taken by electric utilities to influence the amount or timing of customers' energy demand, in order to utilize scarce electric supply resources more efficiently. According to IEA Demand Side Management working group, the term “demand response” refers to a set of strategies which can be used in competitive electricity markets to increase the participation of the demand side in setting prices and clearing the market. The net effect of the demand response is to ease system constraints and to generate security and economic benefits for the market as a whole. Below, there is a full presentation of the definitions that concern the demand response (Table 1.1) [1].

DR Program	Definition
Direct load control and curtailment	Direct control programs are implemented by system operators and are triggered in response to volatility in wholesale pricing, or system and network constraints. This approach necessitates pre-agreed programs with consumers, which establish commercial terms for participation.
Emergency Demand Response Program	Emergency Demand Response Programs are portfolio of measures designed to deal with declared emergencies, during which the continued controlled operation is at risk brownouts and/or blackouts are likely.
Demand Side Bidding	Demand Side Bidding is a term which refers to the opportunity offered by some electricity trading markets for consumers to choose when and how to participate in real-time and day ahead spot markets. The process allows the consumer to be paid a market price for withdrawing load, when required by the market operator, in a similar way that generators are paid to supply.
Time of Use Pricing	Under Time of Use Pricing, the retail price varies in a preset way within certain blocks of time. It is typically divided into three different price categories for three different parts of the day: • On peak. Demand for electricity is highest. • Mid-peak. Demand for electricity is between on-peak and off-peak. • Off-peak. Demand for electricity is the lowest.
Real Time Pricing (RTP)	Under real time pricing tariffs, electricity consumers are charged with prices that vary over short time intervals, typically hourly, and are quoted one day or less in advance to reflect contemporaneous marginal supply costs.

Table 1.1: Definitions by IEA Demand Side Management working group [IEA 2003].

More specifically, Demand-Side Management is used to describe the actions of a utility, beyond the customer's meter, with the objective of altering the end-use of electricity - whether it is used to increase demand, decrease it, shift it between high and low peak periods, or manage it when there are intermittent load demands - in the overall interests of reducing utility costs. In other words DSM is the implementation of those measures that help the customers to use electricity more efficiently so as to reduce the utility costs. DSM can be achieved through:

- Improving the efficiency of various end-uses through better housekeeping correcting energy leakages, system conversion losses, etc;
- Developing and promoting energy efficient technologies, and
- Demand management through adopting soft options like higher prices during peak hours, concessional rates during off-peak hours, seasonal tariffs, interruptible tariffs, etc.

DSM, in a broaden definition, also includes options such as renewable energy systems, combined heat and power systems, independent power purchase, etc. That utility manages to meet the customer's demand at the lowest possible cost. Electricity DSM strategies have also the goal of maximizing end-use efficiency to avoid or postpone the construction of new generating plants.

Often the energy efficiency and DSM terms are used interchangeably. However, it is important to point out that DSM explicitly refers to all those activities that involve deliberate intervention by the utility in the marketplace so as to alter the consumer's load profile. Energy efficiency issued in an all encompassing sense includes any activity that would directly or indirectly lead to an increase in energy efficiency. To make this distinction precise, a program that encourages customers to install energy efficient lighting systems through a rebate program would fall under DSM. On the other hand, customer purchases of energy efficient lighting as a reaction to the perceived need for conservation is not DSM but energy efficiency gains.

As far as the thermal comfort is concerned in order to reach the desired indoor temperature and humidity, the heating/cooling demand should be regulated thus satisfying a DSM strategy. In the framework of this thesis “**Thermal Model Predictive Controller”** is developed implementing super cooling strategies, through which a building or a building part is pre-cooled during low peak periods achieving peak shaving in an acceptable way by the users regarding the thermal comfort issue during summer.

Demand Side Management strategies also play an important role in mitigating electrical system emergencies, avoiding blackouts and increasing system reliability, reducing dependency on expensive imports, reducing high energy prices, providing relief to the power grid and generation plants, avoiding high investments in generation, transmission and distribution network and leading to environmental protection.

Thus it provides significant economical, system reliability and environmental benefits. DSM techniques are the cheapest, fastest and cleanest way to solve electricity problems. These can be immediately implemented and many times at a cheapest way relative to the cost of building new power plants.

1.1 Layout of the Rest of the Report

In this report the development of a Thermal Model Predictive Controller for DSM actions is implemented, investigated and used to control a building situated in Athens, Greece.

In Chapter 2, the examined building in Athens is presented. An Energy Management System (EMS), based on KNX/EIB technology, as well as a Supervisory Control and Data Acquisition (SCADA) system have been installed. A detailed explanation of the data measurements and control functions is given in this.

In Chapter 3, the Thermal Model Predictive Control Concept is illustrated. In Chapter 4, the development of the Finite Difference Calculation (FDC) Method is presented for a building part. The necessary assumptions are made on this stage. The derived heat fluxes and energies of each wall of the examined building part based on the FDC method are described.

In Chapter 5, the development of an anisotropic (Hay-Davies-Klucher-Riendl (HDKR)) sky solar radiation diffuse model is presented. The absorbed solar radiation is estimated. In Chapter 6, the energy losses from internal heat sources (humans, electric devices etc.) and through windows are calculated. The electrical power consumption of the air-conditioning units is also presented in this chapter.

In Chapter 7, the dynamic thermal model of the examined building part is verified using the energy balance equation and predicting the indoor temperature. In Chapter 8, the thermal model is used for taking decisions for the pre-cooling phase. Experimental results are also presented in this chapter. Based on this approach, conclusions are achieved for the duration of the pre-cooling phase and for the reduction of the indoor temperature during this phase.

In Chapter 9, an approach to Thermal Model Predictive Controller design is presented. In Chapter 10, the energy savings between a cooling strategy based on the developed Thermal Model Predictive Controller for DSM actions in comparison with the normal operation are calculated. Conclusions and Recommendations for future work are discussed in Chapter 11.

2 Building Description & Communication System

A building in Athens, Greece, has been chosen for implementing the Thermal Model Predictive Controller for DSM actions. It is called Georgiadis building, it is named after its owner, and it is located in Gerakas city. A DVD Club is situated at the basement of the building. Furthermore, a bookshop and a shop which sells desalination plants are situated in the ground floor. Finally, an apartment with an attic is in the first floor. The Georgiadis building is depicted in the following Figure 2.1.

Figure 2.1: Georgiadis Building in Gerakas of Athens in Greece.

The bookshop has been chosen as the place to accommodate the experiments of this thesis due to the owner's special interest to save energy in this building part. This chapter aims to present the building and the communication system for the use of the Thermal Model Predictive Controller for DSM actions.

2.1 Communication System KNX/EIB

The Thermal Model Predictive Controller is developed on a PC at the first stage. This development requires a communication system in order to acquire all the needed data and measurements from the building and to process them in on-line mode. The controller should be economically attractive and for this reason the following requirements have to be defined:

- Only existing on the market system components are applied; no special designs and developments.

- Basis for the design is a 'normal' building part (bookshop) and no any 'super installation'. Research results should be able to be transferred economically into a product.

These requirements are achieved by concatenation of different networks that exist in modern buildings (Figure 2.2) [2]. However, today they exist in parallel without any concatenation among each other.

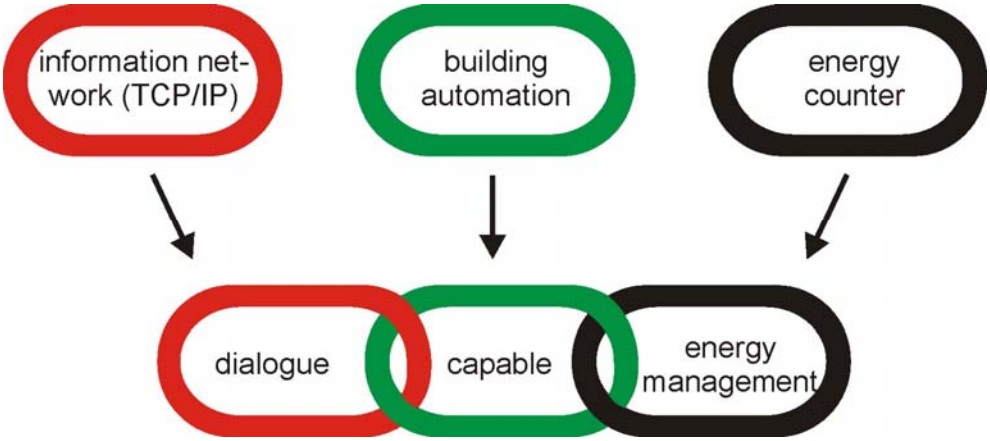

Figure 2.2: Chain of different networks to obtain Thermal Model Predictive Controller.

The realization of the communication process between the Thermal Model Predictive Controller, the building and the user are very important for the acceptance on behalf of the latter and the function of the system. Especially, the remote monitoring and control through Intranet even more via Internet is one of the goals of this thesis. At this point, we should take into consideration the fact that almost all building users have access to a PC that is linked to an Intranet or the Internet which consists of an ideal communication interface for building automation, as well. Therefore, building automation is linked to the information network TCP/IP. Here the building automation is based on KNX/EIB technology, where EIB stands for European Installation Bus.

In the following sections the hardware and the software that allow the communication between the building and the user are described.

2.1.1 The KNX/EIB interface

A Thermal Model Predictive Controller should process energy consumption, outdoor and indoor temperature measurements in order to predict the peak demand and the indoor temperature, so as to regulate the setpoints of a cooling system in an optimal way. For realisation of such an energy management system one can benefit from the recent developments in electrical installation techniques.

According to the electricity principles, electrical loads are supplied with energy via a switch. New applications and new requirements lead this technique to more and more complicated electrical installations. This happens not only because cables have to be installed for energy transmission but also for information transmission. Conventional installation technique reaches soon to its own restrictions. Moreover, an increased installation of cables increases the risk of fire load and under these conditions, regulations no more can be observed [3].

Due to these reasons, installation busses gain more and more recognition. Here, energy and information transmission are separated. The installation bus is the medium on which information transmission occurs. This transmission of information is one of the basic preconditions that a Thermal Model Predictive Controller can operate. For building system technique a variety of bus systems could be applied. Besides EIB there is LON, EHS, BATIBUS or CAN. Konnex Association merges EIB, Batibus and EHS in one bus system named KNX [4], whereas others are in competition.

For the delegable energy management of this application, the KNX/EIB system has been chosen. This bus suffices the requirements of this thesis and with regard to its market presence, the chances to disseminate the “dialog able Thermal Model Predictive Controller for DSM actions” are very positive. More than 15 million installed products, more than 6,500 registered and certified ones are available for KNX/EIB. Except for the twisted pair solution power line, radio frequency and IP media are also available. More than 50.000 KNX/EIB projects of all sizes have been realised world wide [5].

More information on the different bus systems can be found in [6]. In the thesis only the KNX/EIB topology is explained in detail which is more important for the developed Thermal Model Predictive Controller. Details about bus access, telegram description etc. can be found in [3], [7] and [8].

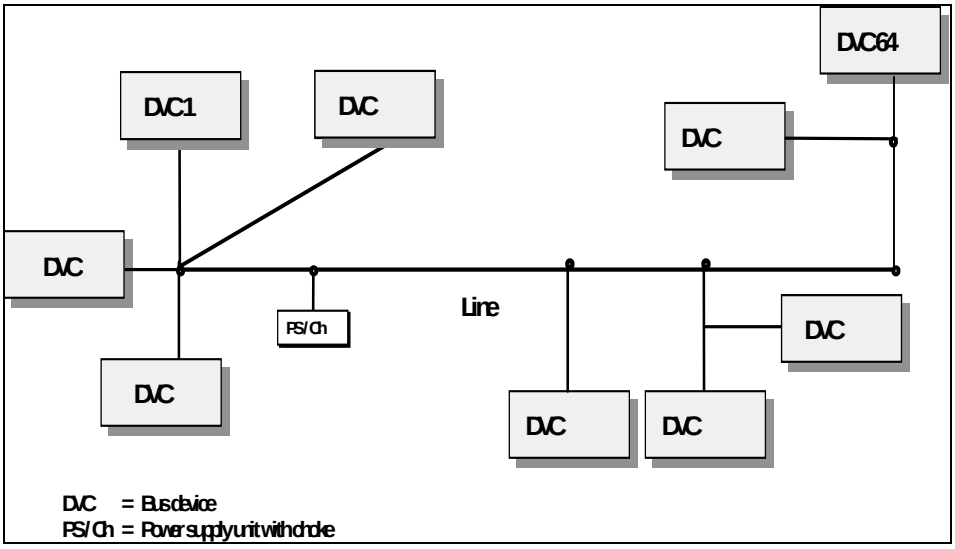

Figure 2.3: Bus Line.

Each bus device (DVC) can exchange information with any other device by means of telegrams [5], [9]. One line consists of a maximum of 4 line segments, each with a maximum of 64 bus devices (Figure 2.3). Each segment requires an appropriate power supply. The configuration of 1 bus line is used in the thesis' building. The Thermal Model Predictive Controller is implemented on a PC, which is connected to the bus through a serial interface.

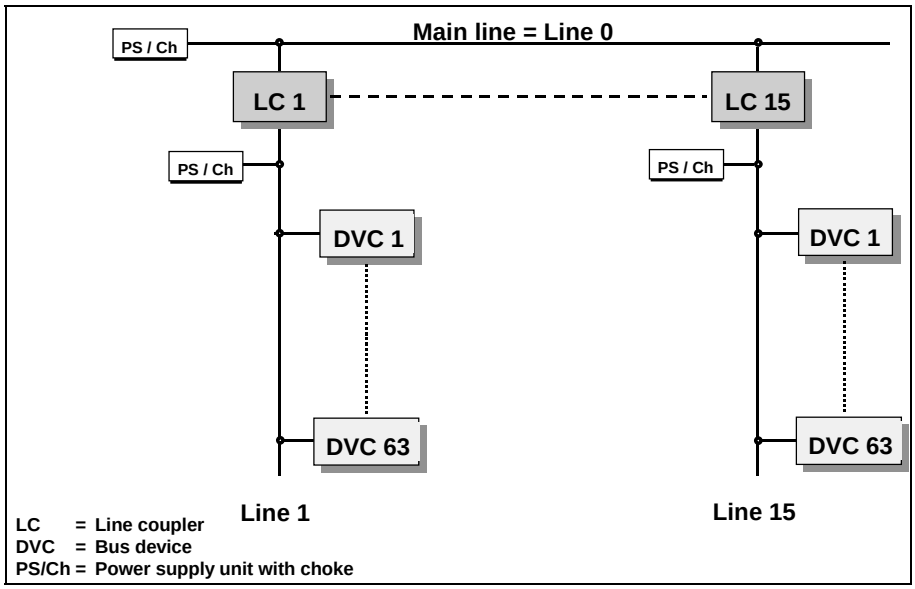

Figure 2.4: Bus Area.

If more than 1 line is to be used or if a different structure is to be selected, then up to 15 lines can be connected to a main line via a line coupler (LC). This is called an area (Figure 2.4). It is also possible to have up to 64 bus devices on the main line. The maximum number of bus devices on the main line decreases by the number of line couplers in use.

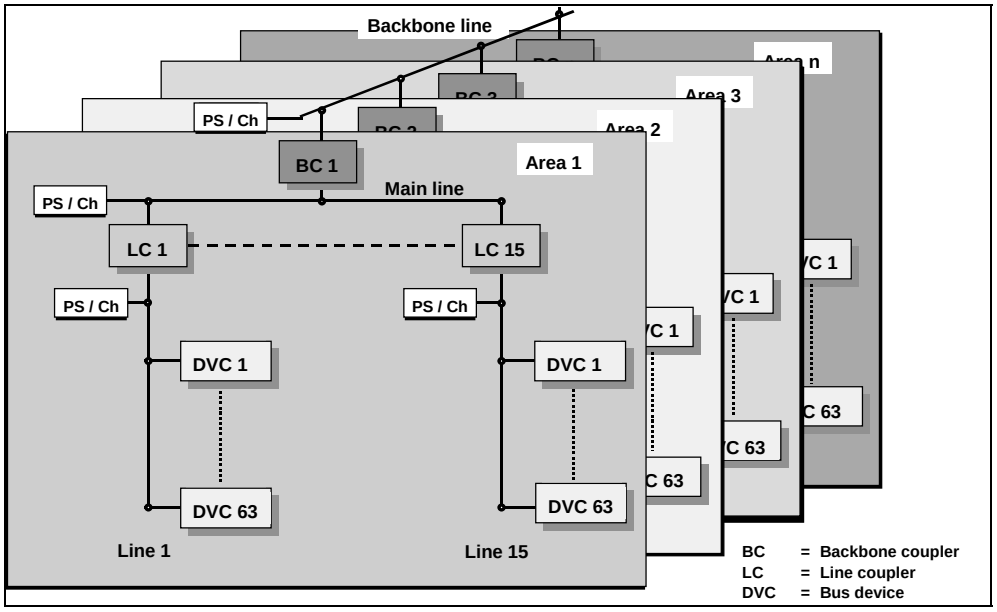

Figure 2.5: Bus Several Areas (Maximum Configuration).

The KNX/EIB TP1 bus can be expanded by means of a backbone line. The backbone coupler (BC) connects its area to the backbone line (Figure 2.5). It is also possible to have bus devices on the backbone line. The maximum number of bus devices on the backbone line decreases by the number of backbone couplers in use. Within a maximum of 15 functional areas, more than 58.000 bus devices can be connected to the bus system. By dividing the KNX/EIB TP1 installation into lines and areas, the functional reliability is increased considerably.

In order to equip the rooms with sensors and actuators a compromise had to be found between two contradictory requirements. On the one hand the necessary measurements should be acquired for the implementation of the Thermal Model Predictive Controller. On the other hand installation expenditure should be kept as small as possible for not becoming too uneconomical. Furthermore, with the number of components the reliability of the installation decreases and the probability of failure increases. As a result of those reasons an installation has been chosen integrating temperature control of a single room and lighting control as well as some devices of a security system. This does not exceed much a standard installation.

Figure 2.6 depicts the layout of the ground floor, where the bookshop and the shop are located. In the bookshop a KNX/EIB thermostat has been installed for controlling the air-conditioning units. Actually, in this room there are 4 air-conditioning units (heat pumps) of total capacity 42.000 Btu/h. However, the 2 air-conditioning units serve as heating/cooling system with total capacity of 21.000 Btu/h. It is noted that the air-conditioning units can be switched on/off only and none of the analogue values can be sent to them [10]. Therefore, KNX/EIB binary outputs activate/deactivate the air-conditioning units.

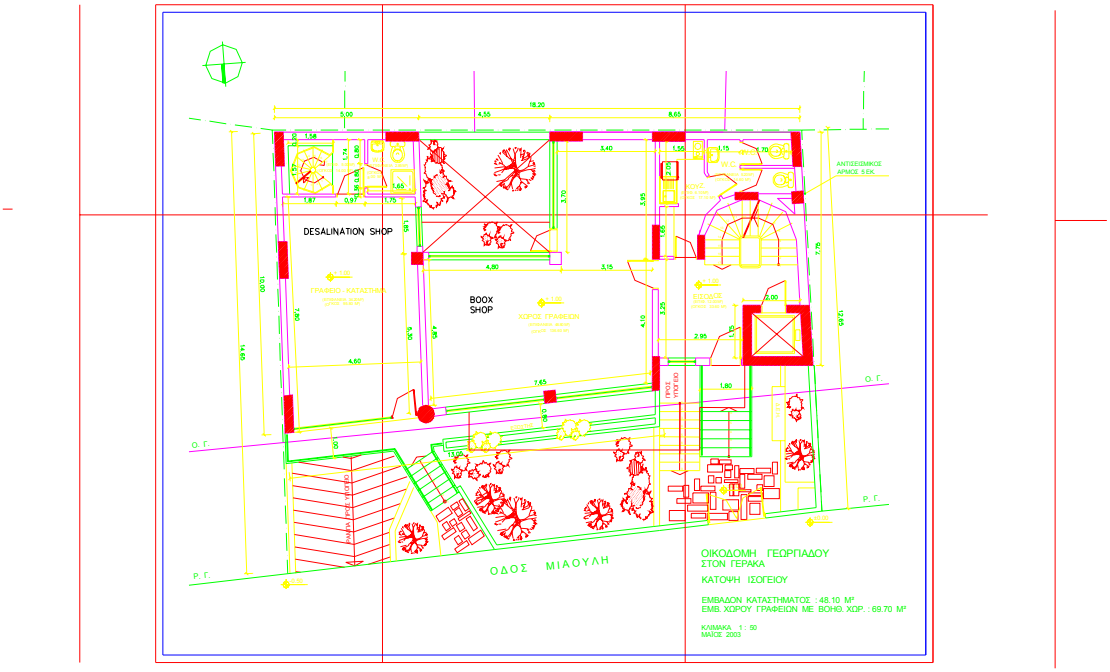

Figure 2.6: Ground floor layout.

The KNX/EIB components are programmed through the ETS (Engineering Tool Software) installed on a PC or Notebook.

Figure 2.7a: KNX/EIB room thermostat.

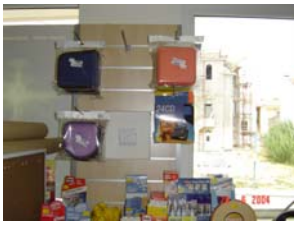

Figure 2.7b: KNX/EIB bookshop thermostat (temperature controller).

- With the KNX/EIB room thermostat (temperature controller) shown in Figure 2.7, the Thermal Model Predictive Controller can influence the heating/cooling system. It gives a large variety of possibilities to set options and programmes. Four temperature modes can be distinguished. Comfort temperature mode, Standby temperature mode, Night and Frost/Heat protection temperature modes. During the normal operation of the bookshop (Boox), Comfort or Standby mode is set by the user. When the windows are opened or while the bookshop is closed, the Frost/Heat protection mode is applied automatically. The Night mode is not used. The thermostat has been programmed so that the range of the setpoint varies from 18 to 21 degrees centigrade during winter and from 24 to 27 degrees centigrade during summer in Comfort mode. In Standby Mode, when the user is not temporarily inside the building part, the setpoint is increased by 2 degrees relatively to the current value in Comfort mode during summer. The indoor and setpoint temperatures of every building room are sent by the KNX/EIB thermostats to a PC, which are going to be used by the Thermal Model Predictive Controller.

Figure 2.8a: KNX/EIB Binary Input Device.

Figure 2.8b: KNX/EIB Boox Binary Input in the distribution board with the Power Supply, the Binary Output, etc.

Figure 2.9a: KNX/EIB Binary Output Device.

- The Security System is connected to the KNX/EIB installed system through a Binary Input Device (Figure 2.8a). So, when the bookshop closes, or when a window opens, the corresponding binary input is activated, the thermostat changes mode from Comfort to Frost/Heat Protection and the air-conditioning units are switched off. On the other hand, when the bookshop opens and all windows are closed, the thermostat goes to Comfort mode and the air-conditioning units are switched on.

- Figure 2.8b shows the KNX/EIB Power Supply 230V/640mA for the used Bus Line (Figure 2.3) in the building, the KNX/EIB Binary Input (BI) and the KNX/EIB Binary Output (BO) Devices. The activation/deactivation of the air-conditioning units is realised via the Binary Output Device. In every building part a KNX/EIB thermostat, BIs and BOs are installed. The Supervisory acquires temperatures from all the rooms and the relative information about the window and room states.

- Figure 2.9.a depicts a typical KNX/EIB Binary Output or Switch Actuator Device. Up to six air-conditioning units can be connected to this BO Device. More details about KNX/EIB bus devices can be found in the sites of the KNX members [11] and [12].

Figure 2.9b: Window reed contact.

- The rooms are equipped with window reed contacts (Figure 2.9.b). These are used by the security system. The above mentioned binary inputs send the windows states to the thermostats and to the Supervisory.

Figure 2.10a: KNX/EIB Delta-Energy Meter.

- A KNX/EIB Delta Energy Meter (Figure 2.10) is installed in the distribution board of the bookshop for measuring the electrical energy consumption and the instantaneous power. This information is sent to the Supervisory on the PC and plays an important role for the evaluation of the Thermal Model Predictive Controller.

Figure 2.10b: KNX/EIB Boox Delta-Energy Meter with the Binary Output and Dimmer Actuator in the distribution board.

- Figure 2.10b depicts the installed KNX/EIB Delta Energy meter with the Binary Outputs for activating/deactivating the air-conditioning units of the bookshop. The Dimmer Actuator Device which dims the lighting of the bookshop through the installed electronic ballasts is also depicted.

Figure 2.11a: KNX/EIB Presence Detector.

Figure 2.11b: Boox KNX/EIB Presence detector next to the lights.

- The Presence Detector (Figure 2.11), with the dimmer actuator (Figure 2.10b) for controlling the digital electronic ballasts and a binary input for the connection of the conventional security system have been installed in the bookshop. When the bookshop is opened and a customer is inside, the lights are controlled by the presence detector according to the solar radiation in the books shop. The brightness value setpoint of the presence detector is set by the user through the SCADA. The switch off time is set by the user via the proper potentiometer of the presence detector.

  When the bookshop is opened and no any customer is inside except for the employee, the presence detector switches the lights off after a certain period, while at the same time the SCADA measures the outside solar radiation and dims the lights to a minimum brightness. This helps the customers outside the shop to realise that the shop is opened, while saving energy.

  When the bookshop is closed, the security system gives this information to the KNX/EIB. The SCADA exploits this information by the OPC Server, and when the outside solar radiation is over a threshold, for instance over 400W/m^2, the lights are switched off, while in the opposite case (during night), they are dimmed to 10%. It is noted that the presence detector controls the lights even if the bookshop is opened or closed or if it is day or night.

Figure 2.12a: KNX/EIB Analogue Input Device.

- Apart from the several rooms which are connected to KNX/EIB components, there are other components which help to complete the range of requirements. These are shown in Figure 2.12b, while Figure 2.12a depicts the KNX/EIB Analogue Input Device for interfacing the above-mentioned components to the KNX/EIB system.

Figure 2.12b: Ambient temperature and solar radiation on a horizontal surface sensors.

- The KNX/EIB Analogue Input Device supplies the Thermal Model Predictive Controller with the following measurements. The transmission happens in periodic cycles and at different minimum changes:
- Ambient Temperature:-10°C to +40°C.
- Global solar irradiation on a horizontal surface.

2.1.2 Supervisory Control and Data Acquisition (SCADA)

The Thermal Model Predictive Controller is developed as a part of a Supervisory Control and Data Acquisition (SCADA) system on a PC. The SCADA is based on LabVIEW Software and operates in on-line mode [13]. The PC is connected to the KNX/EIB installation through a RS232 interface (Figure 2.13), while the LabVIEW Software communicates with the KNX/EIB building automation system via an EIB OPC Server. All the foregoing measurements are acquired from the SCADA and the proper DSM actions are executed by the Thermal Model Predictive Controller.

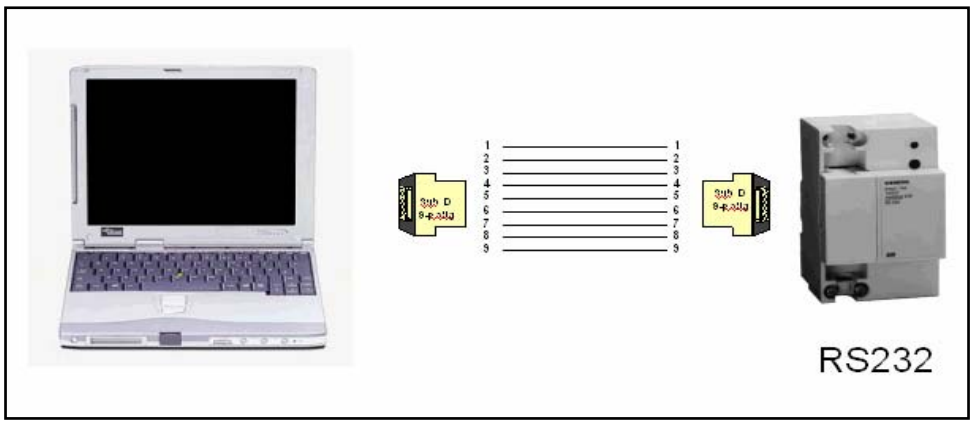

Figure 2.13: Connection between the PC and the KNX/EIB installation.

The following Figure 2.14 depicts the main window of the SCADA, where all indoor and ambient temperatures are monitored as well as the energy consumption and the power of the bookshop. The local time and the solar irradiance on a horizontal surface are also presented on it. With the option **"WALLS ENERGIES",** Inflow, Outflow and Stored Energies of the bookshop are viewed, while the predicted indoor temperature and the measured temperature of the bookshop are shown when the **"PREDICTIONS"** key is chosen.

The absorbed solar radiation by the surface of the outer north wall and the windows, which are also located to the north and by the roof part made of glass are depicted when the tab **"SOLAR ENERGIES"** is pressed, while the estimated instantaneous power and the measured one are shown by choosing **"ESTIMATIONS".** Finally, a graphical view of all temperatures is presented by pressing **"TEMPERATURES".**

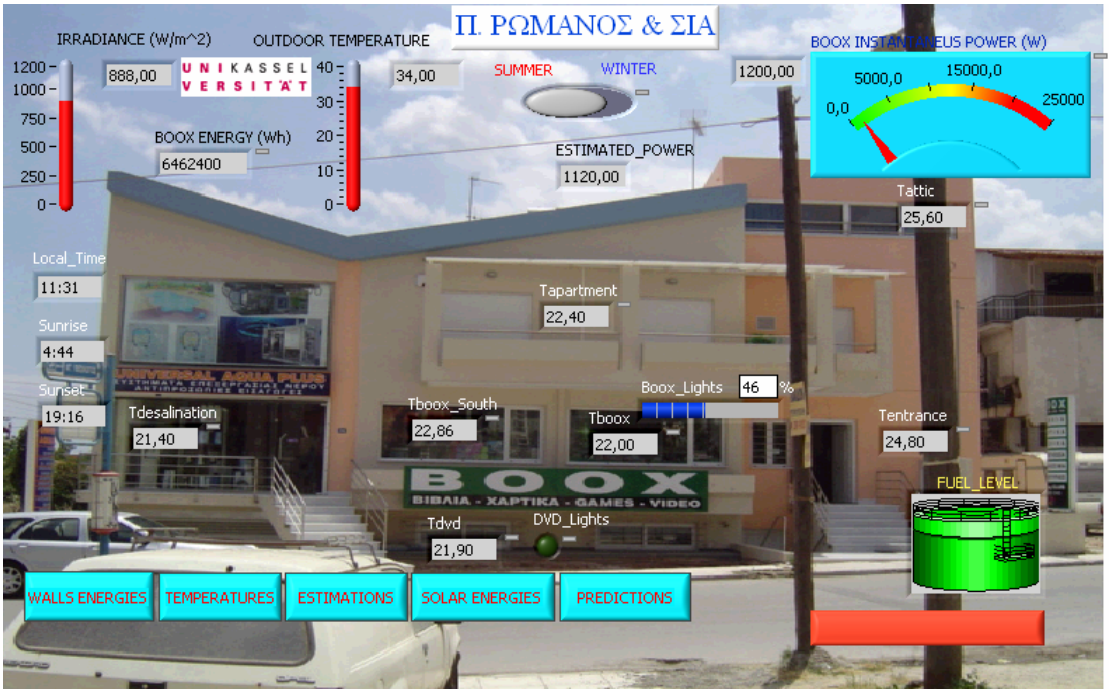

Figure 2.14: The SCADA main window page.

The individual energy management is a motivation to increase acceptance of Building Automation. By using the mouse on each building part, more information and control functions can be viewed for this. A typical window is presented in Figure 2.15, in which the temperatures of the bookshop and the shop selling desalination plants are monitored, as well as the setpoint of each shop. The states of the air-conditioning units are also shown on this panel. Furthermore, by clicking on the air-conditioning units the possibility of activating (green) or deactivating (red) the corresponding ones is realised manually.

The conventional security system monitors the states of the shops. The SCADA receives this information and presents the states of the shops, when one is closed or when its windows are opened (left side in Figure 2.15) and vice-versa. Finally, the dimming level of the lights of the bookshop is viewed on this front panel. All the aforementioned information is saved in daily Excel files, making a useful database for further analysis.

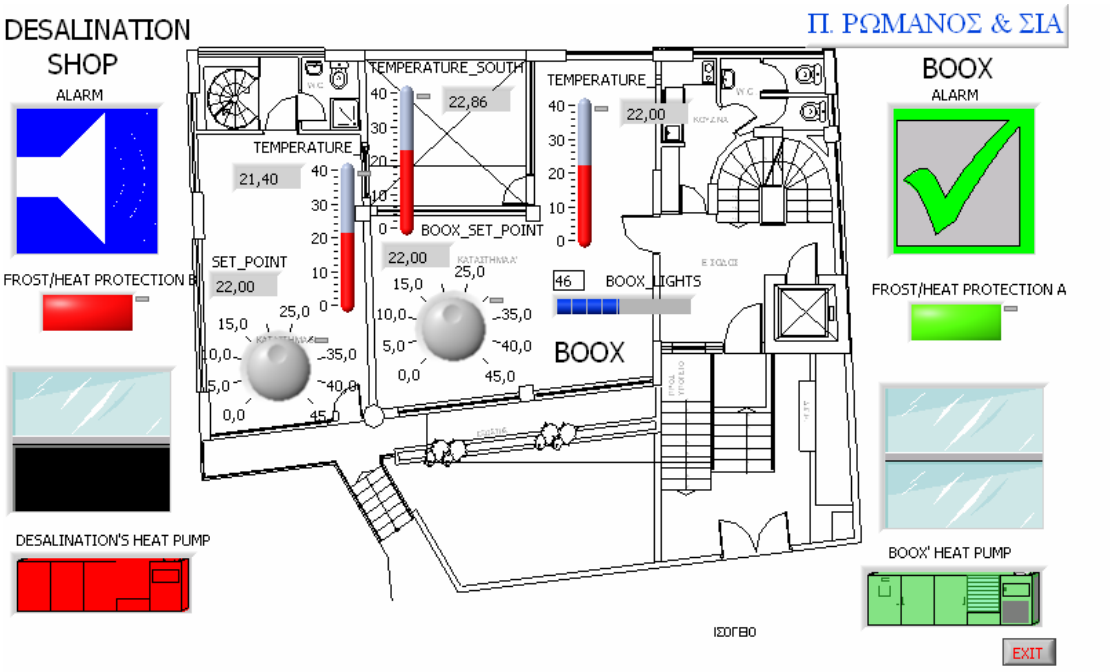

Figure 2.15: Front panel of the Bookshop and shop selling desalination plants.

The requirements for this interface concerning comfortable operation are an intuitive input of information and an ability of operation without reading a manual. The latter can be detrimental for success and flop of all the system. A good example is the above-mentioned room temperature controller described in the previous section. It offers a variety of functionalities which can be programmed with a very few buttons. Experience has shown that even technically versed people don't understand how to program it without reading the technical manual.

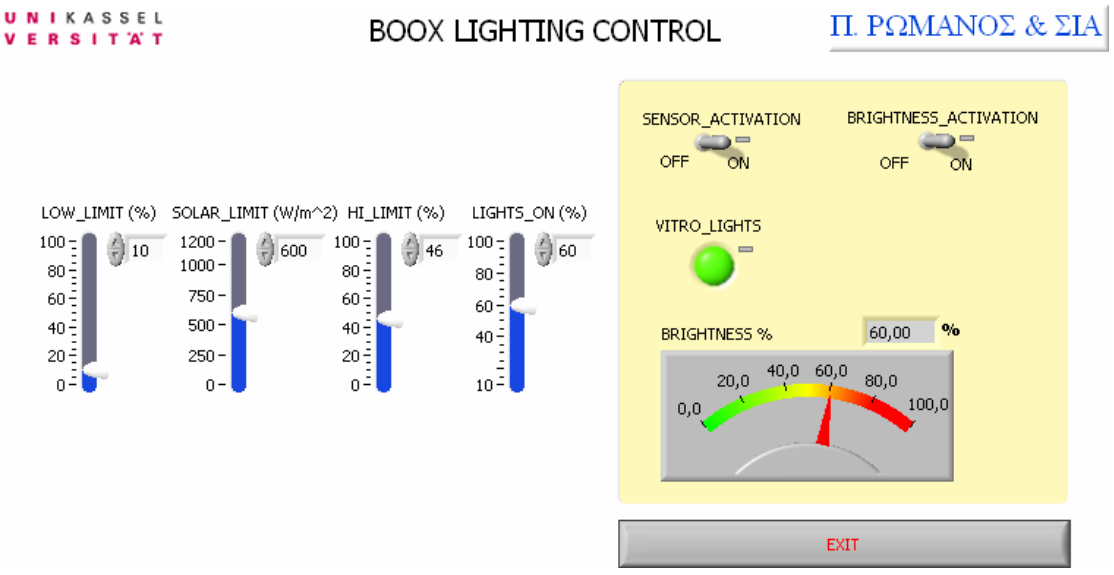

Figure 2.16: Front panel controlling Bookshop lighting.

The above Figure 2.16 presents the visualization front panel concerning the lighting control of the bookshop. The setpoints of the presence detector, which is presented in Figure 2.11, are regulated by this control panel. In this case, if the solar radiation is more than 600W/m^2 the lights are dimmed to 10%, when no any customer is inside, while if it is less than 600W/m^2 the lights are dimmed to 46%. If a customer gets in

the bookshop the presence detector dims the lights according to the existing solar radiation starting from 60%.

For the sake of convenience, the connection of the SCADA system to the Intranet or Internet is useful. Thus, the analysis of the results of the Thermal Model Predictive Controller is achieved faster, while the behaviour of the building is under a better control. The way to implement this communication is realised through LabVIEW software, which has the ability to create remote web panel connections. The following Figure 2.17 depicts such a remote web panel.

It is noted that all the information is available through Intranet or Internet. However, it is not the aim of this report to explain the technical details for programming the KNX/EIB devices through ETS or the communication between the SCADA and the KNX/EIB installation of the building via the OPC SERVER and FALCON Software. In this case a good description can be found in [2].

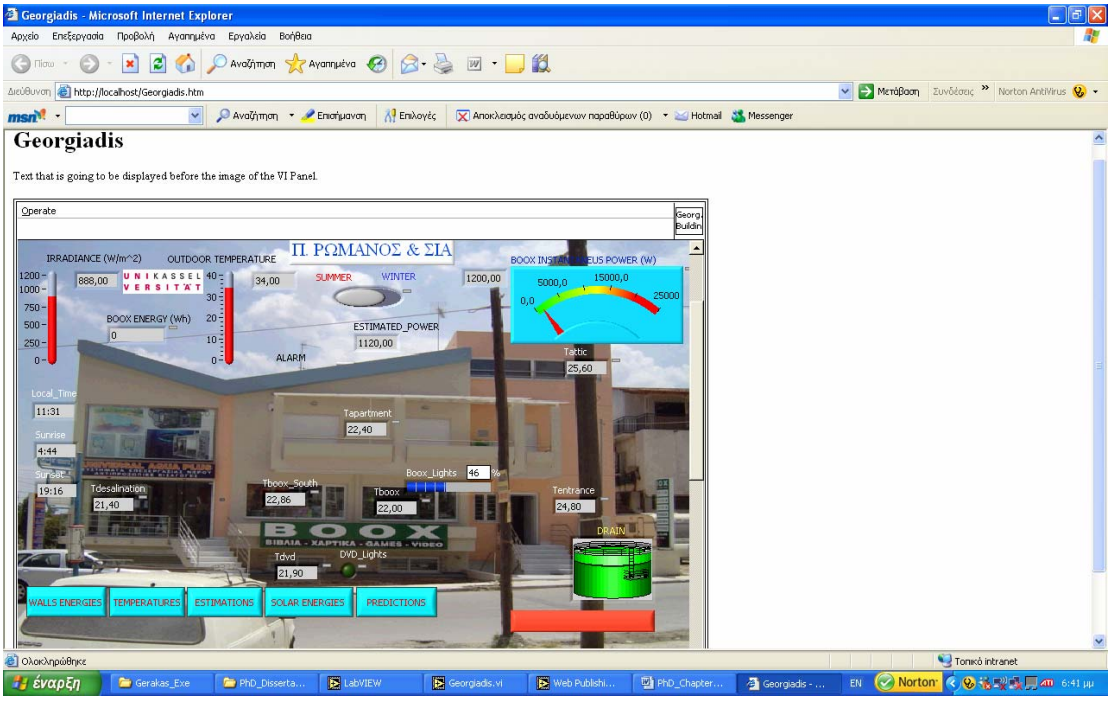

Figure 2.17: Remote Web Panel of the SCADA.

In Chapter 10, there is an explanation by a practical example what the user can earn economically, if he accepts the proposed maximum indoor temperature by the SCADA during the peak period on 19th September 2005, (e.g. 27,5^{o}C instead of 27^{o}C).

The following Figure 2.18 depicts the PC where the SCADA has been developed on, as well as its communication with the KNX/EIB system through the serial interface.

Figure 2.18: The PC with the SCADA and RS-232 interface.

3 Thermal Model Predictive Controller Concept

The concept of the Predictive Control is presented in this chapter. To be more specific, the Thermal Model Predictive Controller for DSM Cooling Strategies (TMPC-DSM) has three major features:

1. The thermal model to predict the indoor temperature during the pre-cooling and peak periods.

2. The stochastic model to predict when the peak period occurs and its duration.

3. Optimization algorithms which produce the optimal controller output sequences over the prediction horizons of the pre-cooling and peak periods, resulting in energy savings and comfortable conditions for the users.

3.1 Predictive Control

Predictive control belongs to the class of model-based controller design concepts, [14]. That is, a model of the process is explicitly used to design the controller, as it is illustrated in Figure 3.1. In this figure u denotes the controller output, y denotes the process output and ω denotes the desired process output. Predictive control is not the only model-based controller design method. Others are, for example, pole-placement control and linear-quadratic (LQ) control. Note that in Figure 3.1 it is assumed that there is a separation between controller design and the controller itself, the control law. For pole-placement control and LQ control it is well known that such a separation exists. For example, in LQ control the controller is usually a state feedback controller. The controller parameters are obtained by solving an optimization problem. In predictive control the above-mentioned separation can, in general, also be obtained, [15], [16] and [17].

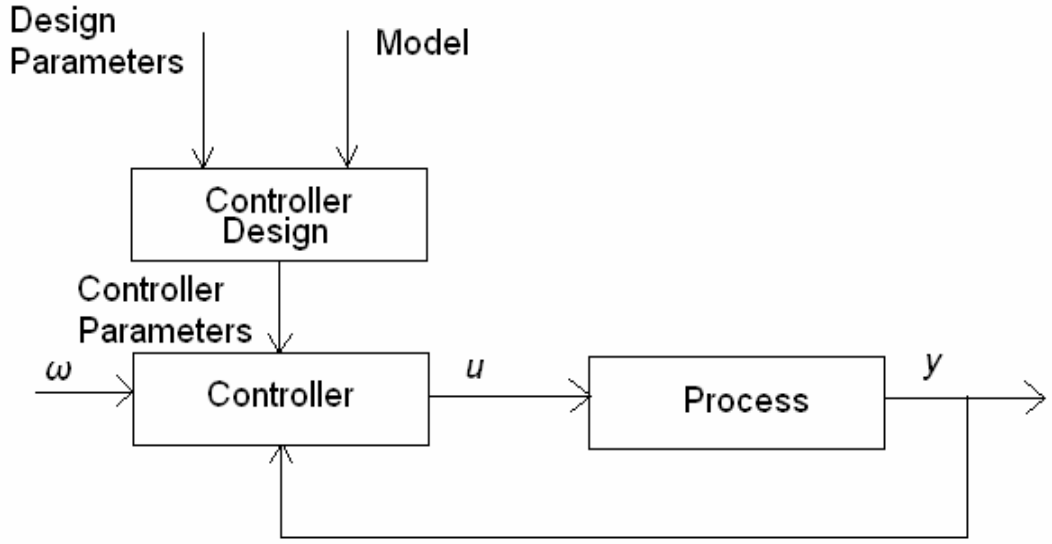

Figure 3.1: Model-based control.

In general, if the process is linear, there are no constraints and the desired process output (the set point or reference trajectory) is simple, then all of the above-mentioned model based controllers can yield approximately the same results. That is, one method is no 'better' than another. This can be explained by the fact that these controller design methods yield linear controllers which after some manipulation are of the same structure and have a sufficient number of degrees of freedom. The controller parameters are, however, determined using a different design methodology. From a designer's point of view, the methods differ in the design parameters that are used to obtain the desired behaviour of the control system.

One of the attractive features of predictive controllers is that they are relatively easy to tune. This makes predictive controllers attractive to a wider class of control engineers and even for people who are not control engineers. Other features of predictive controllers are:

- The concept of predictive control is not restricted to single-input, single-output (SISO) processes. Predictive controllers can be (and have been) derived for and applied to multi-input, multi-output (MIMO) processes. Extending predictive controllers for SISO processes to MIMO processes is straightforward, [18], [19], [20], [21] and [22].

- In contrast to LQ and pole-placement controllers, predictive controllers can also be (and have been) derived for nonlinear processes. A nonlinear model of the process, such as the Thermal Model, is then used explicitly to design the controller, [23], [24] and [25].

- Predictive control is the only methodology that can handle process constraints in a systematic way during the design of the controller.

- Predictive control is an open methodology. That is, within the framework of predictive control there are many ways to design a predictive controller. As a

result, over ten different predictive controllers, each with different properties, have been proposed in the literature over the last decade. Some well-known predictive controllers are GPC (Generalized Predictive Control, [26], [27]), DMC (Dynamic Matrix Control, [28]), EPSAC (Extended Prediction Self-Adaptive Control, [29]), PFC (Predictive Functional Control, [30]), EHAC (Extended Horizon Adaptive Control, [31]) and UPC (Unified Predictive Control, [32], [33]).

- The concept of predictive control can be used to control a wide variety of processes without the designer having to take special precautions. It can be used to control 'simple' processes, as well as 'difficult' processes, such as processes with a large time delay, processes that are nonminimum phase and processes that are open-loop unstable.

- In a natural way feed-forward action can be introduced for compensation of measurable disturbances and for tracking reference trajectories.

- Because predictive controllers make use of predictions, pre-scheduled reference trajectories or set points can be dealt with.

Unavoidably, predictive controller design has some drawbacks. Since predictive controllers belong to the class of model-based controller design methods, a model of the process must be available. In general, in designing a control system two phases can be distinguished: modeling and controller design. Predictive control provides only a solution for the controller design part. The model of the thermal behaviour of the bookshop is obtained by using the Finite Difference Calculation Method.

A second drawback is due to the fact that the predictive control concept is an open methodology. It has already been mentioned that, as a result of this, many different predictive controllers can be derived, each having different properties [34]. Although, at first glance, the differences between these controllers seem rather small, these 'small' differences can yield very different behaviour the closed-loop systems. As a result, it can be quite difficult to select which predictive controller must (or can) be used to solve a particular control problem. Sometimes, one cannot afford the expense designing a control system that one knows will not work in another process and whose cost cannot therefore be spread over a large number of applications.

3.2 Thermal Model Predictive Control Concept for DSM Cooling Strategies

The aim of a DSM strategy is the reduction of the peak demand. Taking into account the fact that the peak demand is mainly caused by the operation of air-conditioning units during summer, the DSM cooling strategy intends to reduce the consumption of these units during the peak periods. However, this reduction should not be against the thermal comfort. This means that the indoor temperature and the humidity should not be increased more than a specified limit, so that the users still feel comfortable in it.

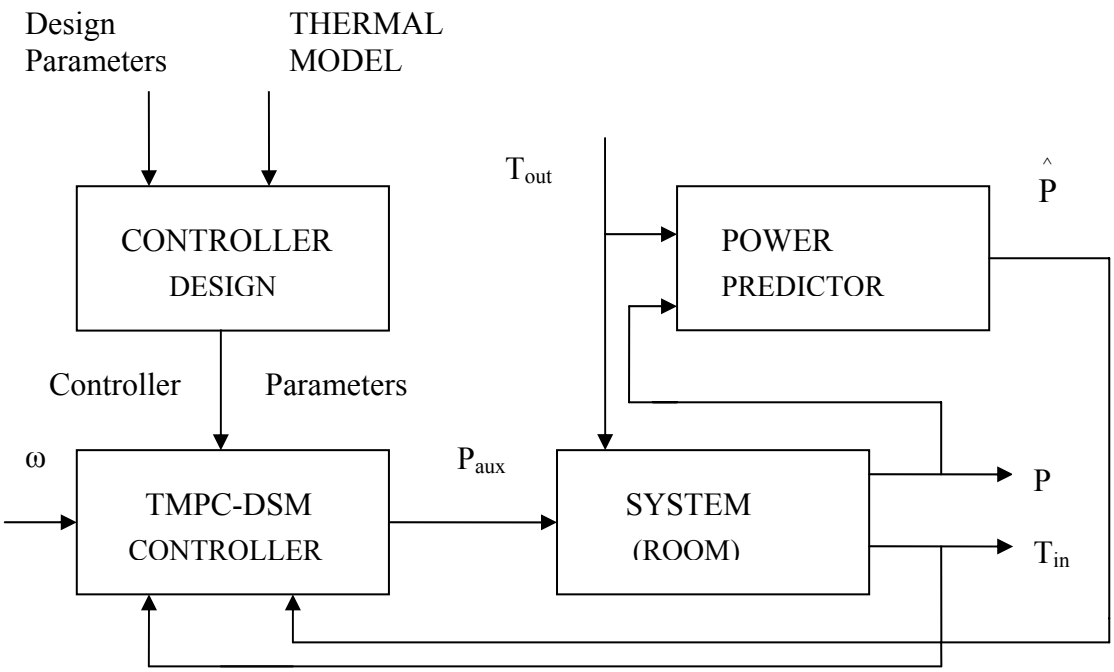

Figure 3.2: Thermal Model-based control.

The block diagram of the Thermal Model Predictive Controller for DSM actions (TMPC-DSM) is illustrated in Figure 3.2. A room of a building is a system which has two inputs: the power of the air-conditioning units P_{aux}, and the ambient temperature T_{out}. It also has two outputs: the indoor temperature T_{in} and the power consumption of the system P. The TMPC-DSM controller controls the power of the air-conditioning units and yields a different indoor temperature T_{in} and power consumption P. The Power Predictor is a stochastic model which predicts the power consumption $\hat{P}$ based on a k-step ahead prediction horizon and informs the controller when the peak demand occurs and its duration, [35], [36] and [37]. The TMPC-DSM pre-cools the system if it is necessary and reduces the peak demand achieving thermal comfort situations for the users.

The operation of the Thermal Model Predictive Controller for DSM cooling actions is illustrated in Figure 3.3. A typical electrical power consumption of a room is shown in Figure 3.3a (red line) and it is assumed that the indoor temperature is kept to 25^{o}C (Figure 3.3b). The indoor temperature is predicted by the thermal model. The Power Predictor predicts the power consumption of the system and informs the controller that the peak demand occurs during the time period from 19:00 until 21:00 in this case.

The Predictive controller pre-cools the room in an optimal way, for example, it starts to pre-cool it 2 hours before the peak demand occurs, at 17:00 (Figure 3.3.a–green area). The indoor temperature is decreased to 24.5^{o}C during that period. The consumption of the air-conditioning units is decreased during the peak demand period using an optimization algorithm and the indoor temperature is not increased more than 27^{o}C, which is the maximum acceptable temperature as far as the users are concerned. The energy saving is depicted in Figure 3.3a by the difference between the typical electrical power consumption (red line) and the electrical power consumption which is derived when the DSM Cooling Strategy is applied (green area).

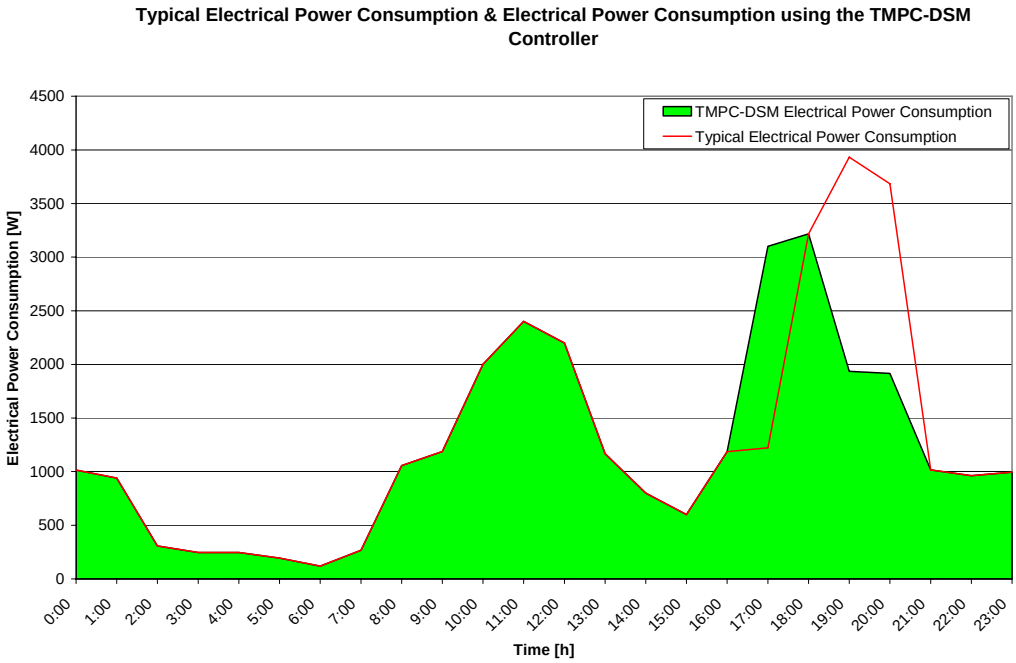

Figure 3.3a: Typical Electrical Power Consumption and Electrical Power Consumption which is derived when the DSM cooling strategy is applied using the TMPC-DSM controller.

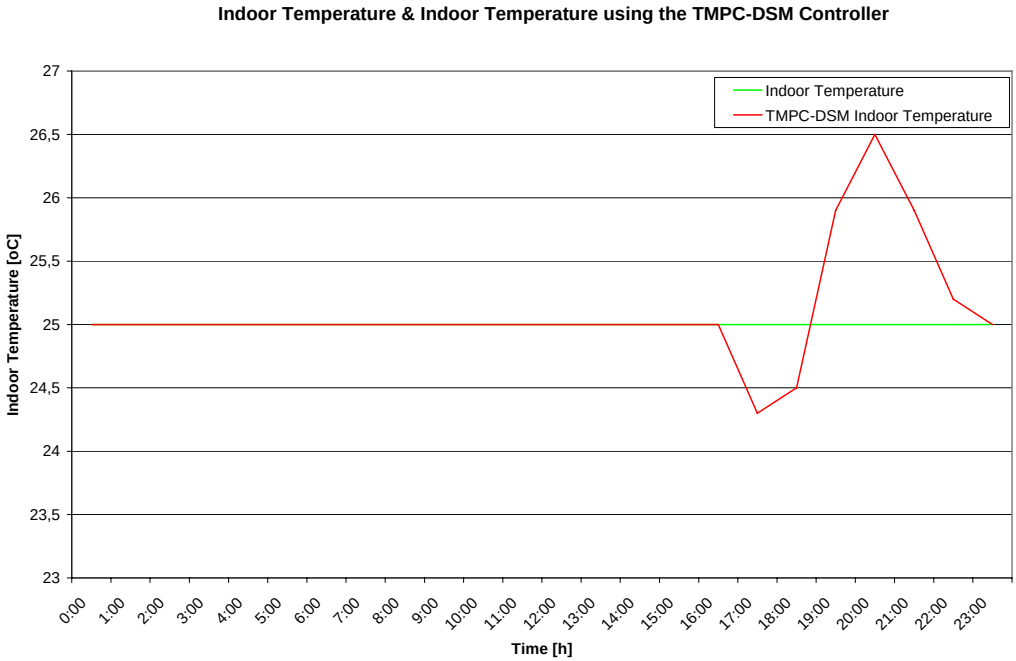

Figure 3.3b: Indoor Temperature and Indoor Temperature which is derived when the DSM cooling strategy is applied using the TMPC-DSM controller.

Obviously, the TMPC-DSM controller operates in three phases every day, as it is shown in Figure 3.3. The period in which the TMPC-DSM controller pre-cools a room is called **Pre-cooling period or Pre-cooling phase,** while the period in which the TMPC-DSM controller acts to air-conditioning units during the peak demand is called **DSM phase**. Moreover, the period in which the TMPC-DSM controller does

not operate or act to air-conditioning units and only receives information from the Power Predictor is called **Inactive phase.** It is noted that the DSM cooling strategy is obtained only by using the TMPC-DSM controller in this thesis.

The reduction of the indoor temperature during the pre-cooling period and its duration as well as the indoor temperature profile during the DSM phase depend on the structure of the examined room, the wall materials, the absorption of solar radiation in it, the internal heat sources such as lighting, the users being inside etc., The analysis of the thermal model defines the indoor temperature reduction during the pre-cooling period with its duration and the power consumption of the air-conditioning units during the peak demand. Therefore, the thermal model is the crucial element for the operation of the Predictive Controller, because it clarifies the system behaviour. For this reason, the FDC Method is chosen and developed in on-line mode, in order to achieve the optimal results.

The stochastic model predicts when the peak demand occurs and its duration. The Predictive Controller uses this information in order to start the pre-cooling period at the right time. The prediction horizon defines how many steps ahead the thermal and stochastic models can predict. Assuming that there are no disturbances and no modeling errors the predicted indoor temperature and room power consumption at time ***t*** are exactly equal to measured indoor temperature and room power consumption at ***t+1.*** The Thermal Model Predictive Controller applies the pre-cooling and DSM phases straightforward. The reason for using the prediction horizon approach is that allows us to compensate for future disturbances or modeling errors. For example, due to a disturbance or modeling error the predicted indoor temperature and room power consumption at time ***t*** are not equal to measured indoor temperature and room power consumption at ***t+1.*** Then, it is intuitive clear that at time ***t+1*** it is better to start the predictions from the measured all around the examined room temperatures and room power consumption, taking into consideration the measured indoor temperature, rather than from the indoor temperature and room power consumption predicted at the previous sample. The predicted indoor temperature and room power consumption are now corrected for disturbances and modeling errors. A feedback mechanism is activated.

As a result of this approach, the prediction horizon over which the indoor temperature and room power consumption are predicted shifts one sample into the future at every sample instant. However, during the Pre-cooling period or DSM phase the prediction horizon is reduced at any sample by one sample, because after the pre-cooling period the controller changes to DSM phase terminating its operation at the end of the DSM phase.

The implementation of the above-mentioned DSM Cooling Strategy must be acceptable by the users. The dialogue-able energy management system, which is reported in [2], can be adapted in order to inform the users for the cost of energy consumption during the peak demand and the economic benefits using the TMPC-DSM controller.

4 Thermal Model based on Finite Difference Calculation

Analytical solutions to transient problems are restricted to simple geometries and boundary conditions. However, in many cases the geometry and/or boundary conditions preclude the use of analytical techniques, and recourse must be made to finite-difference methods. The bookshop has been chosen as a practical system to experiment with because of the owner's special interest to save energy in this part of the building. This chapter aims to derive a thermal model based on Finite Difference Calculation Method in explicit form, [38], [39] and [40].

4.1 Discretization of the Heat Equation: The Explicit Method

The heat diffusion equation is given by:

$$\frac{\partial}{\partial x}\left(\lambda\frac{\partial T}{\partial x}\right)+\frac{\partial}{\partial y}\left(\lambda\frac{\partial T}{\partial y}\right)+\frac{\partial}{\partial z}\left(\lambda\frac{\partial T}{\partial z}\right)+\dot{q}=\rho c_p\frac{\partial T}{\partial t} \tag{4.1}$$

where: λ : thermal conductivity
∂ : spatial derivative
T : temperature distribution
ρ : density
c_p : specific heat
x, y, z : Cartesian coordinates
t : time
$\dot{q}$: Rate of energy generation per unit volume

If the thermal conductivity is a constant, the heat equation is

$$\frac{\partial^2 T}{\partial x^2}+\frac{\partial^2 T}{\partial y^2}+\frac{\partial^2 T}{\partial z^2}+\frac{\dot{q}}{\lambda}=\frac{1}{a}\frac{\partial T}{\partial t} \tag{4.2}$$

where: $a=\lambda/\rho c_p$: thermal diffusivity

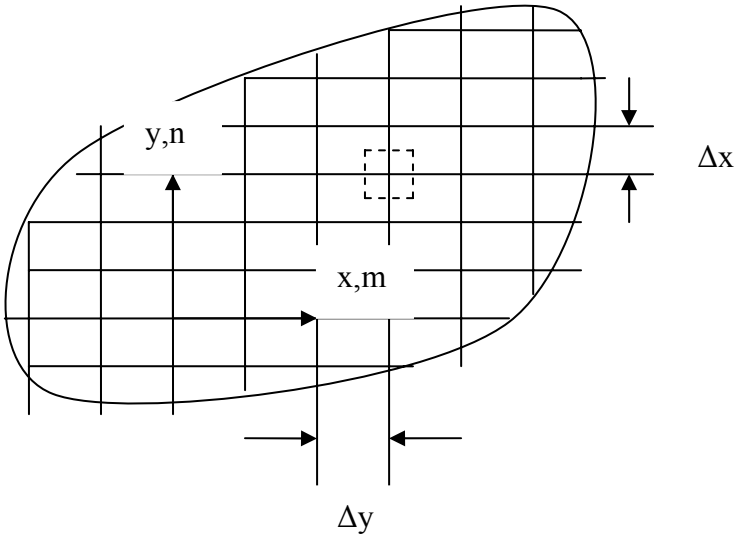

Figure 4.1: Two dimensional conduction.

Consider the two-dimensional system of Figure 4.1. Under transient conditions with constant properties and no internal generation, the appropriate form of the heat equation, Equation (4.2), is

$$\frac{1}{a}\frac{\partial T}{\partial t} = \frac{\partial^2 T}{\partial x^2} + \frac{\partial^2 T}{\partial y^2} \tag{4.3}$$

To obtain the finite-difference form of this equation, we may use the *central-difference* approximations to the spatial derivatives, described by the following Equations (4.7) and (4.8) which are derived through the temperature gradients, Equation (4.4):

$$\left.\frac{\partial^2 T}{\partial x^2}\right|_{m,n} \approx \frac{\partial T/\partial x\big|_{m+1/2,n} - \partial T/\partial x\big|_{m-1/2,n}}{\Delta x} \tag{4.4}$$

The temperature gradients may in turn be expressed as a function of the nodal temperatures. That is,

$$\left.\frac{\partial T}{\partial x}\right|_{m+1/2,n} \approx \frac{T_{m+1,n} - T_{m,n}}{\Delta x} \tag{4.5}$$

$$\left.\frac{\partial T}{\partial x}\right|_{m-1/2,n} \approx \frac{T_{m,n} - T_{m-1,n}}{\Delta x} \tag{4.6}$$

Substituting Equations (4.5) and (4.6) into (4.4), we obtain

$$\left.\frac{\partial^2 T}{\partial x^2}\right|_{m,n} \approx \frac{T_{m+1,n} + T_{m-1,n} - 2T_{m,n}}{(\Delta x)^2} \tag{4.7}$$

Proceeding in a similar fashion, it is readily shown that

$$\left.\frac{\partial^2 T}{\partial y^2}\right|_{m,n} \approx \frac{\partial T/\partial y|_{m,n+1/2} - \partial T/\partial y|_{m,n-1/2}}{\Delta y}$$
$$\approx \frac{T_{m,n+1} - T_{m,n-1} - 2T_{m,n}}{(\Delta y)^2} \tag{4.8}$$

The *m* and *n* subscripts may be used to designate the *x* and *y* locations of *discrete nodal points.* However, in addition to being discretized in space, the problem must be discretized in time. The integer *p* is introduced for this purpose, where

$$t = p\Delta t \tag{4.9}$$

and the finite-difference approximation to the time derivative in Equation (4.3) is expressed as

$$\left.\frac{\partial T}{\partial t}\right|_{m,n} \approx \frac{T_{m,n}^{p+1} - T_{m,n}^{p}}{\Delta t} \tag{4.10}$$

The superscript *p* is used to denote the time dependence of *T*, and the time derivative is expressed in terms of the difference in temperatures associated with the *new (p+1)* and *previous (p)* times. Hence calculations must be performed at successive times separated by the interval *Δt*, and just as a finite-difference solution restricts temperature determination to discrete points in space, it also restricts it to discrete points in time.

If Equation (4.10) is substituted into Equation (4.3), the nature of the finite-difference solution will depend on the specific time at which temperatures are evaluated in the finite-difference approximations to the spatial derivatives. In the *explicit method* of solution, these temperatures are evaluated at the *previous (p)* time. Hence Equation (4.10) is considered to be a *forward-difference* approximation to the time derivative. Evaluating terms on the right-hand side of Equations (4.7) and (4.8) at *p* and substituting into Equation (4.3), the explicit form of the finite-difference equation for the interior node *m, n* is

$$\frac{1}{a}\frac{T_{m,n}^{p+1} - T_{m,n}^{p}}{\Delta t} = \frac{T_{m+1,n}^{p} + T_{m-1,n}^{p} - 2T_{m,n}^{p}}{(\Delta x)^2} + \frac{T_{m,n+1}^{p} + T_{m,n-1}^{p} - 2T_{m,n}^{p}}{(\Delta y)^2} \tag{4.11}$$

Solving for the nodal temperature at the new *(p+1)* time and assuming that $\Delta x = \Delta y$, it follows that

$$T_{m,n}^{p+1} = Fo\left(T_{m+1,n}^{p} + T_{m-1,n}^{p} + T_{m,n+1}^{p} + T_{m,n-1}^{p}\right) + (1 - 4Fo)T_{m,n}^{p} \tag{4.12}$$

where Fo is a finite-difference form of the Fourier number

$$\mathrm{Fo} = \frac{a\Delta t}{(\Delta x)^2} \tag{4.13}$$

If the system is one-dimensional in x, the explicit form of the finite-difference equation for an interior node *m* reduces to

$$T_m^{p+1} = \mathrm{Fo}\left(T_{m+1}^p + T_{m-1}^p\right) + (1 - 2\mathrm{Fo})T_m^p \tag{4.14}$$

Equations (4.12) and (4.14) are *explicit* because *unknown* nodal temperatures for the new time are determined exclusively by *known* nodal temperatures at the previous time. Hence calculation of the unknown temperatures is straightforward. Since the temperature of each interior node is known at $t = 0$ $(p = 0)$ from prescribed initial conditions, the calculations begin at $t = \Delta t$ $(p = 1)$, where Equation (4.12) or (4.14) is applied to each interior node to determine its temperature. With temperatures known for $t = \Delta t$, the appropriate finite-difference equation is then applied at each node to determine its temperature at $t = 2\,\Delta t$ $(p = 2)$. In this way, the transient temperature distribution is obtained by *marching out in time*, using intervals of Δt.

The accuracy of the finite-difference solution may be improved by decreasing the values of Δx and Δt. Of course, the number of interior nodal points that must be considered increases with decreasing Δx, and the number of time intervals required to carry the solution to a prescribed final time increases with decreasing Δt. Hence the computation time increases with decreasing Δx and Δt. The choice of Δx is typically based on a compromise between accuracy and computational requirements. Once this selection has been made, however, the value of Δt may not be chosen independently. It is, instead, determined by *stability* requirements.

An undesirable feature of the explicit method is that it is not unconditionally *stable*. In a transient problem, the solution for the nodal temperatures should continuously approach final (steady-state) values with increasing time. However, with the explicit method, this solution may be characterized by numerically induced oscillations, which are physically impossible. The oscillations may become *unstable*, causing the solution to diverge from the actual steady-state conditions. To prevent such erroneous results, the prescribed value of Δt must be maintained below a certain limit, which depends on Δx and other parameters of the system. This dependence is termed a *stability criterion,* which may be obtained mathematically or demonstrated from a thermodynamic argument. For the temperature distributions of the walls of the bookshop in this thesis, *the criterion is determined by requiring that the coefficient associated with the node of interest at the previous time is greater than or equal to zero.* In general, this is done by collecting all terms involving $T_{m,n}^p$ to obtain the form of the coefficient. This result is then used to obtain a limiting relation involving *Fo*, from which the maximum allowable value of Δt may be determined. Therefore, with Equation (4.14) already expressed in the desired form, it follows that the stability criterion for a one-dimensional interior node is $(1 - 2Fo) \geq 0$, or

$$\mathrm{Fo} \leq \frac{1}{2} \tag{4.15}$$

For prescribed values of Δx and a, these criteria may be used to determine upper limits to the value of Δ*t*.

Equations (4.12) and (4.14) may also be derived by applying the energy balance method to a control volume about the interior node. Accounting for changes in thermal energy storage, a general form of the energy balance equation may be expressed as

$$\dot{E}_{in} + \dot{E}_g - \dot{E}_{out} = \dot{E}_{st} \tag{4.16}$$

where $\dot{E}_{in}$ is the rate at which thermal and mechanical energy enters a control volume

$\dot{E}_g$ is the rate at which thermal energy is generated within the control volume

$\dot{E}_{out}$ is the rate at which thermal and mechanical energy leaves the control volume

$\dot{E}_{st}$ is the rate of increase of energy stored within the control volume.

In the interest of adopting a consistent methodology, it is assumed that all heat flow is *into* the node. Therefore, Equation (4.16) is expressed as

$$\dot{E}_{in} + \dot{E}_g = \dot{E}_{st} \tag{4.17}$$

4.2 FDC Bookshop Thermal Model

The following Figure 4.2 depicts the layout of the bookshop. Obviously, there are 5 different wall parts concerning the materials which consist of:

- Plaster-Brick-Expanded Polystyrene-Brick-Plaster (Green - Yellow Wall)
- Plaster-Expanded Polystyrene-Concrete-Plaster (Red Rectangular & Yellow line Wall)
- Plaster-Brick-Plaster (Red lines – Internal Wall)
- Plaster-Brick-Plaster (Green lines – External Wall)
- Plaster-Concrete-Plaster (Red Rectangular - Internal Wall)

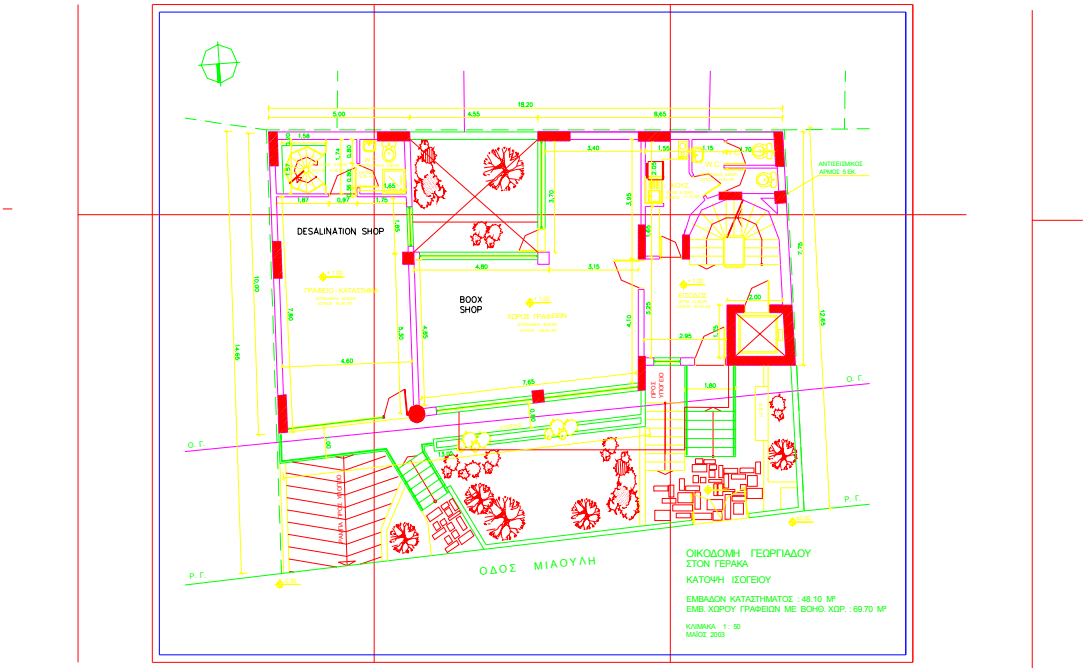

Figure 4.2: Layout of the Bookshop.

In general, each wall part consisting of any materials can be represented by the following Figure 4.3. The explicit form of the finite-difference equation for any interior node of the same material is given by Equation (4.14).

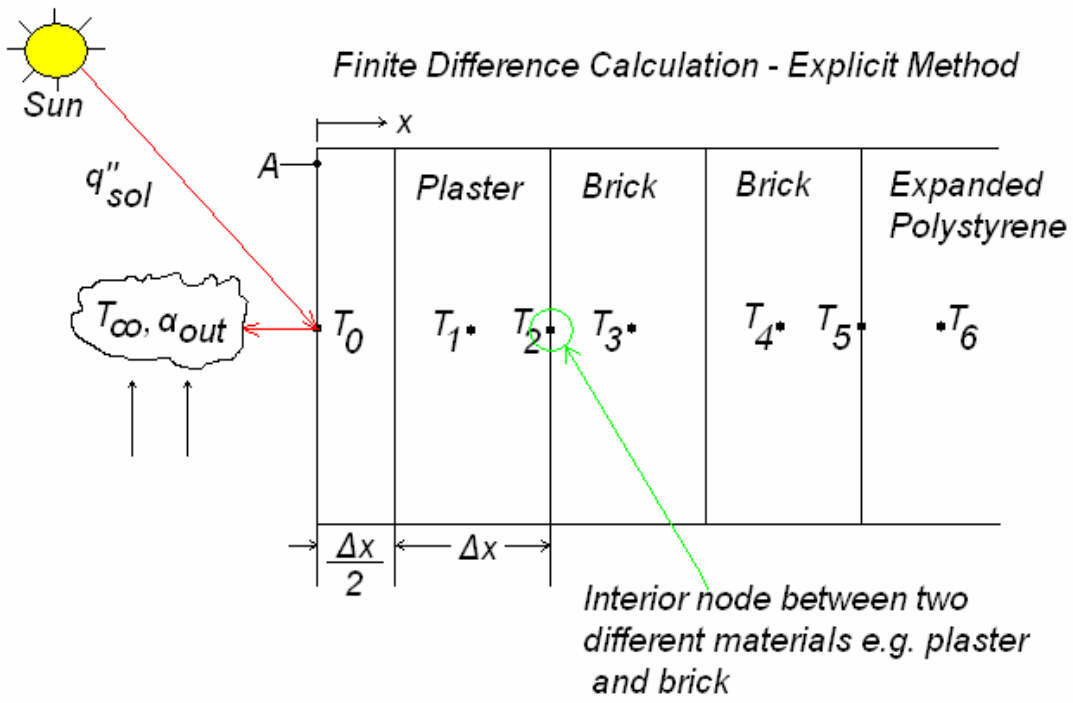

Figure 4.3: Surface node with convection, radiation and one-dimensional transient conduction.

Considering the surface node of the one-dimensional system shown in the above Figure 4.3 and more accurately we determine thermal conditions near the surface, this node has been assigned a thickness that is one-half that of the interior nodes. Assuming that the surface is exposed to radiation, convection transfer from an adjoining fluid (outdoor or indoor air) and no generation, it follows from Equation (4.17) that

$$q''A + \alpha A\left(T_\infty - T_0^p\right) + \frac{\lambda A}{\Delta x}\left(T_1^p - T_0^p\right) = \rho c A \frac{\Delta x}{2}\frac{T_0^{p+1} - T_0^p}{\Delta t} \tag{4.18}$$

where α : Heat transfer coefficient including convection and radiation

or, solving for the surface temperature at $t+\Delta t$

$$T_0^{p+1} = \frac{2a\Delta t}{\Delta x^2}\frac{q''\Delta x}{\lambda} + \frac{2\alpha\Delta t}{\rho c\Delta x}\left(T_\infty - T_0^p\right) + \frac{2a\Delta t}{\Delta x^2}\left(T_1^p - T_0^p\right) + T_0^p \tag{4.19}$$

Recognizing that $(2\alpha\,\Delta t/\rho c\,\Delta x) = 2(\alpha\Delta x/\lambda)(a\,\Delta t/\Delta x^2) = 2$ Bi Fo and grouping terms involving T_0^p, it follows that

$$T_0^{p+1} = 2Fo\left(T_1^p + BiT_\infty + \frac{q''\Delta x}{\lambda}\right) + \left(1 - 2Fo - 2BiFo\right)T_0^p \tag{4.20}$$

The finite-difference form of the Biot number is

$$Bi = \frac{\alpha\Delta x}{\lambda} \tag{4.21}$$

Recalling the procedure for determining the stability criterion, we require that the coefficient for T_0^p be greater than or equal to zero. Hence

$$1 - 2Fo - 2BiFo \geq 0 \tag{4.22}$$

or

$$Fo\left(1 + Bi\right) \leq \frac{1}{2} \tag{4.23}$$

Since the complete finite-difference solution requires the use of Equation (4.14) for the interior nodes, as well as Equation (4.20) for the surface node. Equation (4.23) must be contrasted with Equation (4.15) to determine which requirement is more stringent. Since $Bi \geq 0$, it is apparent that the limiting value of *Fo* for Equation (4.23) is less than that for Equation (4.15).

In the case where an interior node is between 2 different materials e.g. plaster and brick, Equation (4.17) becomes

$$\lambda_{pl}A\frac{\left(T_1^p-T_2^p\right)}{\Delta x}+\lambda_{br}A\frac{\left(T_3^p-T_2^p\right)}{\Delta x}=\rho_{pl}c_{pl}A\frac{\Delta x}{2}\frac{\left(T_2^{p+1}-T_2^p\right)}{\Delta t}+\rho_{br}c_{br}A\frac{\Delta x}{2}\frac{\left(T_2^{p+1}-T_2^p\right)}{\Delta t} \quad (4.24)$$

or

$$\lambda_{pl}A\frac{\left(T_1^p-T_2^p\right)}{\Delta x}+\lambda_{br}A\frac{\left(T_3^p-T_2^p\right)}{\Delta x}=\left(\rho_{pl}c_{pl}+\rho_{br}c_{br}\right)A\frac{\Delta x}{2}\frac{\left(T_2^{p+1}-T_2^p\right)}{\Delta t} \quad (4.25)$$

or

$$2\frac{\lambda_{pl}}{\rho_{pl}c_{pl}+\rho_{br}c_{br}}\frac{\Delta t}{\Delta x^2}\left(T_1^p-T_2^p\right)+2\frac{\lambda_{br}}{\rho_{pl}c_{pl}+\rho_{br}c_{br}}\frac{\Delta t}{\Delta x^2}\left(T_3^p-T_2^p\right)=T_2^{p+1}-T_2^p \quad (4.26)$$

or

$$2F_{pl}\left(T_1^p-T_2^p\right)+2F_{br}\left(T_3^p-T_2^p\right)=T_2^{p+1}-T_2^p \quad (4.27)$$

where

$$F_{pl}=\frac{\lambda_{pl}}{\rho_{pl}c_{pl}+\rho_{br}c_{br}} \quad \text{and} \quad F_{br}=\frac{\lambda_{br}}{\rho_{pl}c_{pl}+\rho_{br}c_{br}} \quad (4.27a)$$

and finally

$$T_2^{p+1}=2F_{pl}T_1^p+2F_{br}T_3^p+\left[1-2F_{pl}-2F_{br}\right]T_2^p \quad (4.28)$$

4.2.1 FDC Bookshop Thermal Model Assumptions

An on-line thermal model of the bookshop has been developed based on LabVIEW Software. The finite difference calculation in one-dimensional conduction has been applied for each different part of the walls. Equations (4.14), (4.20) and (4.28) are solved at each iteration, with the following assumptions to be hold:

- **One dimensional conduction in x.**
- **The indoor and outdoor temperatures are uniform at any time t.**
- **Constant properties (λ, ρ, c, *a*…).**
- **The heat exchange between the plaster of the surface of the outer wall and the surroundings is between a small surface and a much larger enclosure. The radiation is estimated by using the following heat transfer coefficients α_{out} and α_{in}.**
- **The ambient convection and radiation heat transfer coefficient is constant to $\alpha_{out} = 25\ W/m^2K$ [DIN 4701-1].**
- **The indoor convection and radiation heat transfer coefficient is constant to $\alpha_{in} = 8\ W/m^2K$ [DIN 4701-1].**
- **Radiation is developed due to the different temperatures of the surfaces of the opposite inner walls and is given by $5W/m^2K\left(T_{w1}^p-T_{w2}^p\right)$.**

- **The initial conditions for the temperature distributions in the walls are given by equations of the one-dimensional, steady-state conduction.**
- **All internal resistances are neglected.**
- **Heat flows through the floor and the roof are calculated by equations of the one-dimensional, steady-state conduction.**
- **It should be mentioned that because of the fact that we cannot be aware of the temperature conditions of the building which is adjacent to the one we examine, we assume that its outer south wall is an adiabatic surface.**
- **Ventilation and Infiltration effects are neglected.**

Obviously the thermal model is simplified by the use of these assumptions making its application economically attractive. However, a model mismatch is expected.

4.2.2 FDC Equations of the main part of the North Wall

The orientation of the building is in the northern side. The main part of the north wall consists of Plaster (2cm), Brick (9cm), Expanded Polystyrene (5cm), Brick (9cm) and Plaster (2cm). Taking into account Equations (4.14), (4.20) and (4.28) and the above-mentioned assumptions the following equations describe the finite-difference calculation of this wall part. The stability criterion is satisfied by using Δx = 1 cm and Δt = 47 sec.

The surface node of the outer wall follows from Equation (4.20) where

$$T_0^{p+1} = 0{,}4332\left[T_1^p + 0{,}3472T_{out} + 0{,}0139q''_{sol}\right] + 0{,}4164T_0^p \tag{4.29a}$$

The finite-difference solutions to the interior nodes are obtained by using Equations (4.14) and (4.28). Note that the nodes 1 to 27 are the nodes from surfaces of the outer to the inner wall.

$$T_1^{p+1} = 0{,}2166[T_0^p + T_2^p] + 0{,}5668T_1^p \tag{4.29b}$$

$$T_2^{p+1} = 0{,}2138[T_1^p + T_3^p] + 0{,}5724T_2^p \tag{4.29c}$$

$$T_3^{p+1} = 0{,}2111[T_2^p + T_4^p] + 0{,}5778T_3^p \tag{4.29d}$$

T_4^{p+1} up to T_{10}^{p+1} are of the same function as the T_3^{p+1}

$$T_{11}^{p+1} = 0{,}4107T_{10}^p + 0{,}0188T_{12}^p + 0{,}5705T_{11}^p \tag{4.29e}$$

$$T_{12}^{p+1} = 0{,}3462[T_{11}^p + T_{13}^p] + 0{,}3076T_{12}^p \tag{4.29f}$$

T_{13}^{p+1} up to T_{15}^{p+1} are of the same function as the T_{12}^{p+1}

$$T_{16}^{p+1} = 0{,}0188T_{15}^p + 0{,}4107T_{17}^p + 0{,}5705T_{16}^p \tag{4.29g}$$

$$T_{17}^{p+1} = 0.2111[T_{16}^{p} + T_{18}^{p}] + 0.5778T_{17}^{p} \quad (4.29h)$$

T_{18}^{p+1} up to T_{24}^{p+1} are of the same function as the T_{17}^{p+1}

$$T_{25}^{p+1} = 0{,}2138[T_{24}^{p} + T_{26}^{p}] + 0{,}5724T_{25}^{p} \quad (4.29i)$$

$$T_{26}^{p+1} = 0{,}2166[T_{25}^{p} + T_{27}^{p}] + 0{,}5668T_{26}^{p} \quad (4.29j)$$

$$T_{27}^{p+1} = 0{,}4332\left[T_{26}^{p} + 0{,}1111T_{in}^{p} \pm 0{,}0139q''_{aux}\right] + 0{,}5187T_{27}^{p} \quad (4.29k)$$

In Appendix A the thermophysical properties of the materials used in the bookshop are presented, while in Appendix B the finite-difference solutions for every wall part of the bookshop are described in details.

4.2.3 Verification of FDC of the North Wall

The on-line Thermal Model, based on the FDC method, measures the indoor and ambient temperatures with a sampling rate of Δt = 47 sec. The LabVIEW software saves the measurements and the simulation results in daily Excel Files. These files serve to the verification of the Model as well as for a further analysis of the data. Figure 4.4 depicts the ambient, surface node of the outer wall T_0^p, surface node of the inner wall T_{27}^p and indoor temperatures from 17/4/2005 until 16/5/2005.

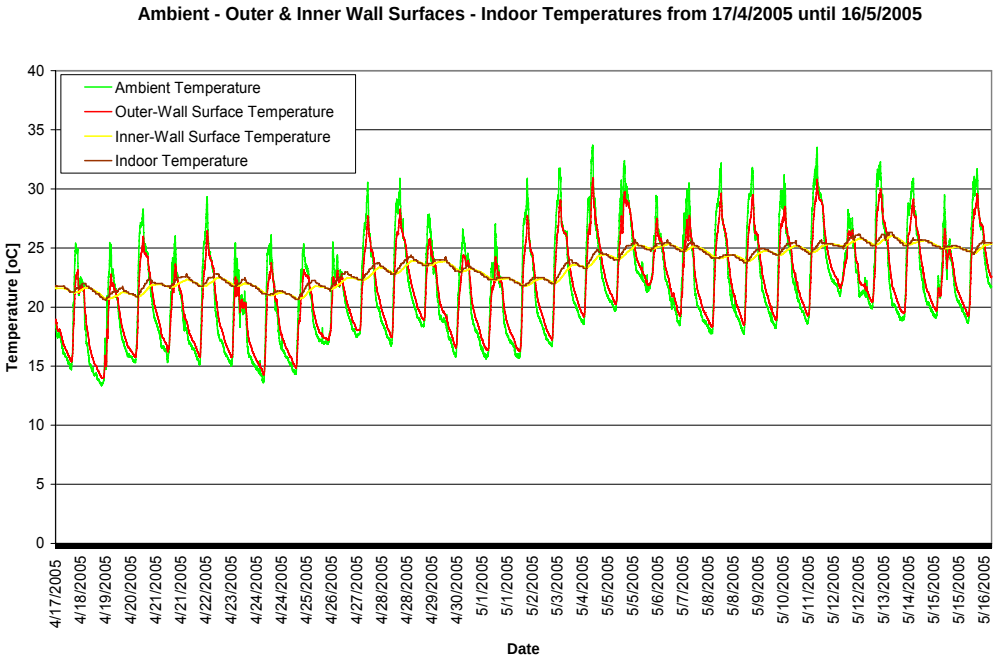

Figure 4.4: Ambient, surface node of the outer wall T_0^p, surface node of the inner wall T_{27}^p and indoor temperatures from 17/4/2005 until 16/5/2005.

The Inflow Heat Flux is proportional to the convection and radiation heat transfer coefficient α_{in} = 8 W/m^{2}K and to the difference between the indoor temperature and

the surface node temperature of the inner wall (*Newton's law of cooling*). Respectively, the Outflow Heat Flux is proportional to the convection and radiation heat transfer coefficient α_{out} = 25 W/m^{2}K and to the difference between the surface node temperature of the outer wall and the ambient (T_∞ or T_{out}^p) temperature. The Inflow and Outflow Heat Fluxes are expressed by Equations (4.30) and (4.31).

$$q''_{in} = \alpha_{in}\left(T_{in}^p - T_{27}^p\right) \tag{4.30}$$

$$q''_{out} = \alpha_{out}\left(T_0^p - T_\infty\right) \tag{4.31}$$

The following Figure 4.5 depicts the inflow and outflow heat fluxes based on Equations (4.30) and (4.31) from 17/4/2005 until 16/5/2005.

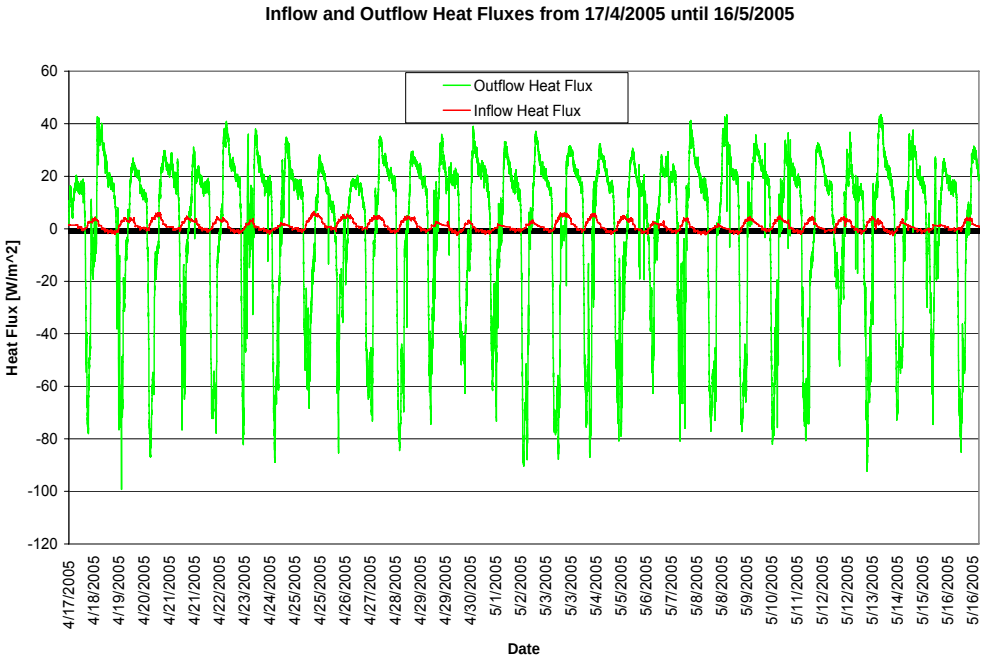

Figure 4.5: Inflow and Outflow Heat Fluxes from 17/4/2005 until 16/5/2005.

Recalling the energy balance Equation (4.16) or (4.17), the thermal model is verified if the energy storage reaches to zero (E_{st} = 0) after 1 month experimental results. For this reason the averages of the simulated Inflow and Outflow Heat Fluxes are calculated at every sample and are shown in Figure 4.6a. Furthermore, the difference between the average of the Inflow Heat Flux and the average of the Outflow Heat Flux is calculated and shown at every sample in the following Figure 4.6b.

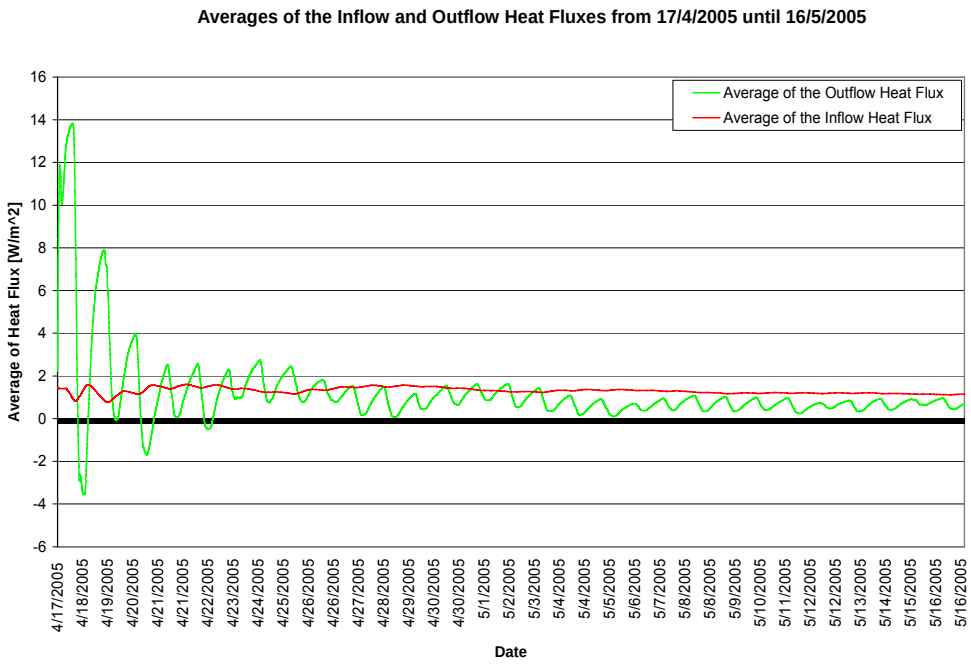

Figure 4.6a: Averages of the Inflow and Outflow Heat Fluxes from 17/4/2005 until 16/5/2005.

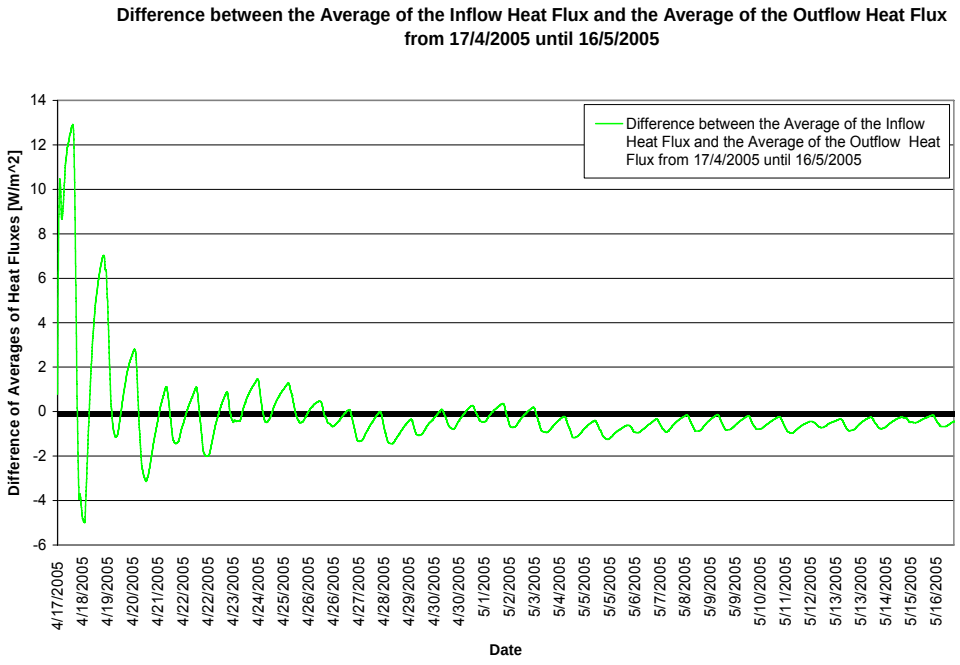

Figure 4.6b: Difference between the Average of the Inflow Heat Flux and the Average of the Outflow Heat Flux from 17/4/2005 until 16/5/2005.

Obviously, the convergence of the Inflow and Outflow Heat Fluxes is achieved very fast, in one day approximately, proving that the choice of $\Delta t = 47$ sec and $\Delta x = 1$ cm is correct. Keeping $\Delta x = 1$ cm for this northern wall part, simulations with different Δt show also this convergence but not so fast. Especially, when Δt increases the convergence deteriorates. This verification process is realized at all different wall parts, where $\Delta x = 1$ cm has been kept in each case. Taking into consideration the

fastest convergences of the fluxes, the respective equations for finite-difference calculation are derived (Appendix B). The on-line Thermal Model of the bookshop is based on these equations.

4.2.4 Heat Fluxes and Energies of the North Wall

After thermal model verification, the Thermal Model Predictive Controller is setup to operate for one week. The KNX/EIB installation was completed in September 2005. Therefore, the Thermal Model Predictive Controller started its operation on 19th September 2005. The following Figure 4.7 presents the outdoor, surface node of the outer wall T_0^p, surface node of the inner wall T_{27}^p and indoor temperatures from 18/9/2005 until 25/9/2005.

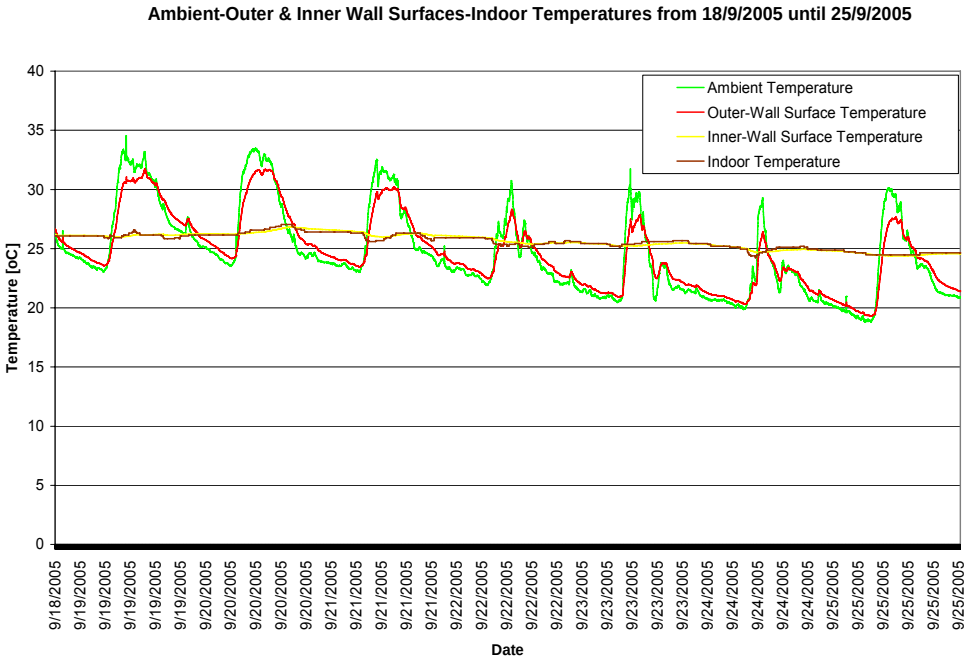

Figure 4.7: Ambient, surface node of the outer wall T_0^p, surface node of the inner wall T_{27}^p and indoor temperatures from 18/9/2005 until 25/9/2005.

The chosen period of September is a typical summer period in Greece as it is depicted in Figure 4.7. The following Figure 4.8 depicts the inflow and outflow heat fluxes based on Equations (4.30) and (4.31) from 18/9/2005 until 25/9/2005.

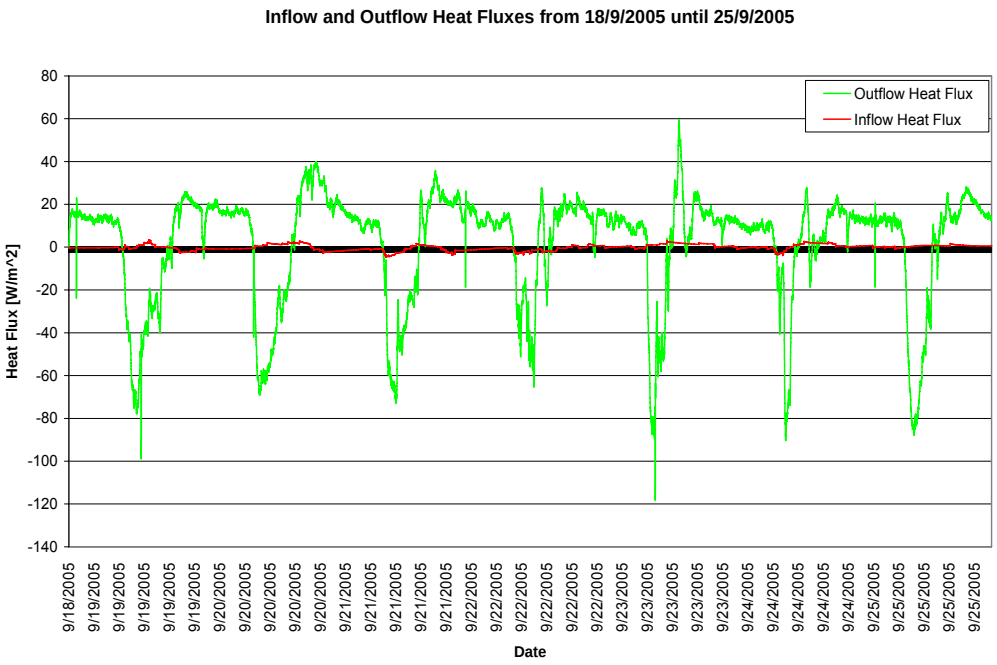

Figure 4.8: Inflow and Outflow Heat Fluxes from 18/9/2005 until 25/9/2005.

The verification process proves that the thermal model is correct as it is shown in the following Figure 4.9. In this figure the Stored Energy converges to zero and the model is verified.

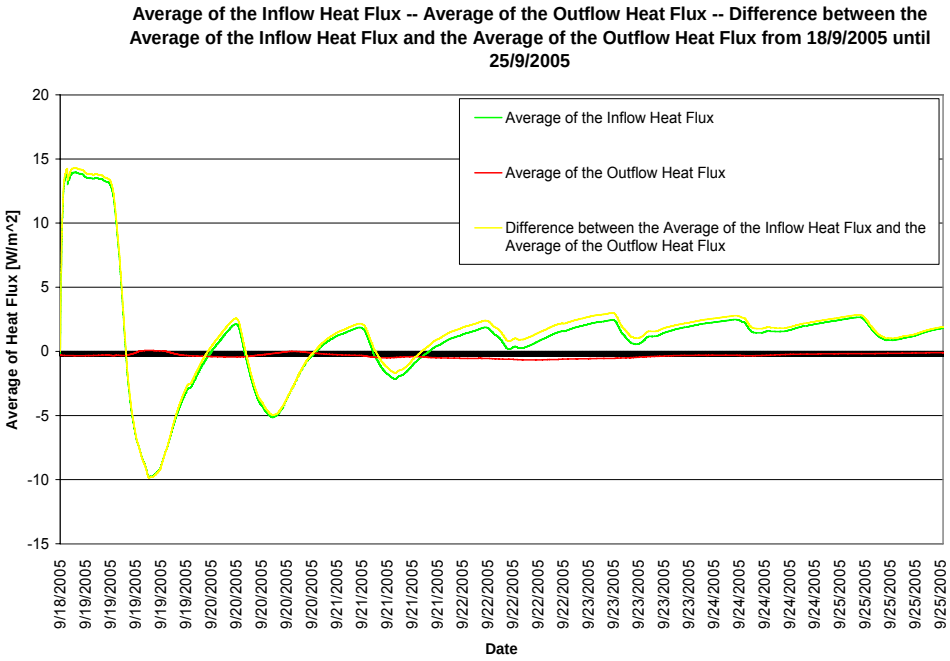

Figure 4.9: Averages of the Inflow and Outflow Heat Fluxes as well as their difference from 18/9/2005 until 25/9/2005.

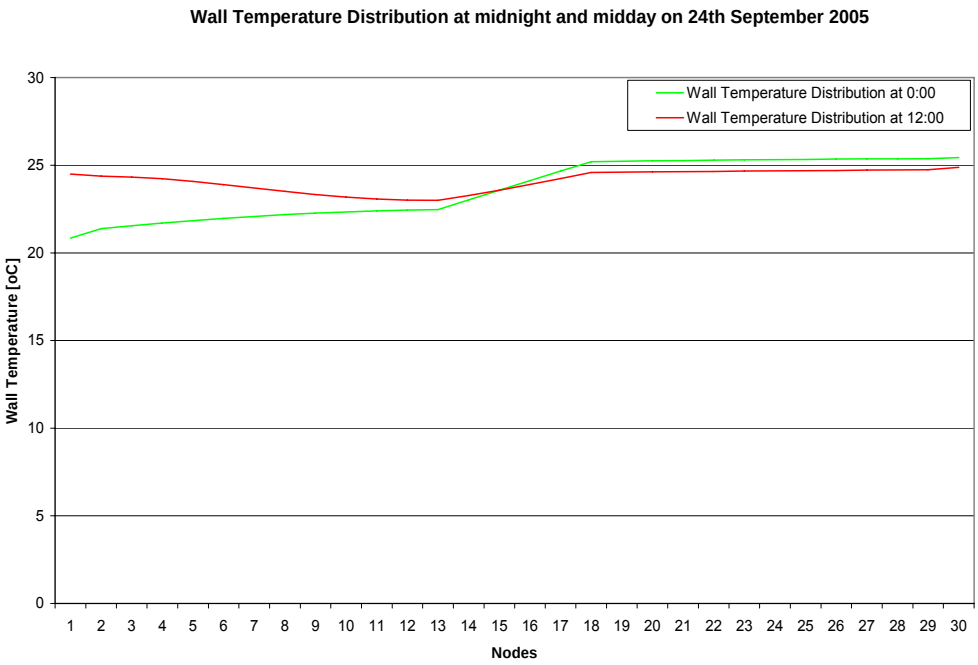

Figure 4.10: Wall Temperature Distribution at midnight and midday on 24th September 2005.

The above Figure 4.10 depicts the temperature distribution of the northern wall part at midday, 12:00, where Stored Energy occurs and at midnight, 0:00, (steady-state). The area of the examined wall is A_w = 9,8635 m^2. Multiplying the heat fluxes of Figure 4.8 with the area A_w by using Equations (4.30) and (4.31), the Inflow and Outflow Energies are derived by their integration and depicted in Figure 4.11.

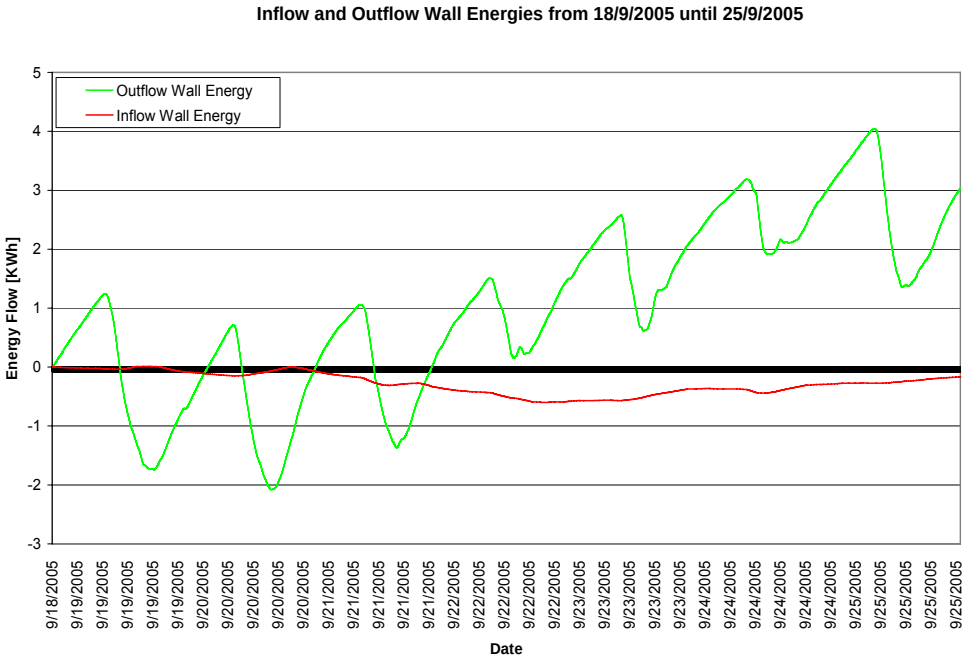

Figure 4.11: Inflow and Outflow Wall Energies from 18/9/2005 until 25/9/2005.

5 Absorbed Solar Radiation

An Anisotropic Solar Radiation diffuse model based on the Hay-Davies-Klucher-Riendl (HDKR) model is presented in this chapter. The HDKR model estimates the absorbed beam, diffuse and ground reflected solar radiation by the surface of the outer wall, the windows and a part of the roof of the bookshop. The orientation of the building is in the north. The latitude of the building is $\phi = 38^o$ and the longitude is $L_{loc} = -23°51'$.

5.1 HDKR Solar Radiation Model

Calculation of the solar radiation onto the surface of the wall is achieved by measuring the total radiation on a horizontal surface with the ISET-Sensor–monocrystalline pyranometer (Figure 2.12), [41]. The directions, from which beam and diffuse components reach onto the surface of the outer wall, are calculated according to the procedure reported in [42].

5.1.a Beam Radiation onto the surface of the outer wall

For the direction of beam radiation, calculation of the sun position is realised. At first, the solar time is calculated. It is relative to the sun and at 12:00 solar time, the sun is located in the meridian of the spectator:

$$Solar\ time - Standard\ time = 4 \cdot (L_{st} - L_{loc}) + E \tag{5.1}$$

where L_{st} is the standard meridian for the local time zone in which the building is located. L_{loc} is the longitude of the building location, and longitudes are in degrees west. For the building in Athens L_{loc} = -23,8497^o. The equation of time E (in minutes) is determined from Equation (5.2):

$$\begin{aligned} E = 229{,}2 \cdot (&0{,}000075 + 0{,}001868 \cdot \cos B - 0{,}032077 \cdot \sin B - \\ &- 0{,}014615 \cdot \cos 2B - 0{,}04089 \cdot \sin 2B \end{aligned} \tag{5.2}$$

where

$$B = (n-1) \cdot \frac{360}{365} \tag{5.3}$$

with n equal to the day of the year. The surface of the outer wall is vertical. In this case the **angle of incidence** θ, which is the angle between the beam radiation on a surface and the normal to that surface, is given by:

$$\cos\theta = -\sin\delta\cos\phi\cos\gamma + \cos\delta\sin\phi\cos\gamma\cos\omega + \cos\delta\sin\gamma\sin\omega \tag{5.4}$$

where:

The **Declination δ** is defined as the angular position of the sun at solar noon with respect to the plane of the equator, north positive and is given by Equation (5.5):

$$\delta = 23{,}45\sin\left(360\frac{284+n}{365}\right) \qquad -23{,}45^{o} \le \delta \le 23{,}45^{o} \tag{5.5}$$

The **Latitude** ϕ is defined as the angular location north or south of the equator, north positive: $-90^{o} \le \phi \le 90^{o}$. For the building in Athens $\phi = 38{,}01210^{o}$.

The **Surface azimuth angle** γ is the deviation of the projection on a horizontal plane of the normal to the surface from the local meridian, with zero due south, east negative and west positive: $-180^{o} \le \gamma \le 180^{o}$.

The **Hour angle** ω is the angular displacement of the sun east or west of the local meridian due to rotation of the earth on its axis at 15^{o} per hour, morning negative, afternoon positive. For this $\omega = 15° \cdot \Delta T$ with ΔT the time to/from midday in hours.

For a horizontal surface θ_z **is the Zenith angle,** the angle between the vertical and the line to the sun, i.e. the angle of incidence of beam radiation on a horizontal surface, and is calculated by the following Equation (5.6):

$$\cos\theta_z = \cos\phi\cos\delta\cos\omega + \sin\phi\sin\delta \tag{5.6}$$

For the azimuth of the sun the following is the case:

$$\gamma_s = C_1 \cdot C_2 \sin^{-1}\left(\frac{\sin\omega\cos\delta}{\sin\theta_z}\right) + C_3 \cdot \left(\frac{1 - C_1 \cdot C_2}{2}\right) \cdot 180 \tag{5.7}$$

with

$$C_1 = \begin{cases} 1 \;\; if \;\; |\omega| < \omega_{ew} \\ -1 \;\; if \;\; |\omega| \ge \omega_{ew} \end{cases} \tag{5.8}$$

$$C_2 = \begin{cases} 1 \;\; if \;\; \phi(\phi - \delta) \ge 0 \\ -1 \quad \text{otherwise} \end{cases} \tag{5.9}$$

$$C_3 = \begin{cases} 1 \;\; if \quad \omega \geq 0 \\ -1 \quad \text{otherwise} \end{cases} \tag{5.10}$$

where

$$\omega_{ew} = \cos^{-1}\left(\frac{\tan\delta}{\tan\phi}\right) \tag{5.11}$$

The geometric factor R_b is the ratio of beam radiation on the surface of the outer wall (vertical) to that on a horizontal surface at any time. It is calculated by the following Equation (5.12):

$$R_b = \frac{G_{b,T}}{G_b} = \frac{G_{b,n}\cos\theta}{G_{b,n}\cos\theta_z} = \frac{\cos\theta}{\cos\theta_z} \tag{5.12}$$

The number of daylight hours N is given by

$$N = \frac{2}{15}\cos^{-1}\left(-\tan\phi\tan\delta\right) \tag{5.13}$$

5.1.b Diffuse Radiation on the surface of the outer wall

The direction from which diffuse radiation is received, i.e., its distribution over the sky dome, is a function of conditions of cloudiness and atmospheric clarity, which are highly variable. Clear day data have led to a description of the diffuse radiation as being composed of three parts. The first is an **isotropic** part, received uniformly from all of the sky dome. The second is **circumsolar diffuse**, resulting from forward scattering of solar radiation and concentrated in the part of the sky around the sun. The third, referred to as **horizon brightening**, is concentrated near the horizon, and is most pronounced in clear skies.

The angular distribution of diffuse is to some degree a function of the reflectance ρ_g (the albedo) of the ground. A high reflectance (such as that of fresh snow, with ρ_g approximately 0,7) results in reflection of solar radiation back to the sky, which in turn may be scattered to account for horizon brightening.

When beam and reflected radiation are added, they provide the means of calculating radiation on a tilted surface from measurements on the horizontal. The incident solar radiation is the sum of a set of radiation streams including beam radiation, the three components of diffuse radiation from the sky, and radiation reflected from the various surfaces “seen” by the surface of the outer wall. The total incident radiation onto the surface of the outer wall can be written as

$$I_T = I_{T,b} + I_{T,d,iso} + I_{T,d,cs} + I_{T,d,hz} + I_{T,refl} \tag{5.14}$$

where the subscripts *iso, cs, hz* and *refl* refer to the isotropic, circumsolar, horizon and reflected radiation streams.

For a surface of the outer wall of area A_w, the total incident radiation can be expressed in terms of the beam and diffuse radiation on the horizontal surface and the total radiation on the surfaces that reflect to the surface of the outer wall. The terms in Equation (5.14) become

$$A_w I_T = I_b R_b A_w + I_{d,iso} A_s F_{s-w} + I_{d,cs} R_b A_w + I_{d,hz} A_{hz} F_{hz-w} + \sum_i I_i \rho_i A_i F_{i-w} \qquad (5.15)$$

The first term is the beam contribution. The second is the isotropic diffuse term which includes the product of sky area A_s (an undefined area) and the radiation view factor from the sky to the surface of the outer wall $F_{s\text{-}w}$. The third is the circumsolar diffuse, which is treated as coming from the same direction as the beam. The fourth term is the contribution of the diffuse from the horizon from a band with another undefined area A_{hz}. The fifth term is the set of reflected radiation streams from the other buildings, fields, etc., to which the surface of the outer wall is exposed. The symbol i refers to each of the reflected streams: I_i is the solar radiation incident on the ith surface, ρ_i is the diffuse reflectance of that surface, and $F_{i\text{-}w}$ is the view factor from ith surface to the surface of the outer wall. It is assumed that the reflecting surfaces are diffuse reflectors. Figure 5.1 shows schematically these five terms of the total incident radiation onto the surface of the outer wall or window.

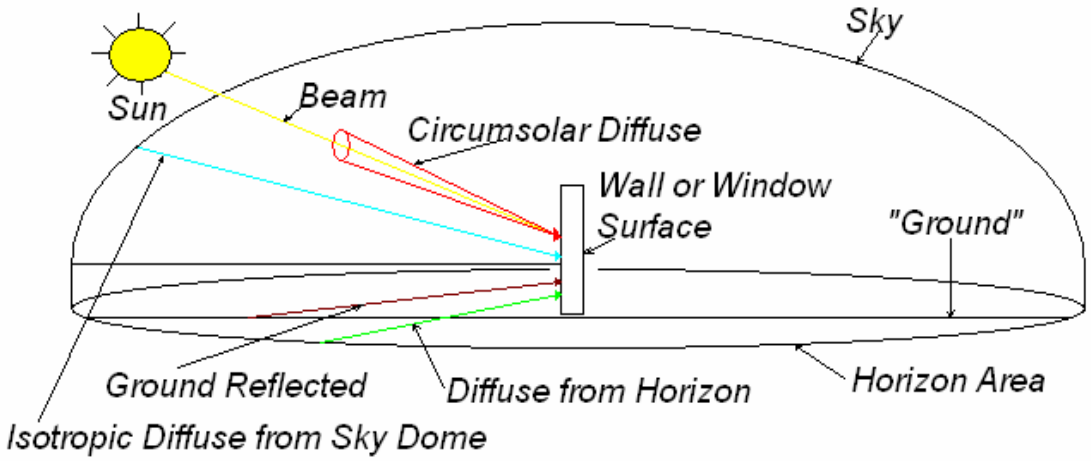

Figure 5.1: Beam, diffuse and ground-reflected radiation onto the surface of the outer wall or window.

In general, it is not possible to calculate the reflected energy term in detail, to account for buildings, trees, etc., the changing solar radiation incident on them, and their changing reflectances. Standard practice is to assume that there is one surface, a horizontal, diffusely reflecting ground, large in extent, contributing to this term. In this case, I_i is simply I and ρ_i becomes ρ_g, a composite "ground" reflectance.

Equation (5.15) can be rewritten in a useful form by interchanging areas and view factors (since the view factor reciprocity relation requires that, for example, $A_s F_{s\text{-}w} = A_w F_{w\text{-}s}$). This eliminates the undefined areas A_s and A_{hz}. The area A_w appears in each term in the equation and cancels. The result is an equation that gives I_T in terms of parameters that can be determined either theoretically or empirically:

$$I_T = I_b R_b + I_{d,iso} F_{w-s} + I_{d,cs} R_b + I_{d,hz} F_{w-hz} + I\rho_g F_{w-g} \tag{5.16}$$

When I_T has been determined, the ratio of total radiation on the surface of the outer wall, to that on the horizontal surface is determined by

$$R = \frac{\text{Total\_radiation\_on\_the\_surface\_of\_the\_outer\_wall}}{\text{Total\_radiation\_on\_a\_horizontal\_surface}} = \frac{I_T}{I} \tag{5.17}$$

The HDKR model is based on the assumption that all of the diffuse can be represented by two parts, the isotropic and the circumsolar. The diffuse radiation on a surface of the outer wall is written as

$$I_{d,T} = I_{T,d,iso} + I_{T,d,cs} \tag{5.18}$$

and

$$I_{d,T} = I_d \left[(1 - A_i) \left(\frac{1 + \cos\beta}{2} \right) + A_i R_b \right] \tag{5.19}$$

where A_i is an **anisotropy index** which is a function of the transmittance of the atmosphere for beam radiation,

$$A_i = \frac{I_{b,n}}{I_{on}} = \frac{I_b}{I_o} \tag{5.20}$$

where I_o is the extraterrestrial radiation on a horizontal surface for an hour period, given by (where ω_2 is the larger)

$$I_0 = \frac{12 \times 3600}{\pi} G_{sc} \left(1 + 0{,}033 \cos \frac{360n}{365} \right) \times \left[\cos\phi \cos\delta (\sin\omega_2 - \sin\omega_1) + \frac{\pi(\omega_2 - \omega_1)}{180} \sin\phi \sin\delta \right] \tag{5.21}$$

where the **solar constant** G_{sc} = 1.367 W/m^2 is the energy from the sun, per unit time, received on a unit area of surface perpendicular to the direction of propagation of the radiation, at mean earth-sun distance, outside the atmosphere.

The anisotropy index determines a portion of the horizontal diffuse which is to be treated as forward scattered: it is considered to be incident at the same angle as the beam radiation. The balance of the diffuse is assumed to be isotropic. Under clear conditions, the A_i will be high, and most of the diffuse will be assumed to be forward scattered. The correction factor $[1+f\sin^3(\beta/2)]$ accounts for horizon brightening both on clear days and for cloudiness, depending by the modulating factor f. The diffuse on the surface of the outer wall is

$$I_{d,T} = I_d \left\{ (1 - A_i) \left(\frac{1 + \cos\beta}{2} \right) \left[1 + f \sin^3 \left(\frac{\beta}{2} \right) \right] + A_i R_b \right\} \tag{5.22}$$

where

$$f = \sqrt{I_b / I} \tag{5.23}$$

5.1.c Absorbed Solar Radiation by the surface of the outer wall

The total incident radiation on a surface of the outer wall is

$$I_T = (I_b + I_d A_i) R_b + I_d (1 - A_i)\left(\frac{1+\cos\beta}{2}\right)\left[1 + f\sin^3\left(\frac{\beta}{2}\right)\right] + I\rho_g\left(\frac{1-\cos\beta}{2}\right) \tag{5.24}$$

where

I: is the total hourly radiation on a horizontal surface measured by the ISET-Sensor–monocrystalline pyranometer and stored by LabVIEW in Excel files.
I_b: is the hourly beam radiation on the horizontal surface.
I_d: is the hourly diffuse radiation on the horizontal surface.
β: is the angle of the surface of the outer wall ($\beta = 90^0$).

An hourly clearness index k_T is defined as

$$k_T = \frac{I}{I_0} \tag{5.25}$$

The Erbls et al. correlation I_d/I is the fraction of the hourly radiation on a horizontal plane which is diffuse, with k_T, the hourly clearness index, and is represented by the following equations:

$$\frac{I_d}{I} = \begin{cases} 1{,}0 - 0{,}09k_T & \text{for } k_T \le 0{,}22 \\ 0{,}9511 - 0{,}1604k_T + 4{,}388k_T^2 - 16{,}638k_T^3 + 12{,}336k_T^4 & \text{for } 0{,}22 < k_T \le 0{,}80 \\ 0{,}165 & \text{for } k_T > 0{,}80 \end{cases} \tag{5.26}$$

The following relation also holds:

$$I = I_b + I_d \tag{5.27}$$

Finally, the total absorbed radiation by a surface of the outer wall is

$$S_T = (I_b + I_d A_i) R_b \alpha_p + I_d (1 - A_i)\left(\frac{1+\cos\beta}{2}\right)\alpha_p\left[1 + f\sin^3\left(\frac{\beta}{2}\right)\right] + I\rho_g\alpha_p\left(\frac{1-\cos\beta}{2}\right) \tag{5.28}$$

or

$$S_T = (I_b + I_d A_i) R_b \alpha_p + I_d (1 - A_i) \alpha_p \left(\frac{1}{2}\right)\left[1 + f \sin^3(45^0)\right] + I \rho_g \alpha_p \left(\frac{1}{2}\right) \qquad (5.29)$$

where

ρ_g is assumed to be 0,4.
α_p is the absorptivity factor for the plaster and it is assumed to be 0,9 [39].

The above Equations (5.28) and (5.29) illustrate how the hourly total absorbed solar radiation S_T by the surface of the outer wall is calculated by measuring the hourly total radiation I on a horizontal surface.

5.1.d Absorbed Solar Radiation by the windows and roof glazing surfaces

Direct-gain passive solar heating depends on absorption of solar radiation in rooms or sunspaces which are cavity receivers with apertures (windows) covered with one or more glazings. The fraction of the incident solar energy that is absorbed by such a receiver for radiation incident on the glazing is given by

$$\tau_c \alpha_{eff} = \tau_c \frac{\alpha_i}{\alpha_i + (1 - \alpha_i)\tau_d \frac{A_\alpha}{A_i}} \qquad (5.30)$$

Here τ_c is the transmittance of the glazing for the incident solar radiation; τ_d is the transmittance of the glazing for isotropic diffuse solar radiation (the solar radiation reflected from the inner walls of the cavity), which is at an effective angle of incidence of about 60^o; A_α is the area of the aperture (the northern windows and roof glazing); A_i is the area of the inside of the room (A_{total} = 213,7 m^2 for the bookshop); and α_i is the absorptance for diffuse radiation of the inner surface of the cavity. The bookshop has various surfaces on floor, walls, ceiling, and furnishing, and a mean value of α_i = 0,45 can be used.

The transmittance τ_c of the double glazing of the northern windows and roof glazing (horizontal glazing) is calculated as a function of the angle of incidence of the solar radiation with extinction length KL = 0,0370 (per glazing), where K is the proportionality constant extinction coefficient and L is the actual path length in the medium ([38]-Figure 4.2 and [42]-Figure 5.3.1.) More specifically, for the northern windows which are vertical, the effective angle of incidence for the beam radiation is calculated by Equation (5.4). The effective angle of incidence of both the diffuse and the ground-reflected radiation is 59^o from Brandemuehl and Beckman ([42]-Figure 5.4.1-1980).

Solar films are mounted on the windows and roof glazing surfaces, [43]. The construction of the films is based on Polyester and the transmittance–absorptance product can be assumed constant and independent of the angle of incidence

(Appendix A). Figure 5.2 shows schematically the absorbed solar radiation by the window.

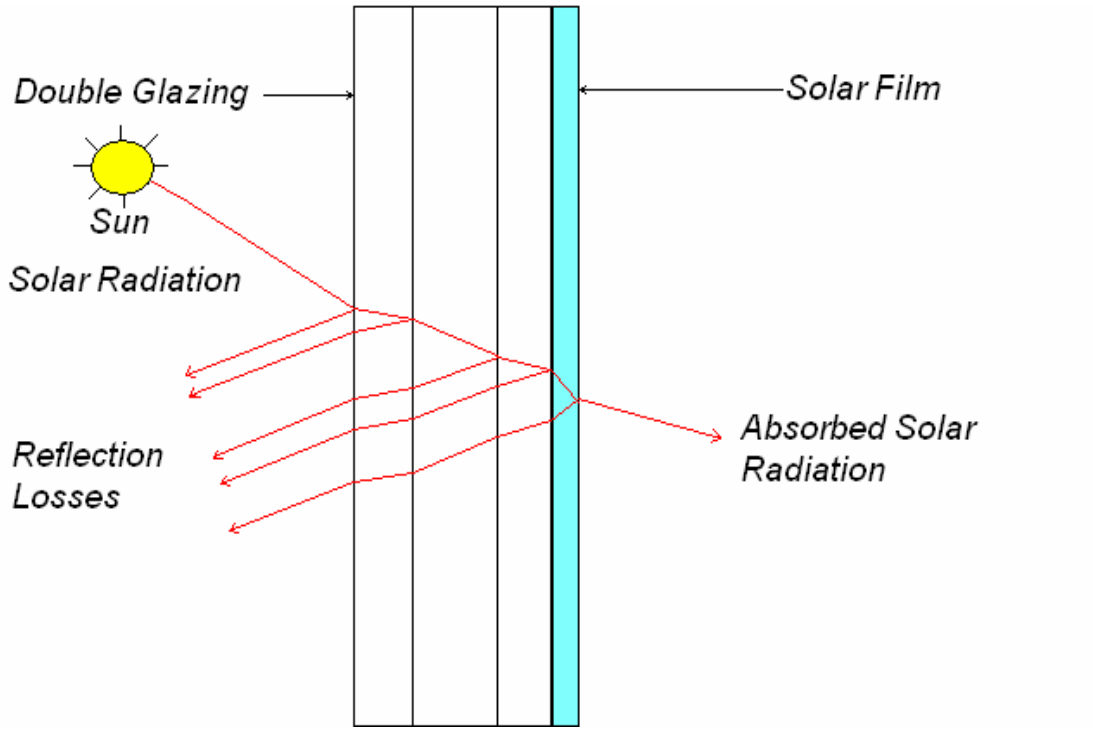

Figure 5.2: Absorbed Solar Radiation by the window.

Using the HDKR model of diffuse radiation, Equation (5.24) can be modified by multiplying each term with the appropriate transmittance-absorptance product. The double glazed window has KL = 0,0370 per sheet. The energy absorbed by the northern windows S_w is given by

$$S_W = \left(I_b + I_d A_i\right) R_b (\tau\alpha)_b (\tau\alpha)_{sf} + I_d \left(1 - A_i\right)\left(\frac{1+\cos\beta}{2}\right)(\tau\alpha)_d (\tau\alpha)_{sf}\left[1 + f\sin^3\left(\frac{\beta}{2}\right)\right] + I\rho_g (\tau\alpha)_g (\tau\alpha)_{sf}\left(\frac{1-\cos\beta}{2}\right) \quad (5.31)$$

where

$(\tau\alpha)_b$ is the transmittance-absorptance product of the beam radiation using Equation (5.30).
$(\tau\alpha)_d$ is the transmittance-absorptance product of the diffuse radiation using Equation (5.30).
$(\tau\alpha)_g$ is the transmittance-absorptance product of the ground radiation using Equation (5.30).
$(\tau\alpha)_{sf}$ is the transmittance-absorptance product of the solar film NG70 which is mounted on the inner glazing of the window, with $(\tau\alpha)_{sf} = 0{,}67$ (Appendix A).
β: is the angle of the surface of the northern windows ($\beta = 90^o$).

A part of the roof, which is made by glass, is under shadow by the wall of the adjacent building for a time period. The following Figure 5.3 explains the condition for which the beam radiation is considered in this case.

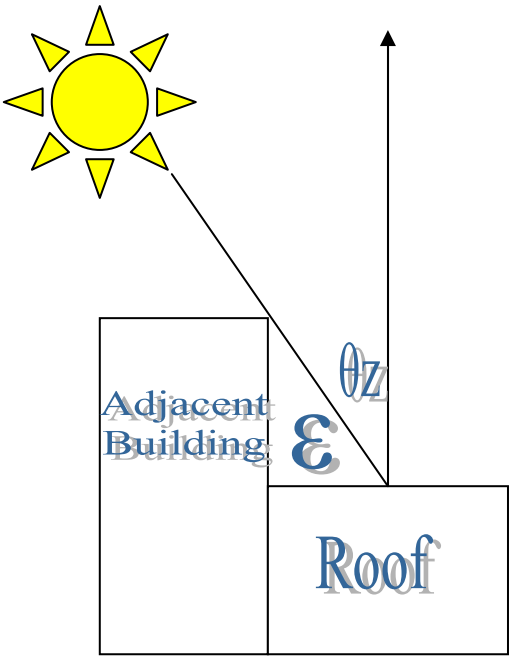

Figure 5.3: The roof glazing of the bookshop is under shadow as $\theta_z > 39^o$.

As it is illustrated in Figure 5.3, the beam radiation on the horizontal glazing is zero when $\theta_z > 39^o$. The calculation of the absorbed radiation by the roof glazing is obtained through the modification of Equation (5.27) by multiplying each term with the appropriate transmittance-absorptance product. It is also assumed that the roof glazing has KL = 0,0370 for the inner single glazing. The absorbed radiation S_r by the roof glazing is

$$S_r = I_b(\tau\alpha)_b(\tau\alpha)_{sf} + I_d(\tau\alpha)_d(\tau\alpha)_{sf} \qquad (5.32)$$

where

$(\tau\alpha)_b$ is the transmittance-absorptance product of the beam radiation using Equation (5.30).
$(\tau\alpha)_d$ is the transmittance-absorptance product of the diffuse radiation using Equation (5.30).
$(\tau\alpha)_{sf}$ is the transmittance-absorptance product of the solar film SDS S220X which is mounted on the outer single glazing of the roof glazing, with $(\tau\alpha)_{sf}$ = 0,2 (Appendix A).
β: is the angle of the surface of the roof glazing ($\beta = 0^o$).

5.2 Total Calculation of the Absorbed Radiation by the surfaces of the Bookshop

The following Figure 5.4 depicts the measured Solar Incident Radiation on a horizontal surface by the ISET-Sensor–monocrystalline pyranometer from 18/9/2005 until 25/9/2005. The Thermal Model Predictive Controller through LabVIEW arranges these measurements in hourly profiles calculating thus radiation *I*.

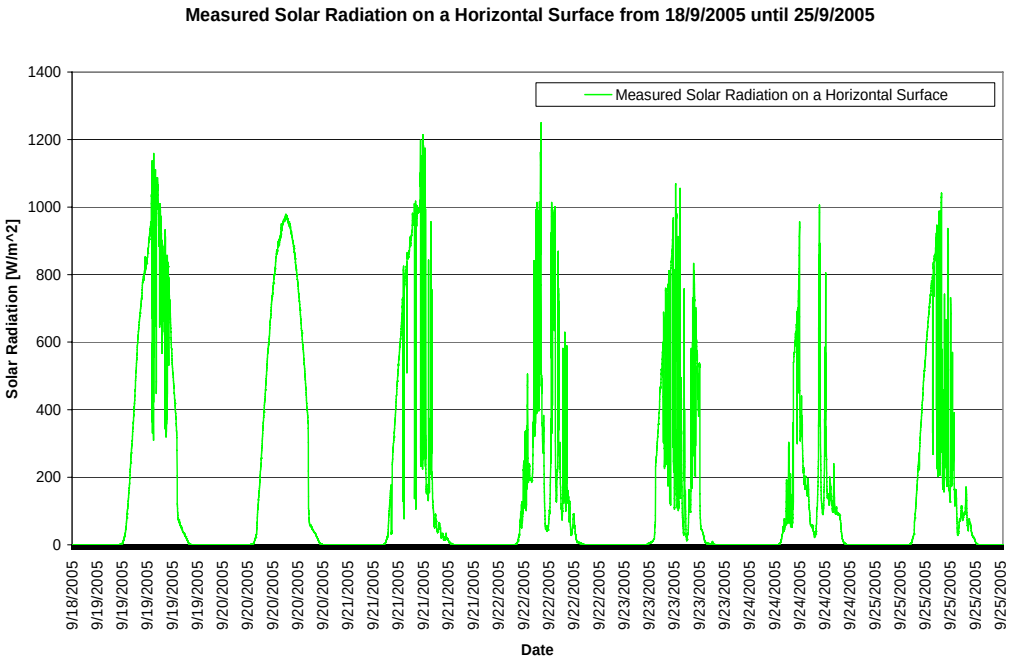

Figure 5.4: Measured Solar Radiation on a Horizontal Surface from 18/9/2005 until 25/9/2005.

After having estimated the absorbed radiation by the surface of the northern wall, the windows and the roof (where A_{wall} = 15,24 m^2, $A_{windows}$ = 9,33 m^2 and $A_{roof\_glazing}$ = 13,76 m^2), we multiply the radiation with every mentioned surface, resulting in calculating the solar energies. Figure 5.5 depicts the above-mentioned energies, while Figure 5.6 shows the profile of the total absorbed solar radiation in the bookshop from 18/9/2005 until 25/9/2005.

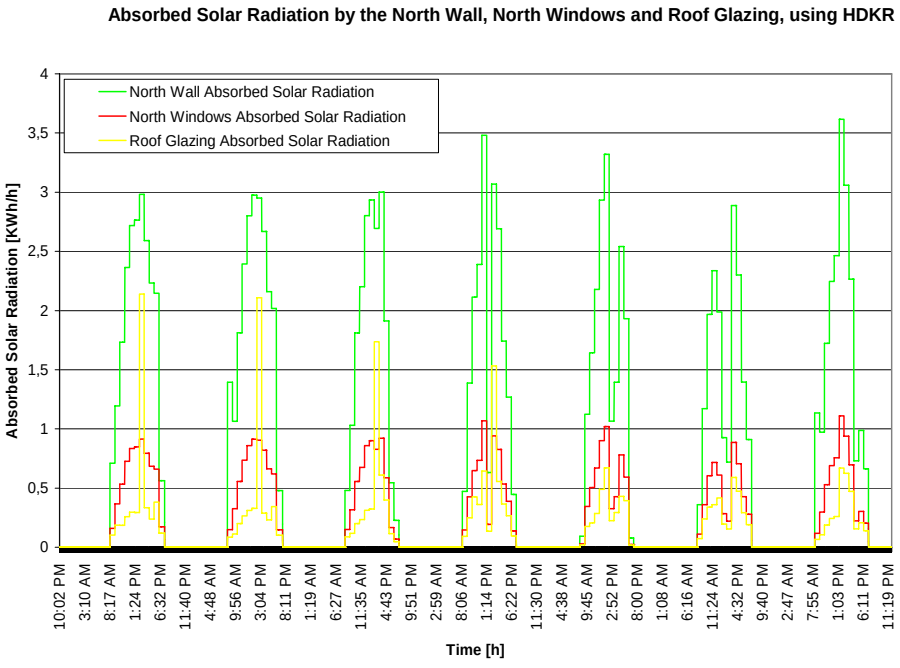

Figure 5.5: Absorbed Solar Radiation by the north wall, north windows and roof glazing from 18/9/2005 until 25/9/2005.

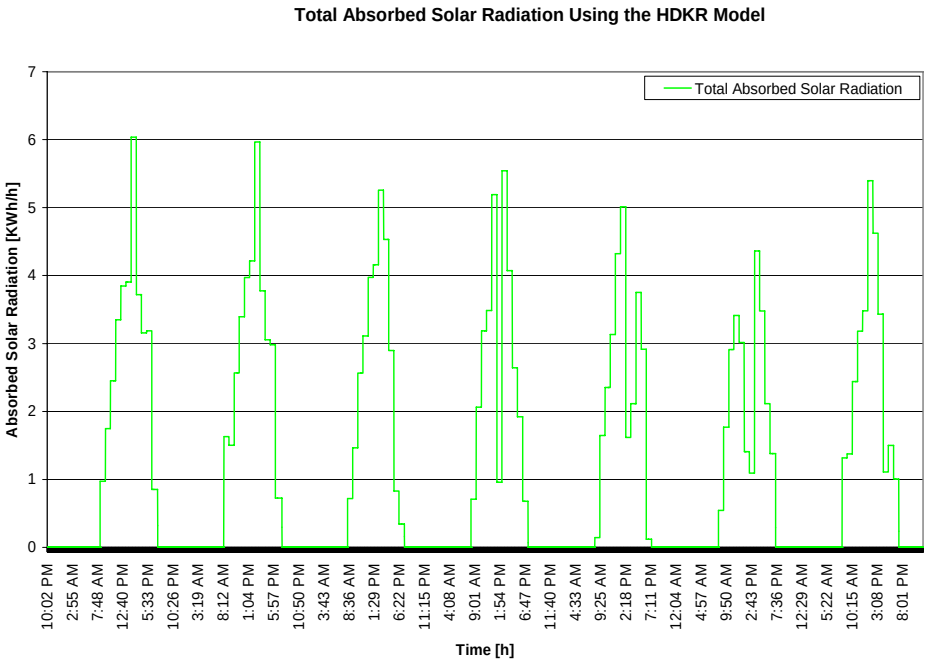

Figure 5.6: Total Absorbed Solar Radiation by the surfaces of the bookshop from 18/9/2005 until 25/9/2005.

6 Internal Heat Sources

The energies of internal heat sources are those from humans and electric devices, such as lighting, PCs, security system, etc. Special effort is given in the calculation of the thermal energy caused by the different temperatures of the surfaces of the opposite bookshop inner walls. The heat losses from the windows and doors are also integrated in the Thermal Model. The air-conditioning units operation is presented in comparison with the electrical power consumption of the bookshop.

6.1 Internal Heat Sources

The SCADA monitors the operation of the bookshop and gets information from the security system when the shop opens and closes respectively. After a statistical approach concerning the existence of humans inside the shop, it is concluded that 2 persons in average are in the shop during its daily operation. Taking into account that each person contributes by 60W, the total heat sources caused by humans are 120W.

The electric energy consumption of the bookshop is recorded without the analytical measurement of the consumption of each electrical load. Therefore a statistical approach is made for the calculation of the energies of the internal heat sources. The following Table 6.1 presents the electrical loads of the bookshop. PABX (Private Automatic Branch eXchange or Internal Telephone Network), security system, cash register and fridge operate continuously. There is one PC with a UPS of 400W which operates only when the shop is opened. The lighting heat sources are calculated in a statistical way by the analysis of the total electrical power consumption of the bookshop.

Device	**Power (W)**
PABX	20
Security System	12
Cash Register	9
PC	400
Lighting (Maximum)	2.200
Fridge	60

Table 6.1: The Electrical loads of the Bookshop.

The SCADA calculates in on-line mode the heat losses from the different temperatures of the surfaces of the opposite inner walls. The following Equation (6.1) calculates these heat losses as

$$\dot{E}_{opp\_wall} = \alpha_{opp\_wall} A (T^{p}_{w1} - T^{p}_{w2}) \quad (6.1)$$

where

$\dot{E}_{opp\_walls}$: Net rate at which energy is being transferred in by the radiation heat transfer due to the different temperatures of the surfaces of the opposite inner walls *at time (p)*
α_{opp_wall} : $5 W/m^2K$
A : Area of the surface
T_{wx} : Surface Temperature of the corresponding inner wall which is calculated by applying the FDC method to the inner surface node of the wall.

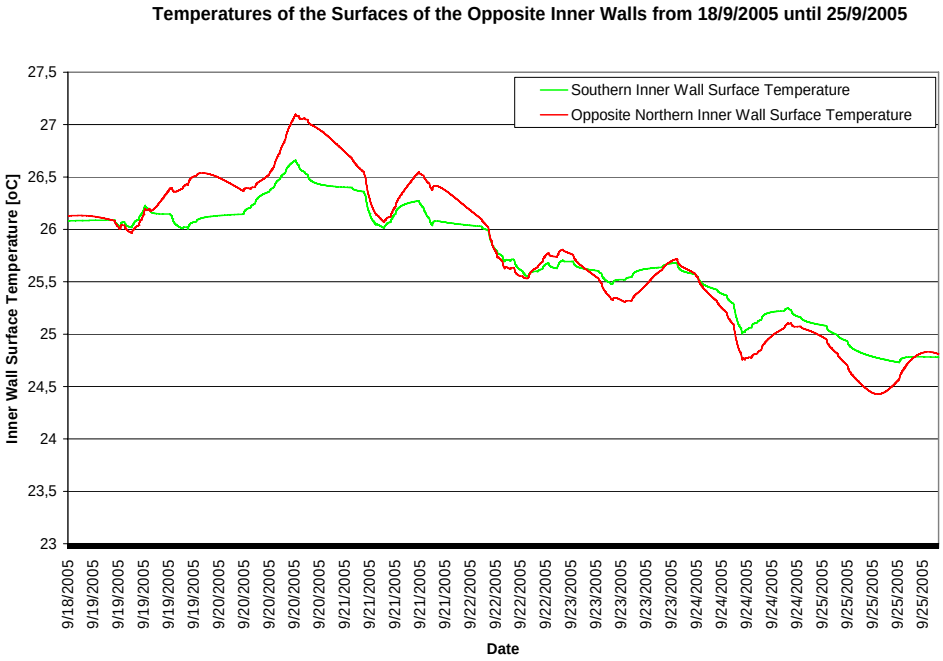

Figure 6.1: Temperatures of the northern and southern surfaces of the opposite inner walls from 18/9/2005 until 25/9/2005.

Figure 6.1 shows the temperatures of the northern and southern surfaces of the opposite inner walls, as they are calculated by the SCADA applying the FDC method to the nodes of the inner surfaces from 18/9/2005 until 25/9/2005. The heat losses from the windows and the eastern door due to the difference between the indoor and the ambient temperatures as well as the heat losses from the western door due to the difference between the indoor and the entrance temperatures are calculated. In addition, the heat losses from the floor due to the difference between the indoor temperature and the temperature of the basement (downstairs) with the heat losses from the roof due to the difference between the indoor temperature and the temperature of the apartment (upstairs) are also estimated on-line. The following Figure 6.2 depicts the foregoing temperatures, while Figure 6.3 presents an analytical view of the heat losses for the examined period.

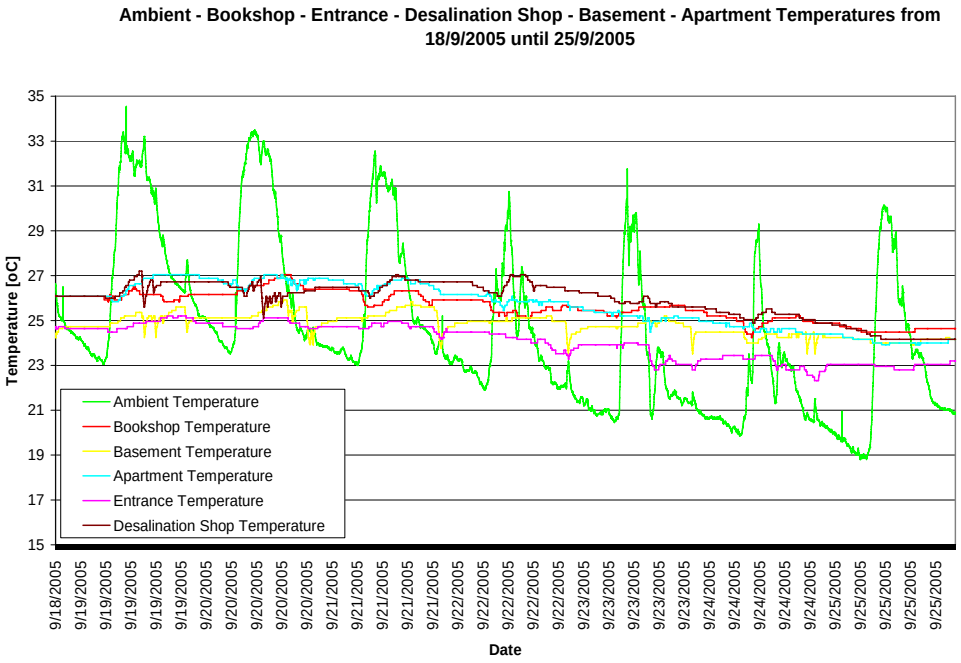

Figure 6.2: Ambient, Bookshop, Basement, Apartment, Entrance and Desalination Shop Temperatures from 18/9/2005 until 25/9/2005.

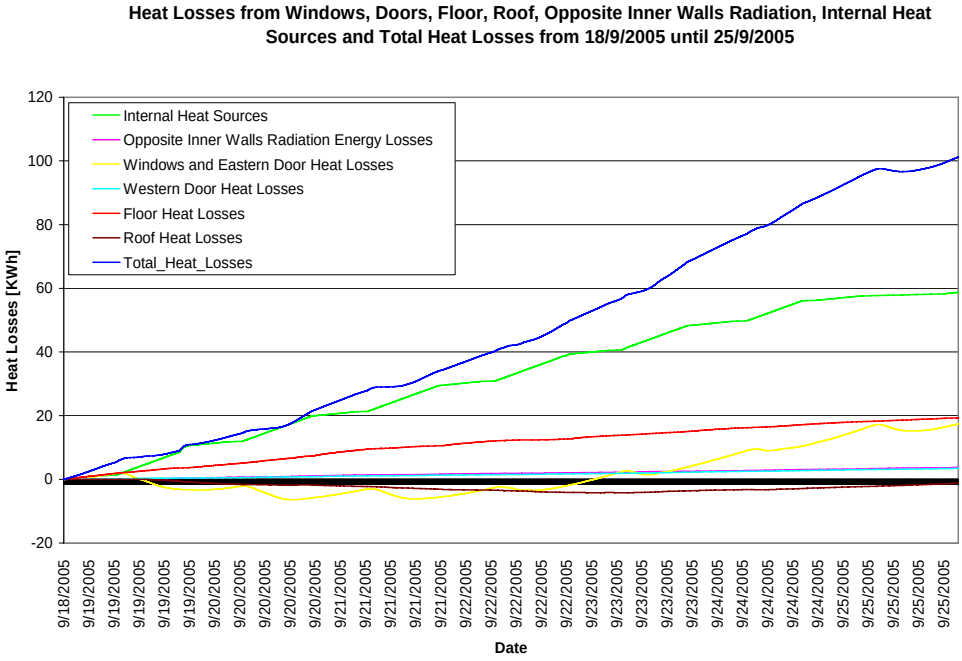

Figure 6.3: Heat Losses from windows, doors, floor, roof, opposite inner walls radiation, internal heat sources and total heat losses from 18/9/2005 until 25/9/2005.

The following Figure 6.4 depicts the indoor temperature on 20th September 2005, which is a typical summer day. It is shown in this figure that the maximum temperature occurs after 16:30. Therefore, the maximum electrical power consumption of the air-conditioning units is required during sunset. Moreover, it is concluded that the use of Photovoltaics is not the optimal solution in this case, because their maximum electrical power is produced at midday.

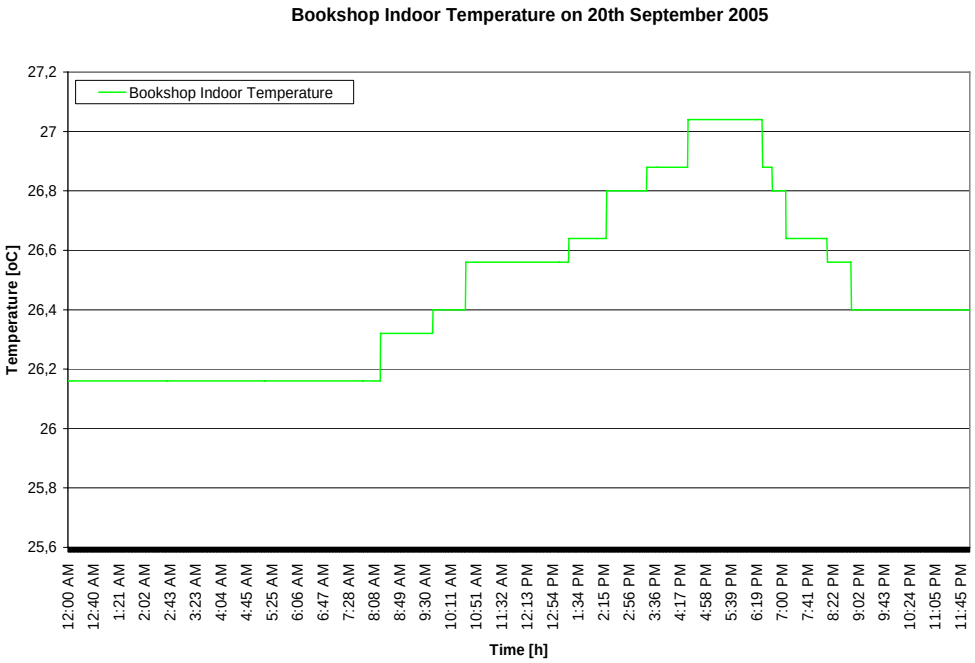

Figure 6.4: Bookshop Indoor Temperature on 20th September 2005.

6.2 Air-Conditioning Units and Bookshop Electrical Power Consumptions

In this section, the description of the dynamics of the bookshop is completed with the presentation of the air-conditioning units operation and the electrical power consumption of the bookshop. The following Figure 6.5 shows the electrical power consumption of the air-conditioning units in comparison with the electrical power consumption of the bookshop from 18/9/2005 until 25/9/2005. It is noted that the nominal capacity of the air-conditioning units is 21.000 Btu/h and the electrical power consumption is 2.220 W during summer, when the outdoor ambient temperature is 35°C and the indoor temperature is 27°C. However, two supplementary air-conditioning units of the same capacity and electrical power consumption with the aforementioned ones have been installed in the bookshop, whether more comfort is required. Furthermore, the SCADA monitors the operation of the air-conditioning units, when they are switched on/off and calculates the rates of heat transfer from these units.

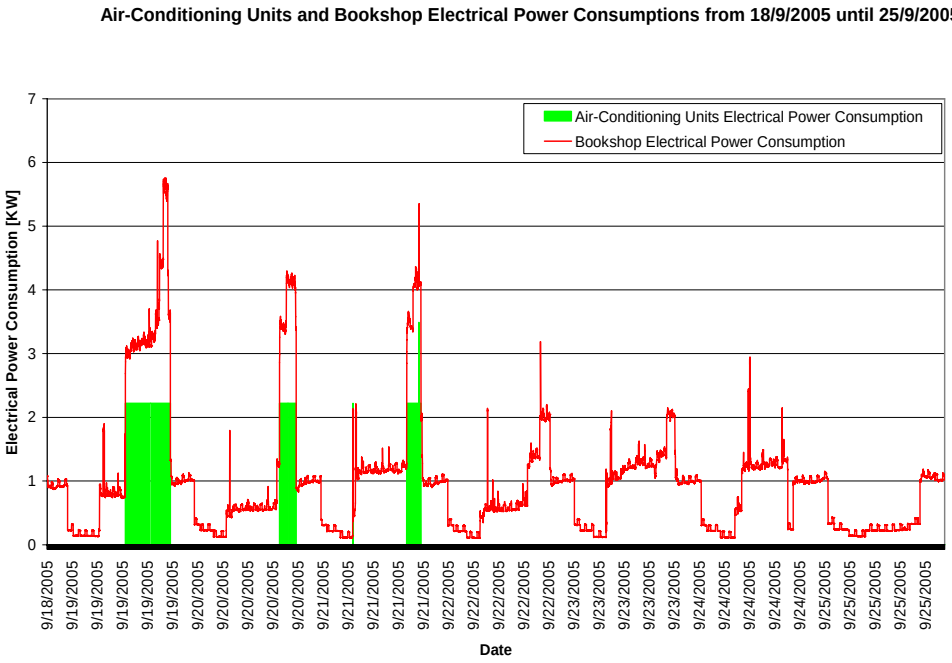

Figure 6.5: Electrical power consumption of the air-conditioning units in comparison with the bookshop electrical power consumption from 18/9/2005 until 25/9/2005.

Based on Figure 6.5, the calculation of the energy consumption of the air-conditioning units is realised by the integration of their electrical power consumptions. The calculated rates of heat transfer from the mentioned units are also integrated to the thermal model. Moreover, this figure illustrates that the peak demand is mainly caused by the operation of the air-conditioning units during summer.

7 Thermal Model Verification

The verification of the Thermal Model is presented in this chapter. This is achieved by the integration of the energies, which have already been presented in Chapters 4, 5 and 6. The thermal model is also verified by the comparison of the measured indoor temperature with the predicted one, which is obtained by using two different methods of prediction.

7.1 Integration of the Bookshop Energies

The integration of the Energies developed in Chapters 4, 5 and 6 includes the Inflow, Outflow Energies in Figure 4.11, the absorbed solar radiation in Figure 5.5, the heat losses in Figure 6.3 and the rates of heat transfer from the air-conditioning units based on Figure 6.5. The following Figure 7.1 depicts the integration of the energies concerning the north wall part only made by plaster, brick and expanded polystyrene.

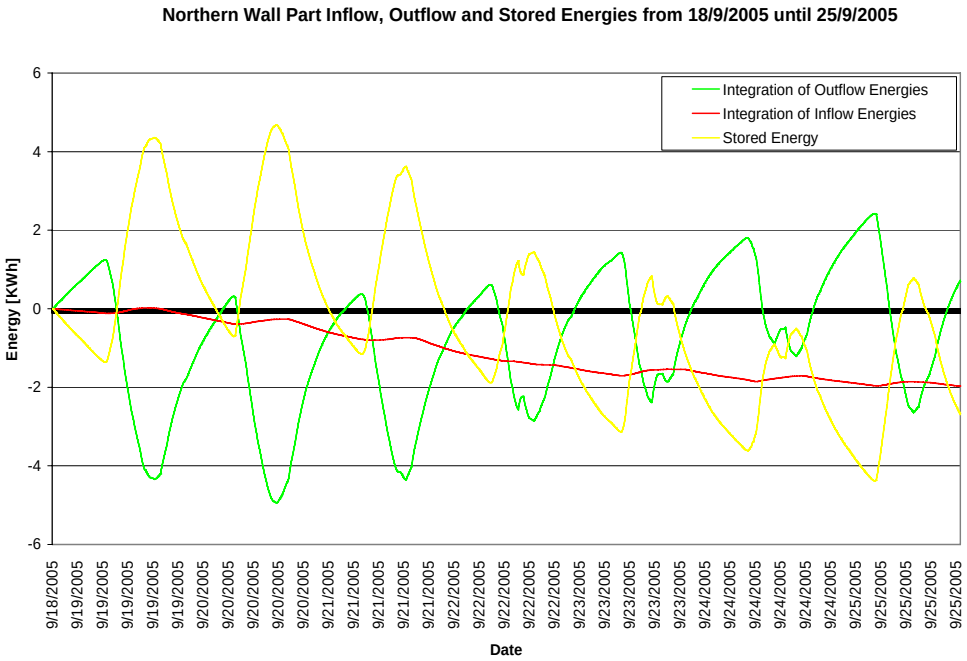

Figure 7.1: Northern wall part Inflow, Outflow and Stored Energies of the Bookshop from 18/9/2005 until 25/9/2005.

Recalling the Energy Balance Equation (4.16)

$$\dot{E}_{in} + \dot{E}_{g} - \dot{E}_{out} = \dot{E}_{st} \tag{4.16}$$

Inflow Energy is considered to be the energy resulting from the heat flux due to the difference between the indoor temperature and the surface temperature of the inner wall. The internal heat sources, the heat losses which are presented in Chapter 6 with the rates of heat transfer from the air-conditioning units leave the shop, interact to the indoor and inner surfaces temperatures and are therefore assumed as Inflow Energies. Respectively, Outflow Energy is the thermal energy due to the difference between the surface temperature of the outer wall and the ambient temperature. The solar radiation is applied onto the surface of the outer northern wall part and is also considered as Outflow Energy.

Figure 7.1 shows that the stored energy changes periodically every day. At first, cooling stored energy increases up to a maximum degree. Afterwards, the cooling stored energy decreases until the stored energy finally reaches zero. Then, heating energy starts to be stored; secondly, it reaches the maximum degree and in the end it gets zero. That means that the energy balance equation holds and the thermal model is verified. The following Figure 7.2 shows the integration of the energies in the entire north wall.

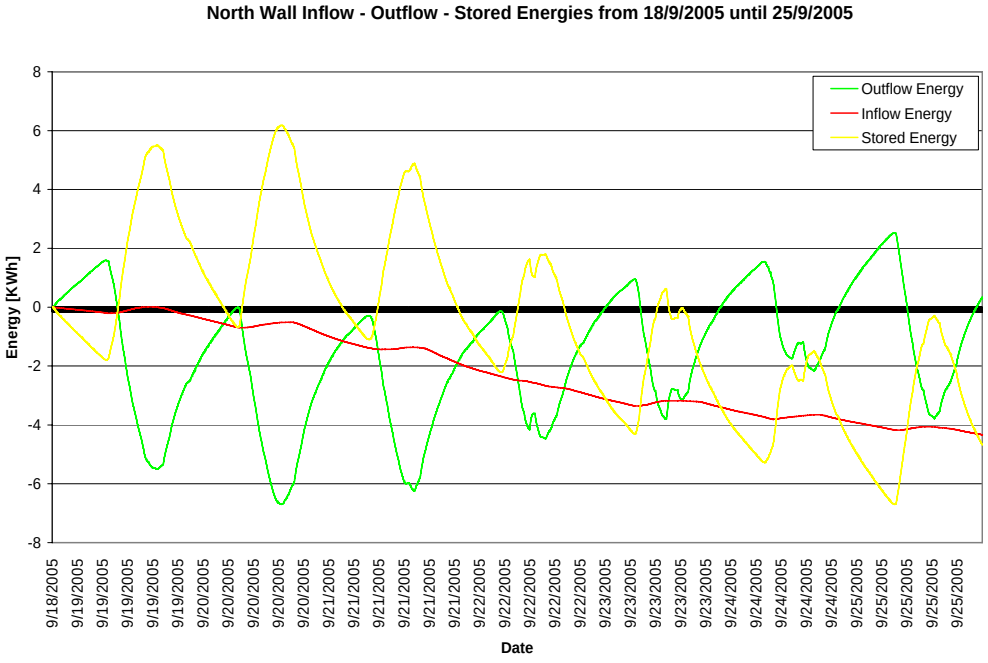

Figure 7.2: North Wall Inflow, Outflow and Stored Energies of the Bookshop from 18/9/2005 until 25/9/2005.

Figure 7.2 also shows that the energy balance equation holds in the entire north wall. The SCADA calculates on-line the total Inflow, Outflow, and Stored Energies in all the walls of the bookshop. The Inflow and Outflow Energies of all walls are depicted in Figure 7.3. In this figure, only the convective heat fluxes to each wall surface are integrated with the absorbed solar radiation by the surface of the northern wall in Figure 5.5.

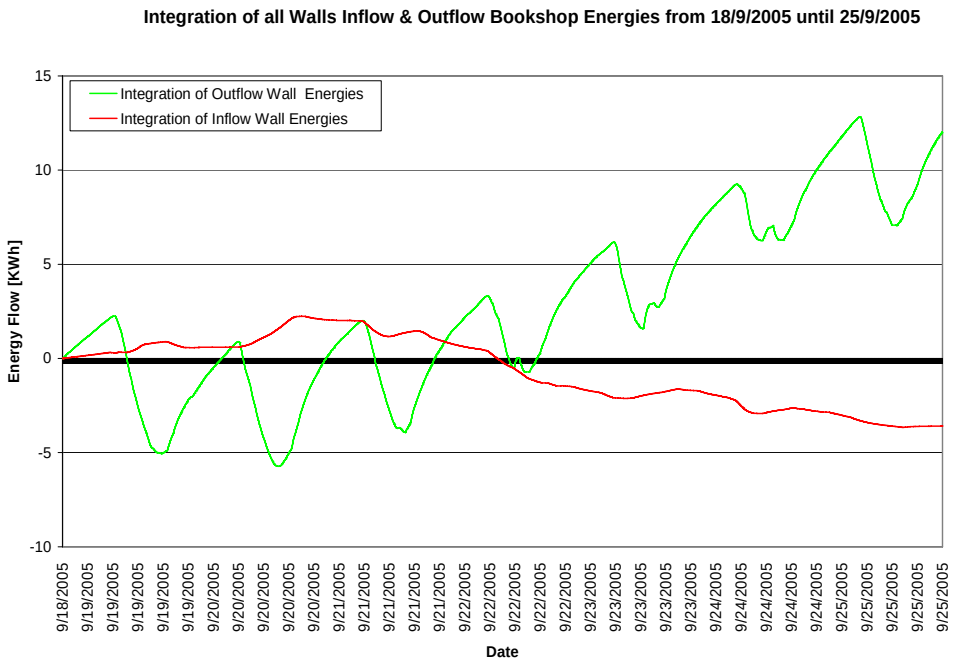

Figure 7.3: Inflow and Outflow Energies of all walls of the Bookshop from 18/9/2005 until 25/9/2005.

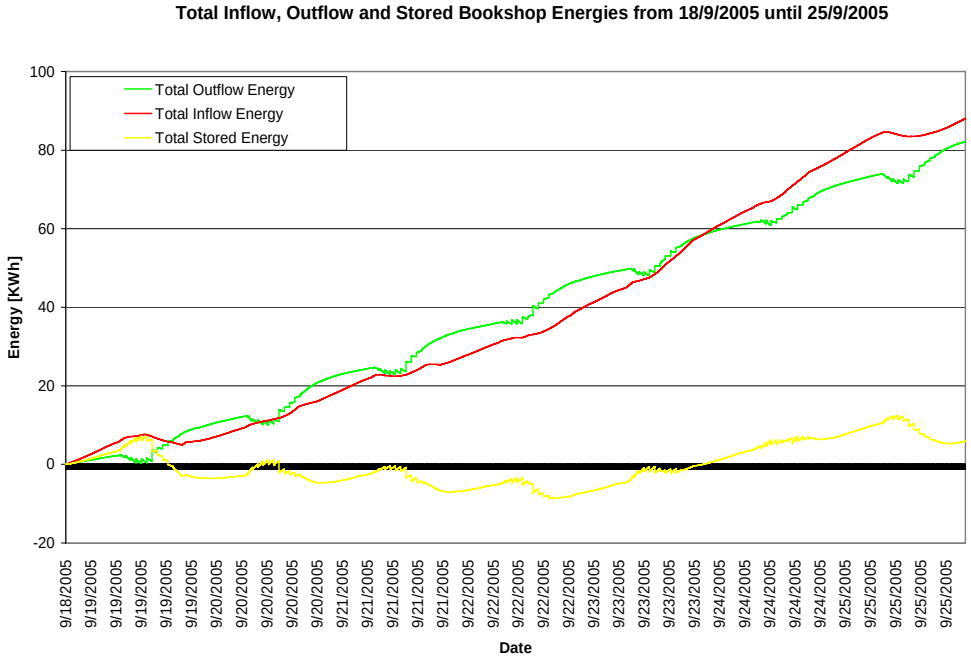

Figure 7.4: Total Inflow, Outflow and Stored Energies of the Bookshop from 18/9/2005 until 25/9/2005.

The Total Inflow Energy is the integration of the Inflow Energy, shown in Figure 7.3, with the heat losses in Figure 6.3 and the rates of heat transfer from the air-conditioning units based on Figure 6.5. Respectively, the Total Outflow Energy is the integration of the Outflow Energy, shown in Figure 7.3, with the absorbed solar radiation by the northern windows and roof glazing in Figure 5.5. Figure 7.4 depicts

the Total Inflow and Total Outflow Energies, verifying the fact that the thermal model is based on the energy balance equation.

7.2 Indoor Temperature Prediction

Two different methods are used for the indoor temperature prediction. Equation (4.20), in Chapter 4, has been used up to this point for the calculation of the Inflow, Outflow and Stored Energies of the northern wall part which is constructed by plaster, brick and expanded polystyrene. This equation is used in this section to predict the indoor temperature $\hat{T}_{in}^{p+1}$, when outdoor (T_{out}^{p} or T_{∞}), and all the around temperatures are known by the measurements. We measure outdoor, desalination, apartment, entrance and basement temperatures. The heat fluxes are calculated at each sample, after having measured all the around temperatures and predicted the indoor temperature. The heat fluxes from the radiation, air-conditioning units and internal heat sources are used as they have been calculated in order to verify the thermal model. Recalling Equation (4.20)

$$T_0^{p+1} = 2Fo\left(T_1^p + BiT_\infty + \frac{q''\Delta x}{\lambda} \right) + (1 - 2Fo - 2BiFo)T_0^p \tag{4.20}$$

For the surface of the inner-wall Equation (4.20) *at the new time (p+1)* becomes

$$T_{27}^{p+1} = 2Fo\left(T_{26}^p + Bi\hat{T}_{in}^p + \frac{q''^p\Delta x}{\lambda} \right) + (1 - 2Fo - 2BiFo)T_{27}^p \tag{7.1}$$

7.2.a 1st Method for Indoor Temperature Prediction

Integrating the heat fluxes in Equation (7.1), we obtain

$$T_{27}^{p+1} = 2Fo\left(T_{26}^p + Bi\hat{T}_{in}^p + \sum\frac{q''^p\Delta x}{\lambda} \right) + (1 - 2Fo - 2BiFo)T_{27}^p \tag{7.2}$$

where $\sum q''^p$ is the integration of all heat fluxes of the bookshop walls, the internal heat sources, the air-conditioning units, the windows, the doors and the solar radiation *at time (p)* and it is given by

$$\begin{aligned}\sum q''^p = &\sum_{i=1}^{n} w_i U_i \left(T_{out}^p - \hat{T}_{in}^p\right) + \sum_{j=1}^{m} w_j U_j \left(T_{des}^p - \hat{T}_{in}^p\right) + \sum_{k=1}^{o} w_k U_k \left(T_{ent}^p - \hat{T}_{in}^p\right) \\ &+ w_{bas} U_{bas} \left(T_{bas}^p - \hat{T}_{in}^p\right) + w_{ap} U_{ap} \left(T_{ap}^p - \hat{T}_{in}^p\right) + w_{rad} q''^p_{rad} + w_{sol} q''^p_{sol} + w_{int} q''^p_{int} \pm w_{aux} q''^p_{aux}\end{aligned} \tag{7.3}$$

where

$\sum_{i=1}^{n} U_i \left(T_{out}^p - \hat{T}_{in}^p\right)$ is the integration of the conduction heat fluxes through all kind of walls, windows, doors and the roof due to the difference between the ambient and the predicted indoor temperatures *at time (p)*.

$\sum_{j=1}^{m} U_j \left(T_{des}^p - \hat{T}_{in}^p\right)$ is the integration of the conduction heat fluxes through all kind of walls, due to the difference between the temperature of the desalination shop and the predicted indoor temperature *at time (p)* (east side).

$\sum_{k=1}^{o} U_k \left(T_{ent}^p - \hat{T}_{in}^p\right)$ is the integration of the conduction heat fluxes through all kind of walls and the door, due to the difference between the temperature of the entrance and the predicted indoor temperature *at time (p)* (west side).

$U_{bas}\left(T_{bas}^p - \hat{T}_{in}^p\right)$ is the conduction heat flux due to the difference between the temperature of the basement and the predicted indoor temperature *at time (p)* (downstairs).

$U_{ap}\left(T_{ap}^p - \hat{T}_{in}^p\right)$ is the conduction heat flux due to the difference between the temperature of the apartment and the predicted indoor temperature *at time (p)* (upstairs).

q''^p_{rad} is the radiation heat flux due to the different temperatures of the surfaces of the opposite inner walls *at time (p)*.

q''^p_{sol} is the heat flux due to the solar radiation *at time (p)*.

q''^p_{int} is the radiation heat flux due to the internal heat sources *at time (p)*.

q''^p_{aux} is the heat flux due to the capacity of the air-conditioning units *at time (p)*.

U is the overall heat transfer coefficient.

$w_i,\ldots,w_{aux}$ are the weighting factors so that the heat fluxes of the northern wall part can be calculated, where

$$w_i = \frac{A_i}{A_T - A_i} \tag{7.4}$$

with

A_i the area in which the corresponding heat flux is applied
A_T the total area of the bookshop ($A_T = 213{,}7\ m^2$)

Assuming that the heat flux which derives from the difference between the predicted indoor temperature and the surface node temperature of the inner wall *at the new time*

(p+1) is equal to the heat flux which derives from the difference between the surface node temperature of the inner wall and the temperature of the last interior node *at the same time (p+1)*, it follows that

$$q'' = \alpha_{in}\left(\hat{T}_{in}^{p+1} - T_{27}^{p+1}\right) = \frac{\lambda\left(T_{27}^{p+1} - T_{26}^{p+1}\right)}{\Delta x} \tag{7.5}$$

where specifically $\hat{T}_{in}^{p+1}$ is calculated as it follows in Equation (7.6)

$$\hat{T}_{in}^{p+1} = T_{27}^{p+1} + \frac{\lambda\left(T_{27}^{p+1} - T_{26}^{p+1}\right)}{\alpha_{in}\Delta x} \tag{7.6}$$

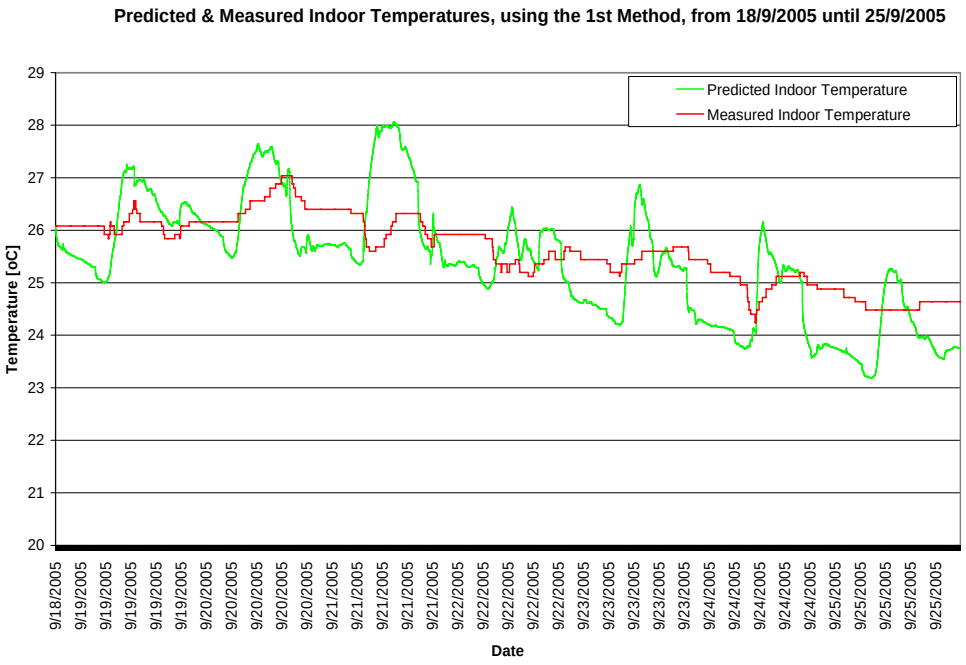

Figure 7.5: Predicted and Measured Indoor Temperatures of the Bookshop, using the 1st Method, from 18/9/2005 until 25/9/2005.

The above Figure 7.5 depicts the predicted indoor temperature of the Bookshop using Equation (7.6). Obviously, the predicted indoor temperature follows quite well the measured one. A model mismatch occurs because of the assumptions in Chapter 4, such as one dimensional conduction, constant properties, neglected ventilation and infiltration effects, etc. This figure verifies the thermal model. It is inferred that this thermal model is the proper one for being used for DSM actions.

7.2.b 2nd Method for Indoor Temperature Prediction

The other approach for predicting the indoor temperature is based on the 1st law of thermodynamics. Assuming that the bookshop is a closed system, the time rate form of the energy balance is obtained as [44]

$$\frac{dE}{dt} = \dot{Q} - \dot{W} \tag{7.7}$$

where

$\frac{dE}{dt}$ is the time *rate of change* of the energy contained within the system *at time t*

$\dot{Q}$ is the net *rate* at which energy is being transferred in by heat transfer *at time t*

$\dot{W}$ is the net *rate* at which energy is being transferred out by work *at time t*

Since the time rate of change of energy is given by

$$\frac{dE}{dt} = \frac{dKE}{dt} + \frac{dPE}{dt} + \frac{dU}{dt} \tag{7.8}$$

where KE is the kinetic energy, PE is the gravitational potential energy and U is the internal energy. Assuming dKE = dPE = 0, Equation (7.7) becomes

$$\frac{dU_{boox}}{dt} = \dot{Q} - \dot{W} \tag{7.9}$$

The mass contained within the control volume remains constant with time, so the term on the left side of the energy rate balance can be expressed as

$$\frac{dU_{boox}}{dt} = \frac{d(m_{boox}u)}{dt} = m_{boox}\frac{du}{dt} \tag{7.10}$$

Hence, the chain rule can be used to write

$$\frac{du}{dt} = \frac{du}{dT}\frac{dT}{dt} = c\frac{dT}{dt} \tag{7.11}$$

With the foregoing considerations the energy rate balance becomes

$$m_{boox}c\frac{dT}{dt} = \dot{Q} - \dot{W} \tag{7.12}$$

The net rate at which energy is being transferred in the bookshop by heat transfer *at time (p)* can be expressed as

$$\begin{aligned}\dot{Q} = \lambda A\frac{\left(T_{26}^{p} - T_{27}^{p}\right)}{\Delta x} + \sum_{i=1}^{n} U_i A_i\left(T_{out}^{p} - \hat{T}_{in}^{p}\right) + \sum_{j=1}^{m} U_j A_j\left(T_{des}^{p} - \hat{T}_{in}^{p}\right) + \sum_{k=1}^{o} U_k A_k\left(T_{ent}^{p} - \hat{T}_{in}^{p}\right) \\ + U_{bas}A_{bas}\left(T_{bas}^{p} - \hat{T}_{in}^{p}\right) + U_{ap}A_{ap}\left(T_{ap}^{p} - \hat{T}_{in}^{p}\right) + \dot{Q}_{rad}^{p} + \dot{Q}_{sol}^{p} + \dot{Q}_{int}^{p} \pm \dot{Q}_{aux}^{p}\end{aligned} \tag{7.13}$$

where

$\lambda A \frac{\left(T_{26}^{p} - T_{27}^{p}\right)}{\Delta x}$ is the net *rate* at which energy is being transferred in by the transient conduction heat transfer due to the difference between the temperature of the last interior node and the surface node temperature of the inner wall *at time (p).*

$\sum_{i=1}^{n} U_i A_i \left(T_{out}^{p} - \hat{T}_{in}^{p}\right)$ is the net *rate* at which energy is being transferred in by the conduction heat transfer through all kind of walls, windows, door and the roof due to the difference between the ambient and the predicted indoor temperatures *at time (p)*.

$\sum_{j=1}^{m} U_j A_j \left(T_{des}^{p} - \hat{T}_{in}^{p}\right)$ is the net *rate* at which energy is being transferred in by the conduction heat transfer through all kind of walls, due to the difference between the temperature of the desalination shop and the predicted indoor temperature *at time (p).*

$\sum_{k=1}^{o} U_k A_k \left(T_{ent}^{p} - \hat{T}_{in}^{p}\right)$ is the net *rate* at which energy is being transferred in by the conduction heat transfer through all kind of walls and the door, due to the difference between the temperature of the entrance and the predicted indoor temperature *at time (p)*.

$U_{bas} A_{bas} \left(T_{bas}^{p} - \hat{T}_{in}^{p}\right)$ is the net *rate* at which energy is being transferred in by the conduction heat transfer due to the difference between the temperature of the basement and the predicted indoor temperature *at time (p)*.

$U_{ap} A_{ap} \left(T_{ap}^{p} - \hat{T}_{in}^{p}\right)$ is the net *rate* at which energy is being transferred in by the conduction heat transfer due to the difference between the temperature of the apartment and the predicted indoor temperature *at time (p)*.

$\dot{Q}_{rad}^{p}$ is the net *rate* at which energy is being transferred in by the radiation heat transfer due to the different temperatures of the surfaces of the opposite inner walls *at time (p)*.

$\dot{Q}_{sol}^{p}$ is the net *rate* at which energy is being transferred in by the heat transfer due to the solar radiation *at time (p)*.

$\dot{Q}_{int}^{p}$ is the net *rate* at which energy is being transferred in by the radiation heat transfer due to the internal heat sources *at time (p)*.

$\dot{Q}_{aux}^{p}$ is the net *rate* at which energy is being transferred in by the heat transfer due to the capacity of the air-conditioning units *at time (p)* (auxiliary cooling).

U is the overall heat transfer coefficient.

A is the area in which heat transfer occurs.

Taking into account also that $\dot{W} = 0$ the energy rate balance becomes

$$m_{boox} c \frac{d\hat{T}_{in}}{dt} = \lambda A \frac{\left(T_{26}^{p} - T_{27}^{p}\right)}{\Delta x} + \sum_{i=1}^{n} U_i A_i \left(T_{out}^{p} - \hat{T}_{in}^{p}\right) + \sum_{j=1}^{m} U_j A_j \left(T_{des}^{p} - \hat{T}_{in}^{p}\right)$$
$$+ \sum_{k=1}^{o} U_k A_k \left(T_{ent}^{p} - \hat{T}_{in}^{p}\right) + U_{bas} A_{bas} \left(T_{bas}^{p} - \hat{T}_{in}^{p}\right) + U_{ap} A_{ap} \left(T_{ap}^{p} - \hat{T}_{in}^{p}\right) + \dot{Q}_{rad}^{p} + \dot{Q}_{sol}^{p} + \dot{Q}_{int}^{p} \pm \dot{Q}_{aux}^{p} \quad (7.14)$$

The solution of the differential Equation (7.14) is given by

$$\hat{T}_{in}^{p+1} = \hat{T}_{in}^{p} e^{\frac{-\left[\sum_{i=1}^{n} U_i A_i + \sum_{j=1}^{m} U_j A_j + \sum_{k=1}^{o} U_k A_k + U_{bas} A_{bas} + U_{ap} A_{ap}\right]}{mc} t} +$$
$$+ \left[\frac{\left[\lambda A \frac{\left(T_{26}^{p} - T_{27}^{p}\right)}{\Delta x} + \sum_{i=1}^{n} U_i A_i T_{out}^{p} + \sum_{j=1}^{m} U_j A_j T_{des}^{p} + \sum_{k=1}^{o} U_k A_k T_{ent}^{p} + U_{bas} A_{bas} T_{bas}^{p} + U_{ap} A_{ap} T_{ap}^{p} + \dot{Q}_{rad}^{p} + \dot{Q}_{sol}^{p} + \dot{Q}_{int}^{p} \pm \dot{Q}_{aux}^{p} \right]}{\sum_{i=1}^{n} U_i A_i + \sum_{j=1}^{m} U_j A_j + \sum_{k=1}^{o} U_k A_k + U_{bas} A_{bas} + U_{ap} A_{ap}} \right] \times \quad (7.15)$$
$$\times \left[1 - e^{\frac{-\left[\sum_{i=1}^{n} U_i A_i + \sum_{j=1}^{m} U_j A_j + \sum_{k=1}^{o} U_k A_k + U_{bas} A_{bas} + U_{ap} A_{ap}\right]}{mc} t} \right]$$

The following Figure 7.6 depicts the predicted indoor temperature based on Equation (7.15) in comparison with the measured indoor temperature from 18/9/2005 until 25/9/2005.

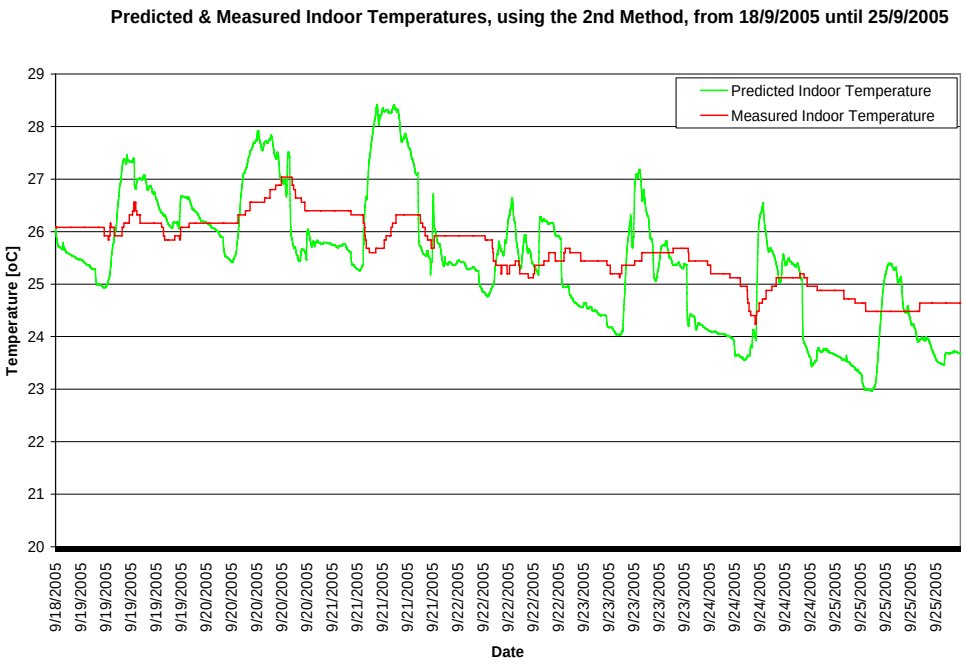

Figure 7.6: Predicted and Measured Indoor Temperatures of the Bookshop, using the 2nd Method, from 18/9/2005 until 25/9/2005.

Defining the Prediction Error (PE) as

$$PE = \sum_{p=1}^{n} \left(T_{in}^{p} - \hat{T}_{in}^{p} \right)^2 \tag{7.16}$$

where

T_{in}^{p} is the measured indoor temperature *at time (p)*
$\hat{T}_{in}^{p}$ is the predicted indoor temperature *at time (p)*
n is the number of investigated samples

For the examined period, the PE based on Equation (7.6) is 8.976 while the PE based on Equation (7.15) is 11.545. Consequently the prediction based on Equation (7.6) is proved to be more accurate relatively to the one on Equation (7.15).

It is noted that the volume of the bookshop is V = 175,17 m^3, the air density is ρ = 1,177 kg/m^3, the air mass of the bookshop is m = 206,15 Kg and the air specific heat is c = 0,718 KJ/KgK at 300K (Appendix A), [44], [45].

8 Pre-Cooling Phase

The Thermal Model is used for taking decisions for the pre-cooling phase. Experimental results are also presented in this chapter. Based on this approach, conclusions are achieved for the duration of the pre-cooling phase and for the reduction of the indoor temperature during this phase.

8.1 Super-Cooling Experimental Results

Several super-cooling experiments were realised in September 2005. The most extreme one is presented in Figures 8.1 and 8.2. Especially, Figure 8.1 shows the electrical power consumption of the air-conditioning units in comparison with the electrical power consumption of the bookshop on 8th September 2005. The air-conditioning units were operated from 3:00 until 17:00.

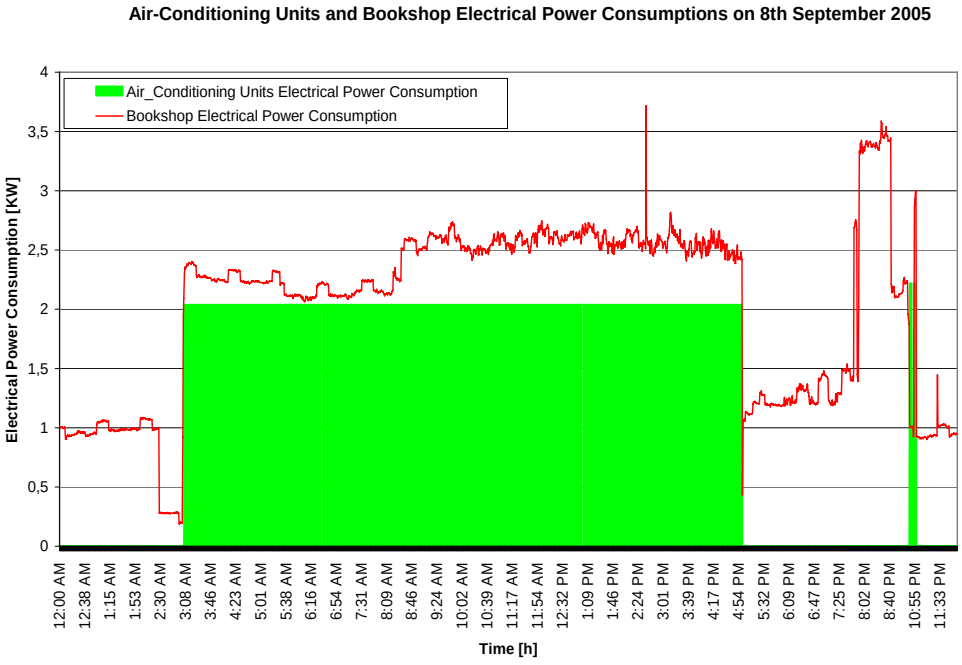

Figure 8.1: Electrical power consumption of the air-conditioning units in comparison with the bookshop electrical power consumption on 8th September 2005.

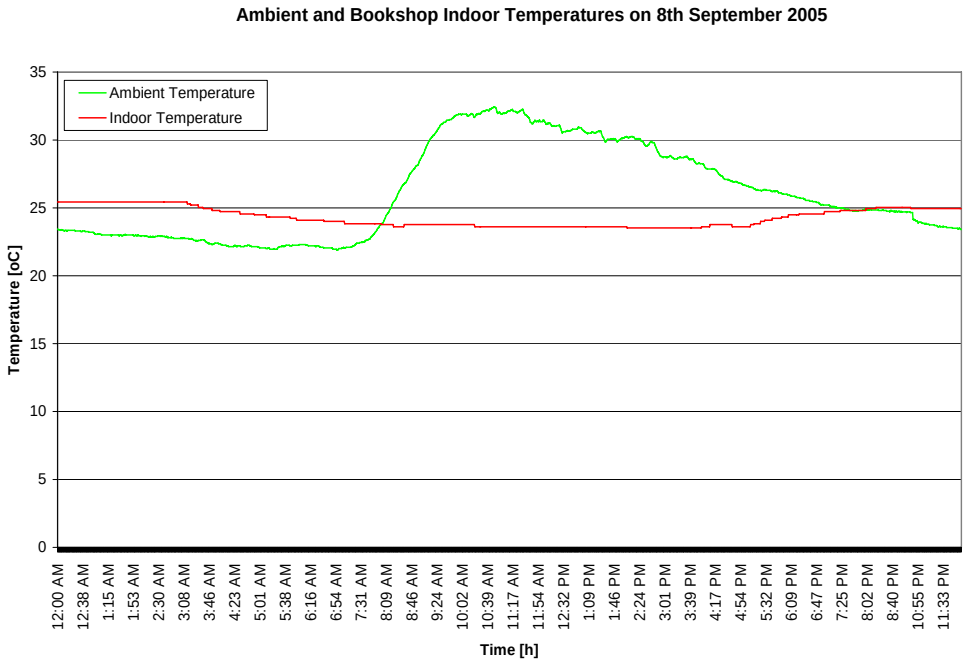

Figure 8.2a: Ambient and Indoor Temperatures on 8th September 2005.

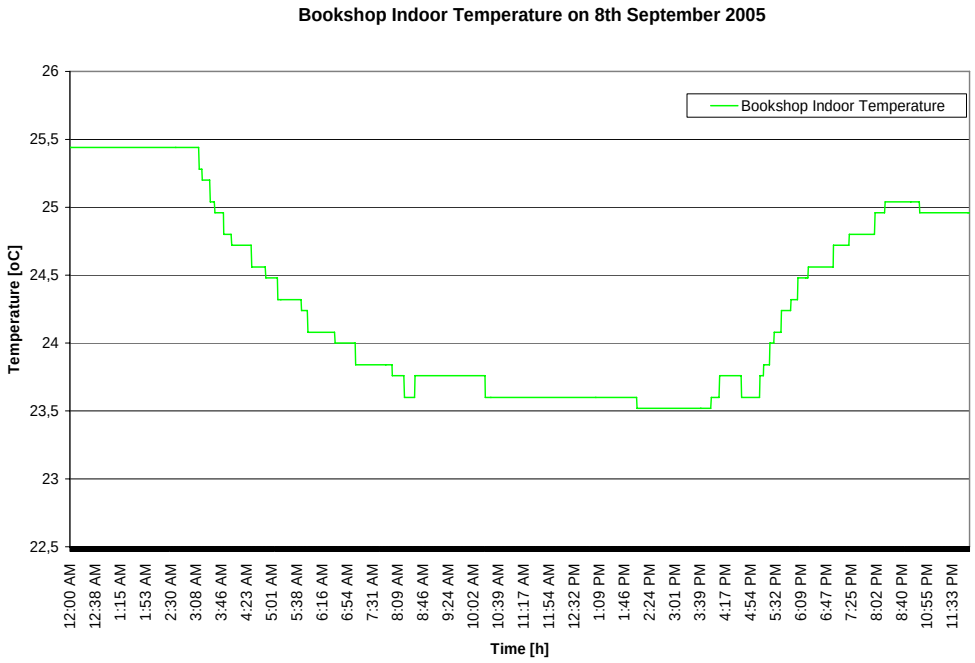

Figure 8.2b: Bookshop Indoor Temperature on 8th September 2005.

The above Figures 8.2a and 8.2b show the ambient and bookshop indoor temperatures on 8th September 2005. It is obviously that the indoor temperature is not increased more than 25°C during the peak period. The following Figure 8.3 presents the electrical power consumption of the air-conditioning units in comparison with the electrical power consumption of the bookshop on 15th September 2005, which is also a typical summer day. Comparing Figures 8.1 and 8.3 it is inferred that there is a significant peak reduction (approximately 30%), when the super-cooling experiment is realised on 8th September.

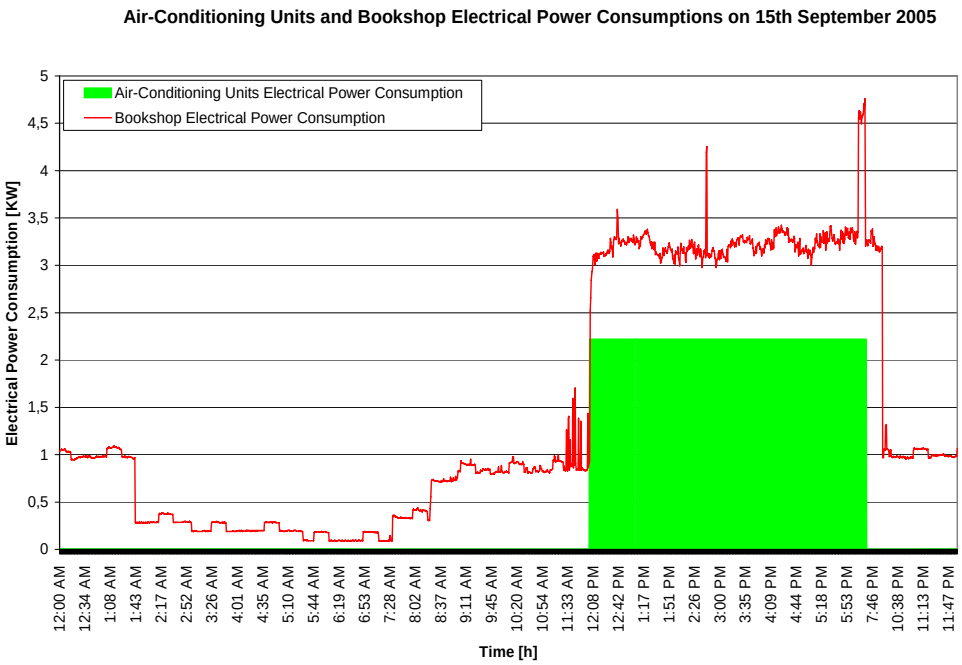

Figure 8.3: Air-conditioning units and bookshop electrical power consumptions for a typical summer day, on 15th September 2005.

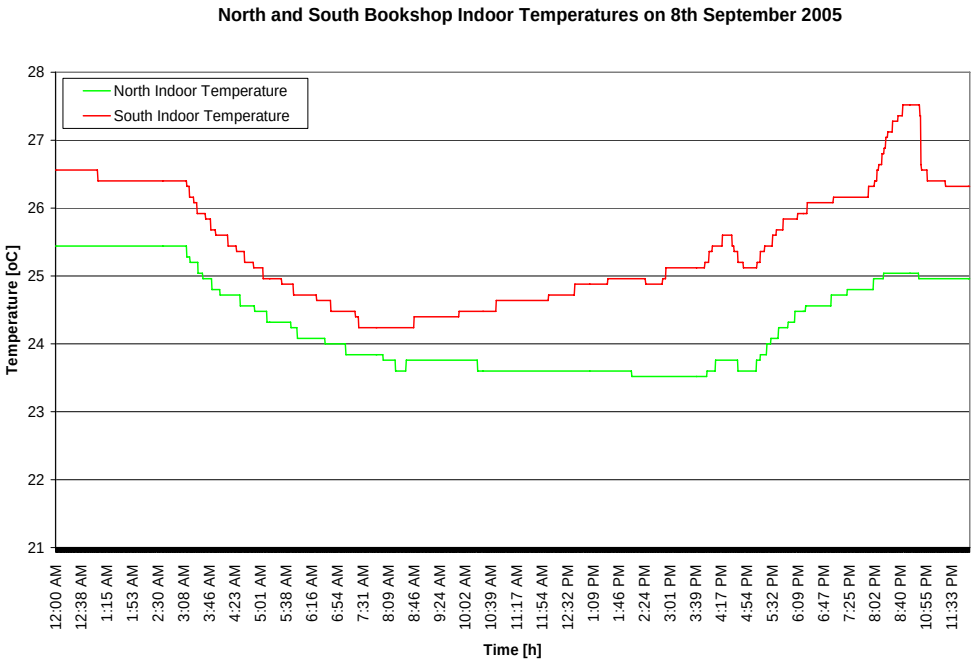

Figure 8.4: North and South Bookshop Indoor Temperatures on 8th September 2005.

The above Figure 8.4 depicts the south and north bookshop indoor temperatures on 8th September 2005. The north temperature is the reference temperature in all the experiments in this thesis. The roof glazing of the bookshop is built in the south side and its area is one quarter of the total roof. However, its lighting power is about 1KW, approximately equal to all other bookshop lighting electrical power consumption. The result was that the temperature in this specific area was increased about to 28°C on 8th September, making the situation uncomfortable for the users. This is the reason why

the owner didn't permit the application of a Demand Side Management Strategy in the bookshop. The conclusions for the pre-cooling phase are derived through simulation results and presented in the following section.

8.2 Super-Cooling Simulation Results

Using the Thermal Model derived in Chapters 4, 5, 6 and 7, the indoor temperature is predicted as in Figure 7.5 or 7.6, based on Equations (7.6) and (7.15) respectively. In the following simulations, the air-conditioning units are switched on at 18:00 on 19th September 2005. Three cases are examined, where the indoor temperature is decreased by 1°C, 10°C and 15°C respectively. The following Figures 8.5, 8.6 and 8.7 depict the simulation results for these cases.

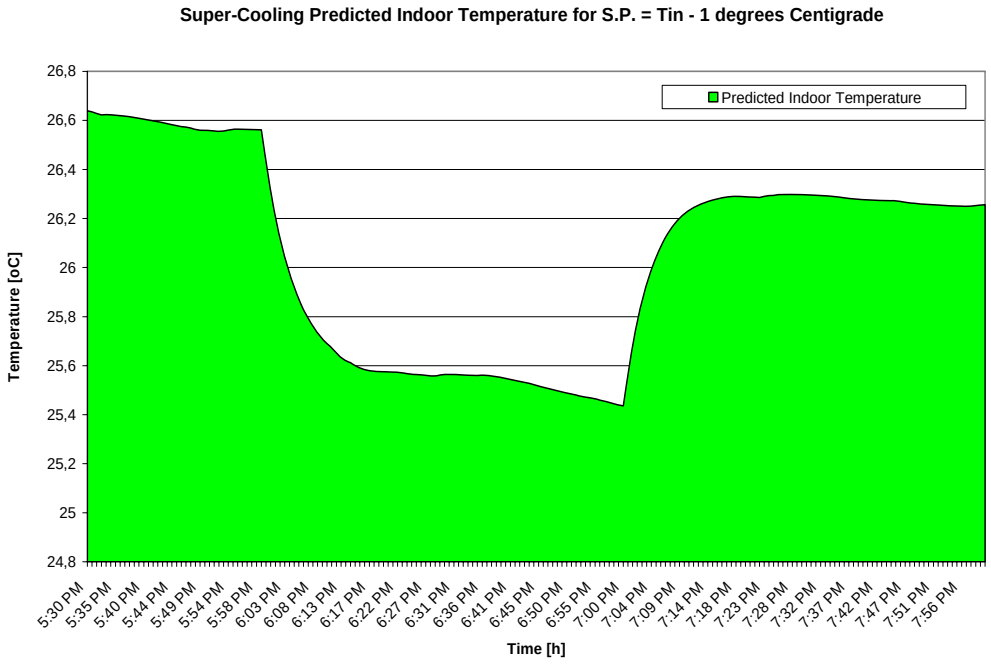

Figure 8.5: Predicted Bookshop Indoor Temperature for S.P = Tin – 1°C on 19th September 2005.

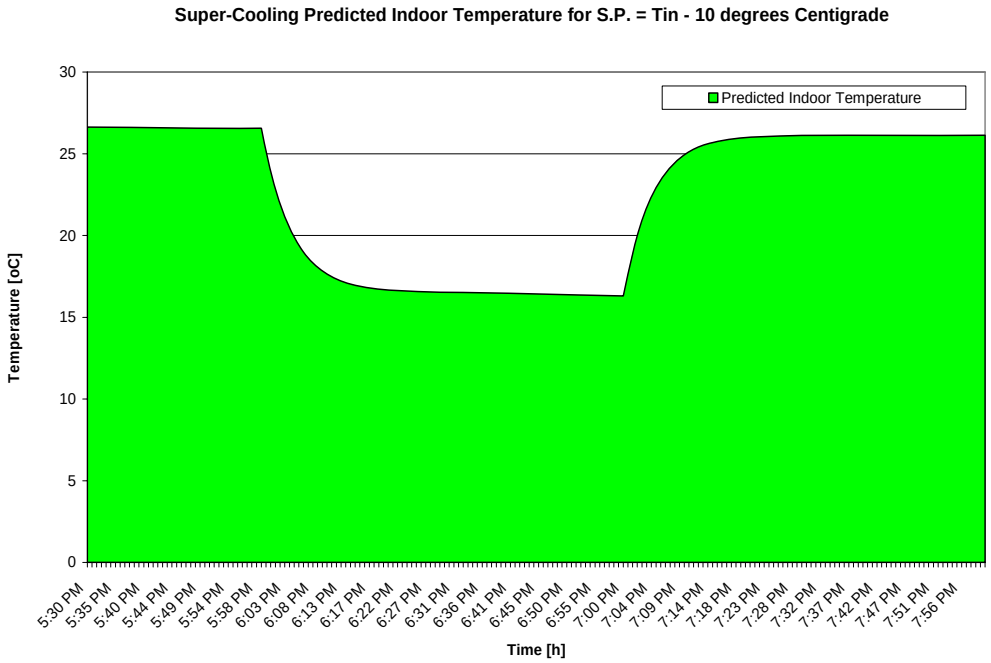

Figure 8.6: Predicted Bookshop Indoor Temperature for S.P = Tin – 10^{o}C on 19th September 2005.

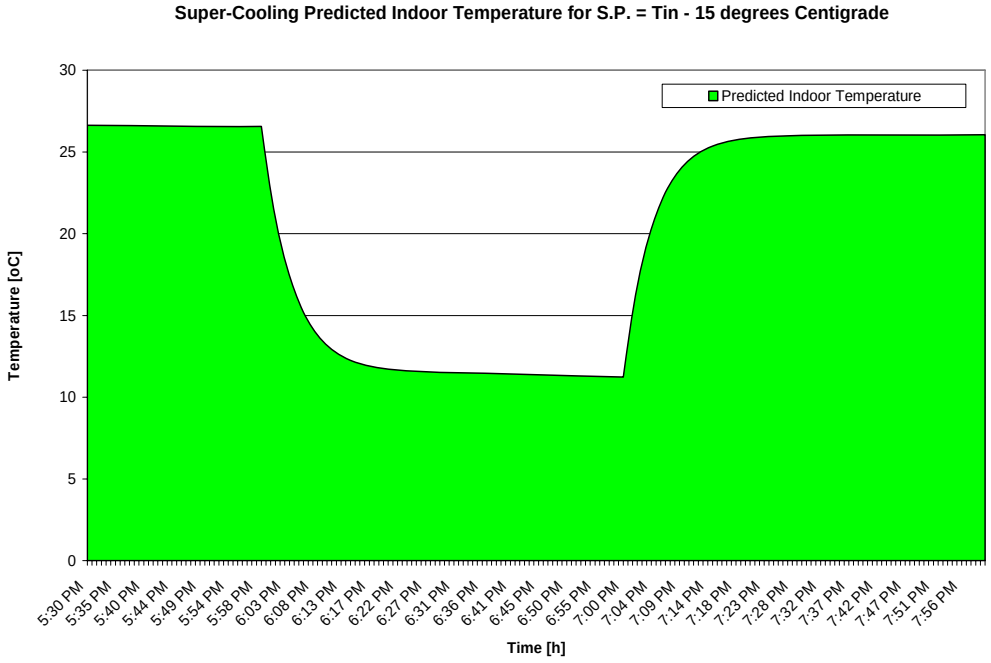

Figure 8.7: Predicted Bookshop Indoor Temperature for S.P = Tin – 15^{o}C on 19th September 2005.

The simulation results from the above Figures 8.5, 8.6 and 8.7 illustrate that the predicted indoor temperature is decreased by 1^{o}C, or 10^{o}C or 15^{o}C in 26 minutes. Taking into account that at 18:00 the indoor temperature was approximately 26,5^{o}C, the indoor temperature is decreased to 25,5^{o}C, or to 16,5^{o}C, or to 11,5^{o}C in 26 minutes and is increased again to 26,5^{o}C at the same time, when the air-conditioning units are switched off. Therefore, the conclusions are the followings:

- **the pre-cooling period is independent from the indoor temperature reduction**
- **the pre-cooling period must be 26 minutes at maximum**
- **during the peak period, the air-conditioning units can be switched off for the pre-cooling period of 26 minutes, keeping thermal comfort for the users.**

The above-mentioned conclusions are of paramount importance for Thermal Model Predictive Controller design and analysis.

9 Thermal Model Predictive Controller Design

An approach to Thermal Model Predictive Controller (TMPC-DSM) design is presented in this chapter. This is realised by using the Thermal Model derived in Chapters 4, 5, 6, 7 and the conclusions for the pre-cooling phase obtained in Chapter 8. Optimization algorithms which produce the optimal controller output sequences over the prediction horizons of pre-cooling and DSM phases are developed and shown in the present chapter. Further, the development of a Power Predictor, which informs the controller when the peak demand occurs and its duration, completes the requirements of TMPC-DSM design.

9.1 Optimization Algorithms

The Thermal Model Predictive Controller acts during the pre-cooling and DSM phases. For each phase, an optimization algorithm is developed and implemented for the controller output. This algorithm is under the constraints of:

- maximum peak demand P_{peak},
- minimum indoor temperature T_{in_min}
- maximum indoor temperature T_{in_max}

and

- maximum permitted electrical power consumption of air-conditioning units P_{cool_max}.

9.1.a Pre-cooling Optimization Algorithm

The pre-cooling period algorithm aims to reduce the indoor temperature to a certain temperature $T_{cooling}$, which is defined by the analysis of the thermal model. The prediction horizon H_p is the number of samples equal to the pre-cooling period. It is reminded that the sampling time is defined by the thermal model when the stability criterion is satisfied according to the finite difference calculation. The necessity of the pre-cooling phase is decided by predicting the indoor temperature during the peak period, assuming that no any special action occurs during the pre-cooling phase. In the case where the pre-cooling phase is needed, an indoor temperature reduction of about 1^oC is enough in order a DSM cooling strategy to be applied.

The Pre-cooling optimization algorithm is based on a uniform search where we decide beforehand the points at which the functional evaluations are to be made [46]. The interval of uncertainty is defined by the difference between the predicted indoor temperature at the end of the Pre-cooling phase ($\hat{T}_{in}^{p+Hp}$) and the desired $T_{cooling}$ one at

this sample (p+Hp). This interval is divided into smaller subintervals via the grid points $u_i = u_i + \mu$, where μ is a small increase of the electrical power consumption of the air-conditioning units for the entire prediction horizon. The difference between the predicted indoor temperature at the end of the Pre-cooling phase and the desired $T_{cooling}$ one is evaluated at each increase of the electrical power consumption of the air-conditioning units (u_i). If this difference is small enough to be acceptable $\left|\hat{T}_{in}^{p+Hp} - T_{cooling}\right| \le \varepsilon$, optimal solution is achieved and only the first element of the controller output sequence (u_1) is used to control the process. At the next sample (hence, at p+1), the whole procedure is repeated, while the prediction horizon is adaptive and at every sample is reduced by one, until the controller changes to DSM phase.

When no optimal solution is found and the electrical power consumption of the air-conditioning units reaches at its maximum permitted value, the first element of the controller output sequence with this maximum electrical power consumption of the air-conditioning units is used to control the process ($u_1 = P_{cool\_max}$). It is obviously, that if we desire a small final interval of uncertainty, then a large number of function evaluations must be made. The Pre-cooling algorithm is:

Pre-cooling Algorithm

Step 1: Initialization step. $\mathbf{u_0} = [u_1, \ldots, u_{Hp}]$, where Hp is the prediction horizon, $\mathbf{u_0} = \text{old}\mathbf{u} = \mathbf{0}$ and $\text{old}\left|\hat{T}_{in}^{p+1} - T_{cooling}\right|$ is a huge number.

Step 2: Using the Thermal Model predict $\hat{T}_{in} = \left[\hat{T}_{in}^{p+1}, \cdots, \hat{T}_{in}^{p+Hp}\right]$.

Step 3: **If** $\left|\hat{T}_{in}^{p+Hp} - T_{cooling}\right| \le \varepsilon$ and $\forall \hat{T}_{in}^{p+i}$, $T_{in\_min} \le \hat{T}_{in}^{p+i} \le T_{in\_max}$, where $0 \le i \le Hp$ and ε is a small number, Optimal solution found

End If

Go to step 4

Else if $\left|\hat{T}_{in}^{p+Hp} - T_{cooling}\right| > \text{old}\left|\hat{T}_{in}^{p+Hp} - T_{cooling}\right|$ formulate $\forall u_i \quad u_i = \text{old}u_i$ for $0 \le i \le Hp$, Optimal solution found

Go to step 4

End If

Else

Formulate $\text{old}\left|\hat{T}_{in}^{p+Hp} - T_{cooling}\right|$ and $\forall u_i \quad \text{old}u_i = u_i$ for $0 \le i \le Hp$

Calculate $\forall u_i$, $u_i = u_i + \mu$, for $0 \le i \le Hp$, where μ is a small increase of the controller output and $\exists$ an integer κ which satisfies $\kappa \bullet \mu = P_{cool\_max}$.

If $\forall u_i, u_i < P_{cool\_max}$

End If

Go to step 2

Else

$\forall u_i \quad u_i = \text{old}u_i$ for $0 \le i \le Hp$

Step 4: Apply u_1 to air-conditioning units

$\kappa = \kappa$-1
If $\kappa > 0$
End If
Wait until next step
Else
Termination of Pre-cooling Phase

In every sample, the controller output is initialised by the vector of dimension 1 X Hp, $\mathbf{u_0} = [u_1, \ldots, u_{Hp}]$, containing the variables for which the criterion is optimised. However, the initialization of the algorithm assumes that the air-conditioning units are switched off, $\mathbf{u_0} = [0, \ldots, 0]$. This way, the search direction is always positive. Further, κ denotes the maximum number of iterations and μ denotes the step size in the search direction. A special case is the one in which the air-conditioning units can be controlled to discrete values, e.g. every 1KW. In this case $\mu = 1$ KW.

It is noted that the term *old* denotes a vector or a scalar at the previous sample. Note also that at each sample holds: $u_1 = u_2 = \ldots = u_{Hp}$.

9.1.b DSM Optimization Algorithm

Respectively, the DSM algorithm aims to reduce the peak at a feasible minimum value, where the maximum permitted electrical power consumption of the air-conditioning units is P_{cool_max}. The prediction horizon H_p is the number of samples equal to the peak period. The DSM optimization algorithm is also based on a uniform search as the Pre-cooling one, where we decide beforehand the points at which the functional evaluations are to be made. The predicted indoor temperatures by the thermal model as well as the predicted electrical power consumptions of the air-conditioning units are evaluated at each sample of the prediction horizon. If the predicted electrical power consumptions of the air-conditioning units are less than a threshold electrical power consumption at each sample ($u_i < P_{cool\_max}$), while the predicted indoor temperatures yield thermal comfort during the DSM phase ($\hat{T}_{in}^{p+i} \leq T_{in\_max}$), then optimal solution is achieved. Further, only the first element of the controller output sequence (u_1) is used to control the process. At the next sample (hence, at p+1), the whole procedure is repeated, while the prediction horizon is adaptive and at every sample is reduced by one until the controller terminates the DSM phase.

If the predicted indoor temperature is greater than a desired maximum limit (T_{in_max}) at one sample, then the controller output is increased by $u_i = u_i + \mu$, where μ is a small increase of the electrical power consumption of the air-conditioning units for the entire prediction horizon. If the increase of the controller output results in the electrical power consumption of the air-conditioning units to reach at its maximum permitted value ($u_i = P_{cool\_max}$), then the SCADA asks the user to accept an increased indoor temperature explaining the economic benefits. If the user accepts it, the process continues normally. If he does not accept it, the controller changes to manual mode and the Thermal Model Predictive Controller is deactivated. The DSM algorithm is:

DSM Algorithm

Step 1: Initialization step. $\mathbf{u_0} = [u_1, \ldots, u_{Hp}]$, where Hp is the prediction horizon, $\mathbf{u_0} = \mathbf{0}$

Step 2: Using the Thermal Model predict $\hat{T}_{in} = \left[\hat{T}_{in}^{p+1}, \cdots, \hat{T}_{in}^{p+Hp}\right]$

Step 3: **If** $\forall u_i$, $u_i < P_{cool\_max}$ and $\forall \hat{T}_{in}^{p+i}$, $\hat{T}_{in}^{p+i} \le T_{in\_max}$, where $0 \le i \le Hp$ Optimal solution found

End If

Go to step 4

Else If $\forall u_i$, $u_i = P_{cool\_max}$ SCADA suggests the user to accept the predicted indoor temperature explaining the economic benefits

If the user accepts the SCADA suggestion

End If

Go to step 4

Else turn to **Manual Mode**

Termination of DSM phase

Else

Calculate $\forall u_i$, $u_i = u_i + \mu$, for $0 \le i \le n$, where μ is a small increase of the controller output and $\exists$ an integer κ which satisfies $\kappa \bullet \mu = P_{cool\_max}$.

Go to step 2

Step 4: Apply u_1 to air-conditioning units

$\kappa = \kappa - 1$

If $\kappa > 0$

End If

Wait until next step

Else

Termination of DSM Phase

As in the Pre-cooling optimization algorithm, in every sample, the controller output is initialised by the vector of dimension 1 X Hp, $\mathbf{u_0} = [u_1, \ldots, u_{Hp}]$, containing the variables for which the criterion is optimised. The initialization of the algorithm also assumes that the air-conditioning units are switched off, $\mathbf{u_0} = [0, \ldots, 0]$. This way, the search direction is always positive. Further, κ denotes the maximum number of iterations and μ denotes the step size in the search direction. Note that at each sample holds: $u_1 = u_2 = \ldots = u_{Hp}$.

9.2 Power Predictor

The Power Predictor, which is mentioned in Chapter 3, is a stochastic model based on a k-step ahead prediction horizon and informs the TMPC-DSM controller when the peak demand occurs and its duration. This stochastic model can be developed as an ARMAX (Auto Regressive eXogenous Moving Average) Model, or a NARMAX (Nonlinear ARMAX) Model, or a FIR (Finite Impulse Response) Model, or a Model based on Neural Networks, etc. [15], [35], [36] and [37]. It is noted that the peak period of the bookshop is predicted by the SCADA Power Predictor, which has been developed as an ARMAX Model (Figure 2.14 – tab **"ESTIMATIONS"**). However, the analysis of the TMPC-DSM controller is based on simulation results in Chapter

10, and it is assumed that the Power Predictor predicts the peak demand without modelling errors.

10 Thermal Model Predictive Controller Analysis

The behaviour of the Thermal Model Predictive Controller is analysed in this chapter. Comparisons of energy and cost savings through different cooling strategies are presented. The European Energy Exchange (EEX) data are used for this purpose [47]. Different price scenarios are also investigated during the peak period.

10.1 European Energy Exchange (EEX) Data

Figure 10.1 presents the hourly prices of electricity from 18/9/2005 until 25/9/2005 taken by EEX. Obviously, the maximum cost of electricity occurs at 9:00 and 18:00 every day. It is noted that the hours are given in U.T.C. time normal. According to the analysis of the electrical power consumption of the bookshop, the air-conditioning units start to operate usually after 11:00. Therefore, a DSM cooling strategy can not be applied during morning, when the peak price occurs at 9:00.

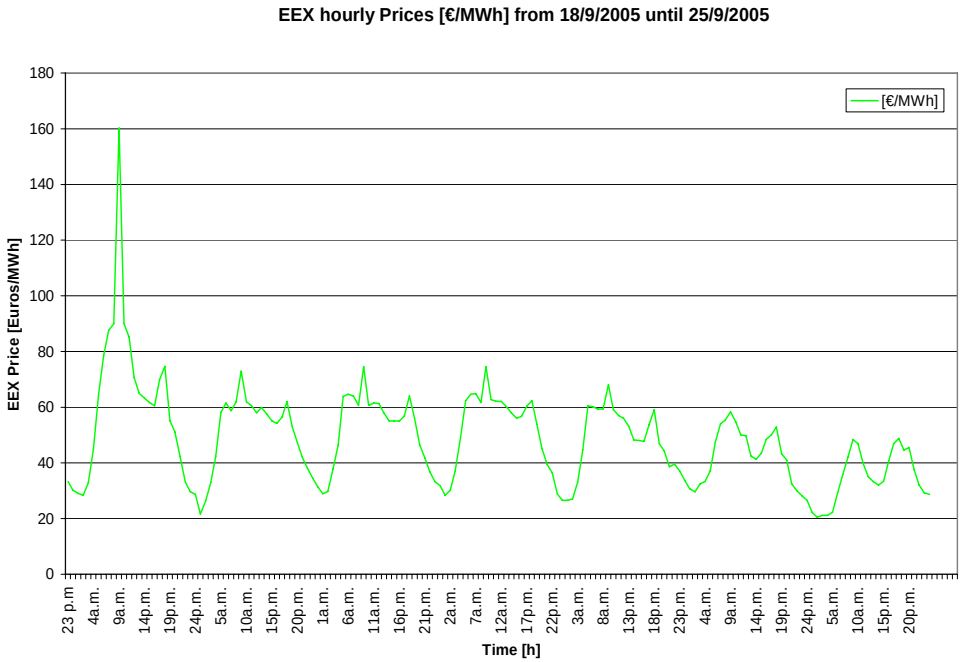

Figure 10.1: EEX hourly prices from 18/9/2005 until 25/9/2005.

10.2 Thermal Model Predictive Controller Analysis for DSM Cooling Strategies

Recalling Figure 6.5, the peak demand of the bookshop occurs at 19:00 and its duration is 2 hours, which is the prediction horizon of the DSM phase. It is reminded that the pre-cooling period is 26 minutes at maximum. Therefore, the prediction horizon of the pre-cooling phase is also 26 minutes and is reduced by 47 seconds at every sample. The maximum desired predicted indoor temperature is defined to T_{in_max} = 27^{o}C. The following Figure 10.2 depicts the predicted indoor temperature using the TMPC-DSM controller in comparison with the predicted and measured indoor temperatures from 18/9/2005 until 25/9/2005. It is noted that in this chapter, the analysis of the TMPC-DSM controller is carried out by means of simulations based on the 1st Method for Indoor Temperature Prediction in Chapter 7, Equation (7.6), while the predicted and measured indoor temperatures are also shown in Figure 7.5.

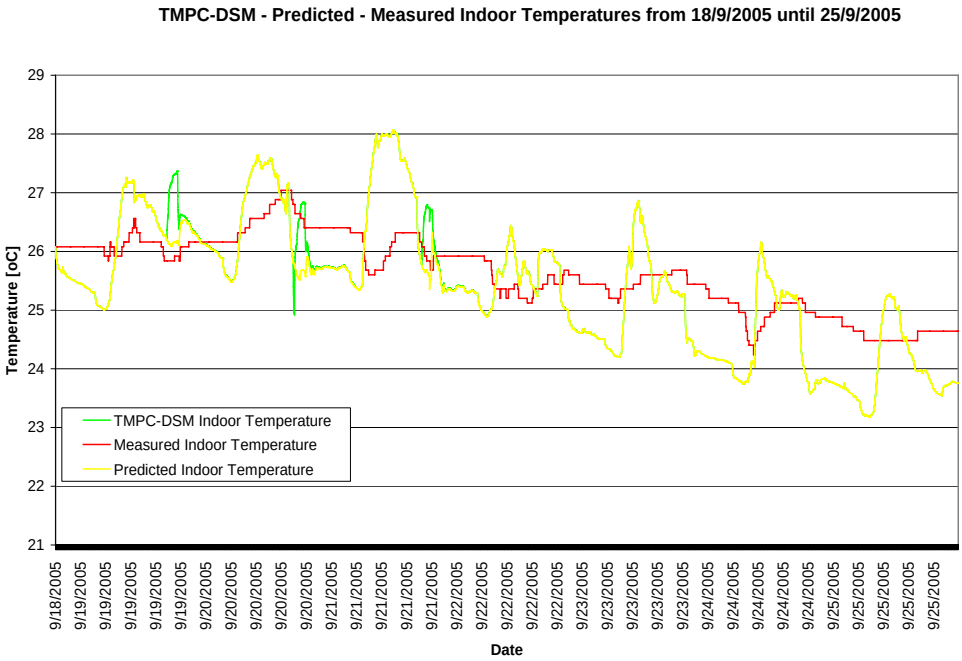

Figure 10.2: Predicted indoor temperature using the TMPC-DSM controller in comparison with the predicted and measured indoor temperatures from 18/9/2005 until 25/9/2005.

More details for the above-mentioned simulation results are shown in the following Figures 10.3, 10.4 and 10.5, which depict the predicted indoor temperatures during the Pre-cooling and DSM phases in comparison with the predicted and measured indoor temperatures on 19th, 20th and 21st September 2005. Three different cases are investigated respectively these days, when the bookshop is opened during afternoon.

More specifically, Figure 10.3 illustrates that the SCADA suggests the user to accept the indoor temperature which reaches 27,5^{o}C on 19th September. The SCADA informs the user that if the indoor temperature is decreased to 27^{o}C during the peak demand for that day, then an additional electric energy consumption of 1,67 KWh will occur. That will cost him €0,12 due to the increased operation of the air-conditioning units during the Pre-cooling and DSM phases. It is assumed that the user accepts this

increase of the indoor temperature in our simulation results. If he does not accept it, the Thermal Model Predictive Controller will be deactivated and the indoor temperature will be regulated by the KNX/EIB thermostat (Figure 2.7). In this case, the SCADA will inform him about the economic benefits from applying the DSM cooling strategy. It is reminded that the DSM cooling strategy is obtained only by using the TMPC-DSM controller in this thesis.

Furthermore, according to the indoor temperature prediction during the peak period, the Pre-cooling Phase is needed only on 20th September as it is shown in Figure 10.4. Both, the Pre-cooling and DSM optimization algorithms are applied for that day.

Finally, Figure 10.5 depicts that the predicted indoor temperature reaches 27^{o}C on 21st September during the DSM phase and without the use of the Pre-cooling phase. Only the DSM optimization algorithm is applied for this day.

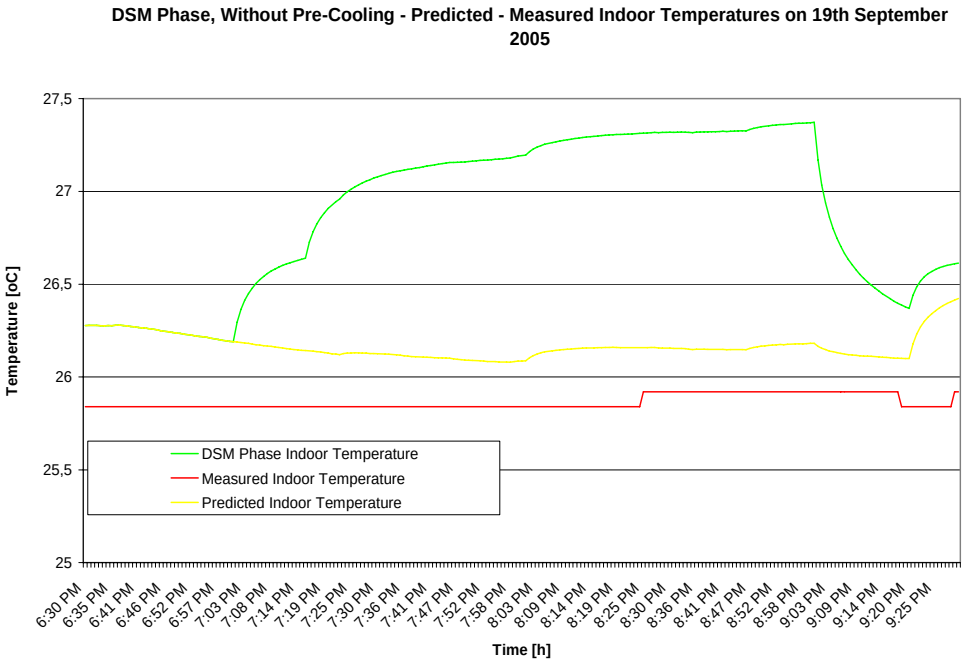

Figure 10.3: Predicted indoor temperature during the Pre-cooling and DSM phases in comparison with the predicted and measured indoor temperatures on 19th September 2005.

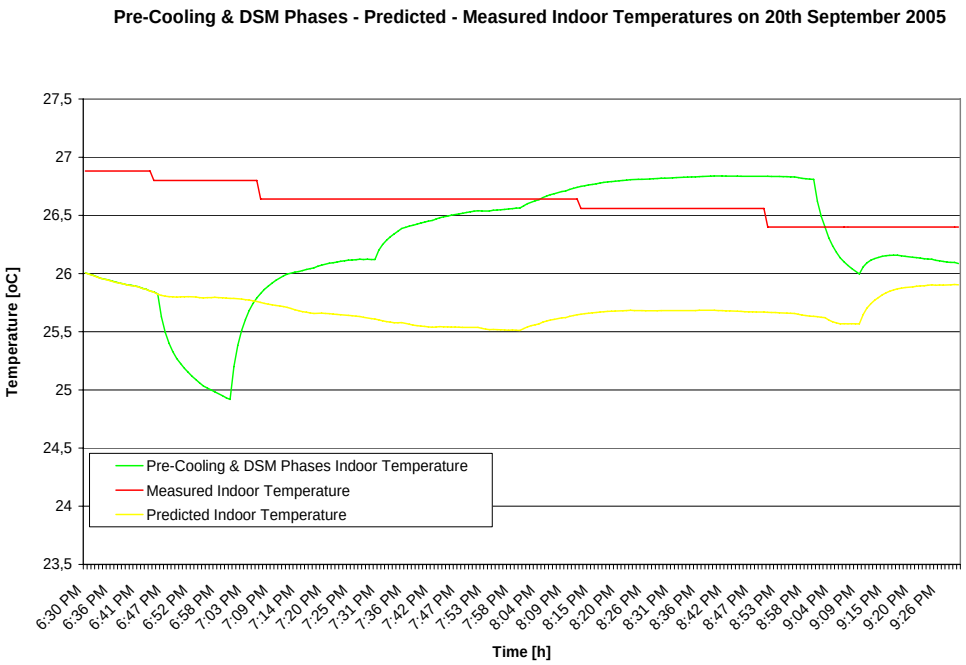

Figure 10.4: Predicted indoor temperature during the Pre-cooling and DSM phases in comparison with the predicted and measured indoor temperatures on 20th September 2005.

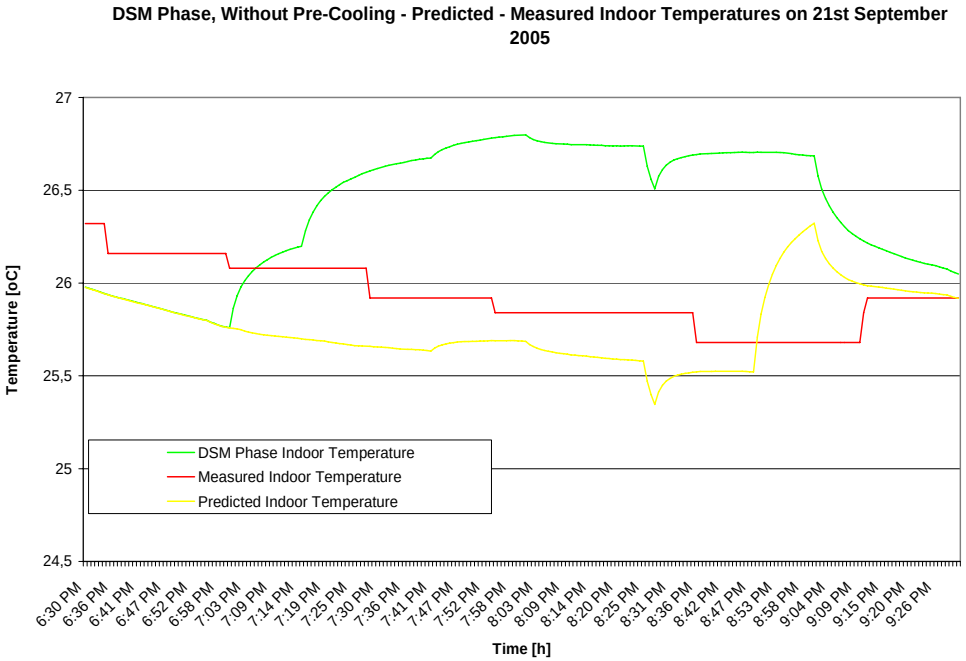

Figure 10.5: Predicted indoor temperature during the Pre-cooling and DSM phases in comparison with the predicted and measured indoor temperatures on 21st September 2005.

The following Figure 10.6 depicts the measured electrical power consumption of the bookshop in comparison with that which will be derived if the DSM cooling strategy is applied from 18/9/2005 until 25/9/2005.

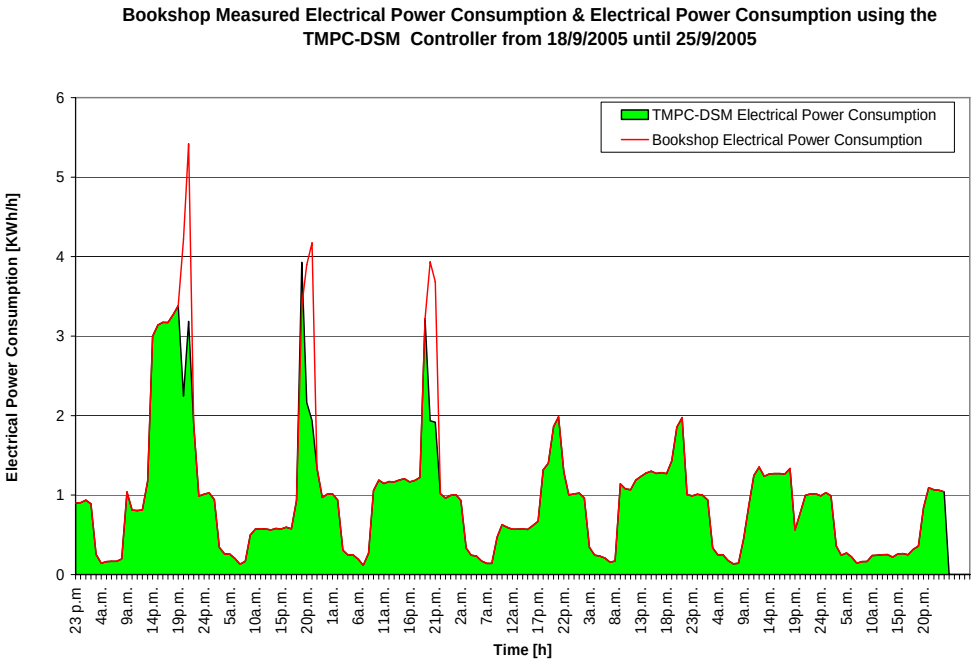

Figure 10.6: Measured electrical power consumption of the bookshop in comparison with that from applying the DSM cooling strategy from 18/9/2005 until 25/9/2005.

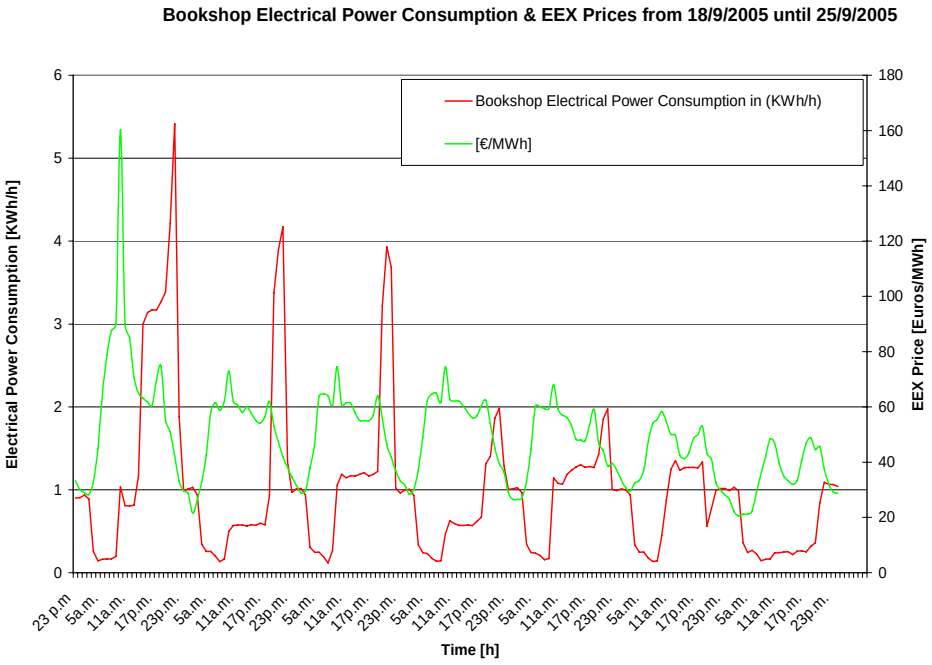

Figure 10.7a: Measured electrical power consumption of the bookshop and EEX prices from 18/9/2005 until 25/9/2005.

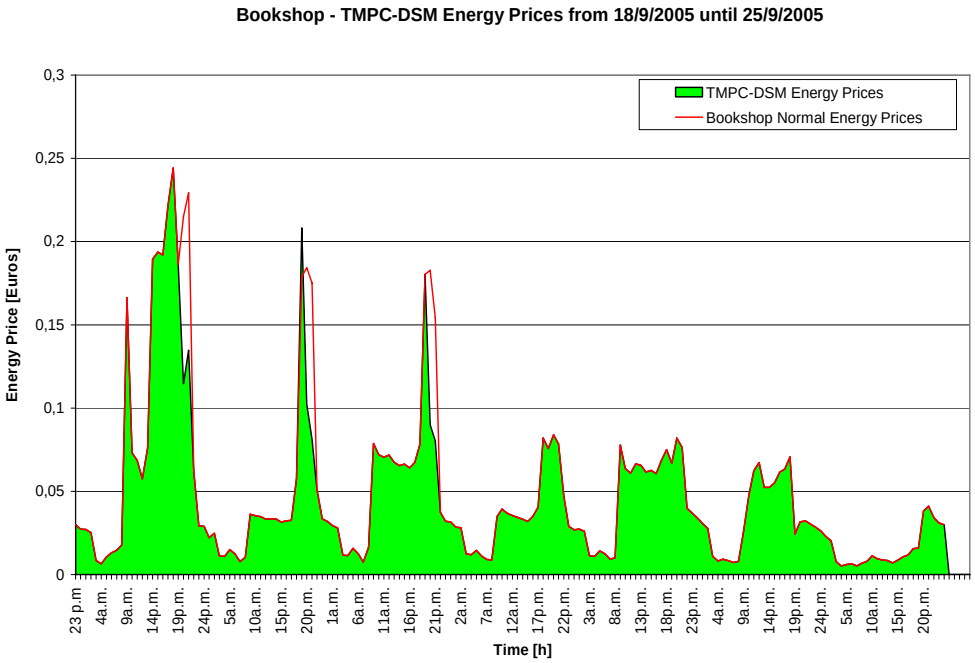

Figure 10.7b: Prices of the measured electric energy consumption of the bookshop and the prices which will be derived if the DSM cooling strategy is applied from 18/9/2005 until 25/9/2005.

The analysis of Figures 10.6, 10.7a and 10.7b shows that the electric energy consumption of the bookshop is 168.558,3 Wh with €8,2 cost from 18/9/2005 until 25/9/2005. By applying the DSM Cooling Strategy, the energy consumption is reduced to 157.183 Wh with €7,69 cost for the same period. Therefore, **energy savings of 6,75% with cost savings of 6,19% are achieved by applying the DSM cooling strategy using the TMPC-DSM controller.**

In the case where the maximum EEX prices occur during the peak demand as it is shown in Figure 10.8a, the following Figure 10.8b depicts the cost profile of the energy consumption of the bookshop with the maximum prices during the electric peak demand and the prices which will be derived if the DSM cooling strategy is applied from 18/9/2005 until 25/9/2005. In this case the energy savings are the same as in Figure 10.6; however, the cost of energy is reduced from €9,3 to €8,56 by using the TMPC-DSM controller; **attaining cost savings of 7,94%.**

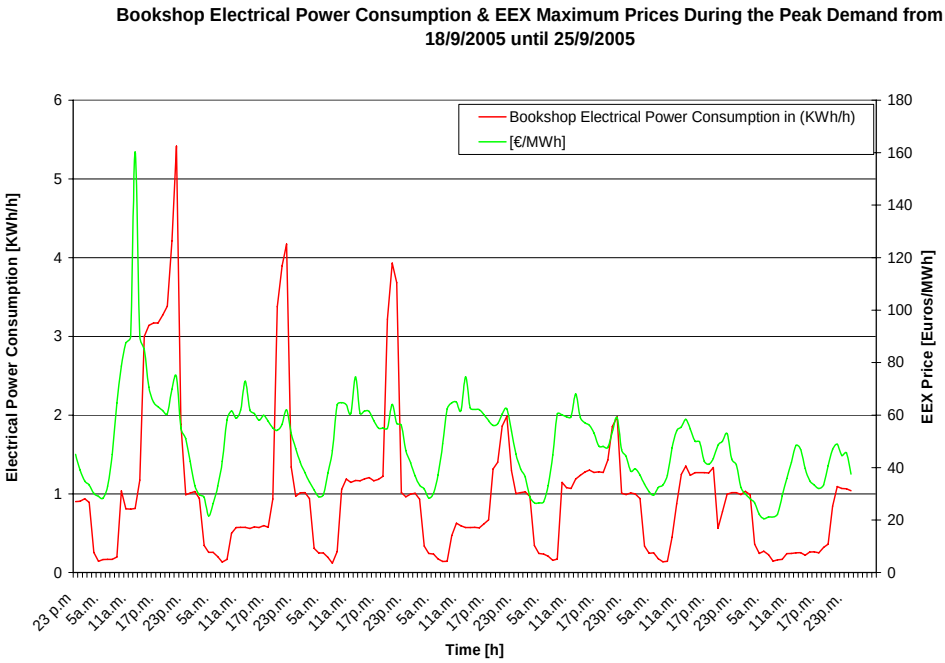

Figure 10.8a: Measured electrical power consumption of the bookshop and EEX prices where the maximum ones occur during the peak demand from 18/9/2005 until 25/9/2005.

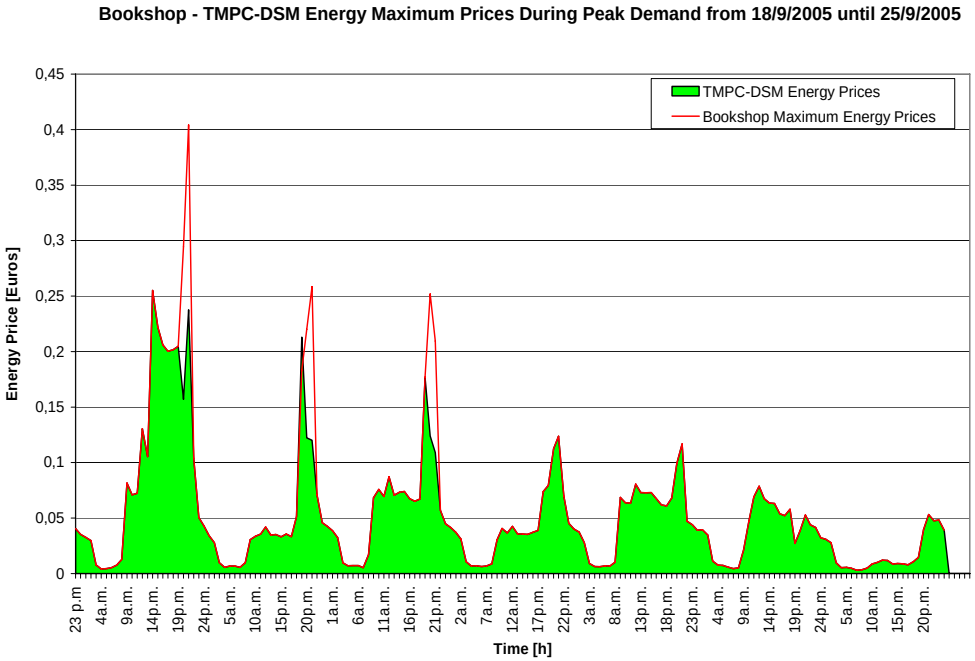

Figure 10.8b: Cost profile of the measured electric energy consumption of the bookshop with the maximum prices during the peak demand and the prices which will be derived if the DSM cooling strategy is applied from 18/9/2005 until 25/9/2005.

The following Table 10.1 illustrates the total with the daily energy and cost savings, by the application of the TMPC-DSM controller.

Date	Without TMPC-DSM (KWh)	TMPC-DSM (KWh)	Energy Savings (%)
19/9/2005	40,2	36	10,44
20/9/2005	24,14	20,73	14,14
21/9/2005	28,84	25,08	13,05
Total (3 Days)	**93,18**	**81,81**	**12,21**
Total (week)	**168,6**	**157,19**	**6,75**

Table 10.1a: Total and daily energy savings using the TMPC-DSM controller.

Date	Without TMPC-DSM (€)	TMPC-DSM (€)	Cost Savings (%)
19/9/2005	2,75	2,45	11,05
20/9/2005	1,29	1,09	15,96
21/9/2005	1,63	1,4	14,05
Total (3 Days)	**5,67**	**4,93**	**13,03**
Total (week)	**9,3**	**8,56**	**7,94**

Table 10.1b: Total and daily cost savings using the TMPC-DSM controller.

It is noted that the term of the daily savings is the percentage of daily savings by using the TMPC-DSM controller in comparison with the bookshop energy consumption or energy cost for that day. For example, the energy savings on 19th September according to Table 10.1a are:

$$\frac{40,2-36}{40,2}\bullet 100\% = 10,44\% \tag{10.1}$$

Respectively, the term of the total week savings is the percentage of week savings by using the TMPC-DSM controller in comparison with the bookshop energy consumption or energy cost for that week. For example, the cost savings on this examined week in September according to Table 10.1b are:

$$\frac{9,3-8,56}{9,3}\bullet 100\% = 7,94\% \tag{10.2}$$

Normally, the bookshop is opened during afternoon only three days per week. If the foregoing calculations concerning the energy and cost savings are taken into consideration only the days when the air-conditioning units are activated during afternoon (19th, 20th and 21st September 2005), the energy savings are 12,21% and the cost is reduced from €5,67 to €4,93 **yielding cost savings of 13%.**

11 Conclusions and Recommendations

11.1 Conclusions

A Thermal Model Predictive Controller for DSM Cooling Strategies is presented in this report. One of the attractive results of the approach adopted in the report is that a simplified thermal model based on finite difference calculation, assuming that there is one-dimensional conduction in x, can describe adequately the dynamics of the system. Furthermore, the Thermal Model Predictive Controller is applied to a bookshop in Athens, which is examined in this report.

The Thermal Model Predictive Controller has three basic elements. First, the Thermal Model is used for the prediction of the indoor temperature during pre-cooling and DSM phases. In addition, it calculates the heat fluxes of the walls and the Inflow, Outflow and Stored energies of the examined room. The Thermal Model plays a significant role in order to define the duration of the pre-cooling phase. General conclusions are derived for this phase:

- the pre-cooling period is independent from the indoor temperature reduction.
- the pre-cooling period is defined as the time period which is needed for the reduction of the indoor temperature by e.g. $1^{o}C$ before the peak demand occurs.
- during the peak period, the air-conditioning units can be switched off for the time of the pre-cooling period, keeping thermal comfort for the users.

The second basic element of the TMPC-DSM controller is the Power Predictor. This is a Stochastic Model which predicts the total power consumption based on a k-step ahead prediction horizon. The Stochastic Model informs the Predictive Controller for the time period, where the peak demand occurs. Further, optimization algorithms are developed in order to produce the optimal controller output sequences over the prediction horizons of the pre-cooling and peak periods. These algorithms integrate the TMPC-DSM controller. Moreover, it is simple for the TMPC-DSM to be applied or to be integrated in Energy Management Systems.

User behaviour has a large influence on energy consumption of buildings. In addition, there is a lack of knowledge about energy consumption, energy costs and energy processes in general. Building automation can contribute significantly to energy savings. However, a full automated building is against its user’s control. This makes the user to feel uncomfortable in it avoiding any energy saving functions.

In this thesis, an energy management system is developed allowing a communication between the user and the building. The main developments and results of the work are:

1. Interconnection of building automation (here the Konnex - European Installation Bus, KNX/EIB) with Intranet/Internet and energy counter. This information structure allows the distribution of information between the building and any other user.

2. There is a communication process between the user and the building automation. The functions of Thermal Model Predictive Control for DSM actions, heating/cooling and lighting control are integrated in a flexible energy management system using a Supervisory Control and Data Acquisition system (SCADA). The user decides the maximum limits of the indoor temperature and energy consumption for DSM phases during summer. Moreover, the user chooses the automation options which are applied in a single room. This achieves the transparency of the installation, which supplies the users with lots of comfort and increases energy savings.

3. The communication between the building automation and the user, part 1: from which the user gets information about energy consumption, its emissions and its costs via the web browser. This allows the user to evaluate his energy consumption and he can change his behaviour. Only this transparency achieves energy savings.

4. The communication between the building automation and the user, part 2: from which the information structure of the bus system allows the evaluation of the bus telegrams. Its capabilities are similar to a human energy consultant. More specifically, the Thermal Model Predictive Controller consults the user to accept a small violate of an indoor temperature maximum limit, explain him the cost and energy savings by this action during the DSM phase.

Finally, the application of Thermal Model Predictive Control for Demand Side Management Cooling Strategies proves that energy saving of 7% is feasible. The cost savings by using the TMPC-DSM controller depend on the prices of the energy during the peak periods. It is concluded that cost savings between 6% and 8% can be achieved.

11.2 Recommendations

A Thermal Model based on finite difference calculation is derived in this report. However, it would be interesting to apply two-dimensional conduction instead of one. It would also be interesting to develop thermal models based on finite element method or use other computational heat transfer methods. An investigation of ventilation and infiltration results will also prove the efficiency of the Thermal Model in this thesis.

The Thermal Model is developed for a building in Greece and it is investigated for cooling demand during summer. An expansion of this model for heating with the optional integration of renewable energy sources and especially of cogeneration systems because of the fact that the maximum temperature occurs during sunset for

this building part, can also be used in any kind of building, such as an office, other residents, industries, factories etc. Moreover it will be possible for us to launch this controller in the market as an industrial product. For this purpose, databases of wall constructions from different materials should be developed.

A General Thermal Model Predictive Control requires optimization algorithms which should be developed for a unified predictive controller for DSM strategies. These optimization algorithms should be examined theoretically and in practice as far their convergence to the optimal solution is concerned.

The development of a general database, SQL, Oracle etc, could be a basis of an information system which can increase overview, stability, thermal comfort and energy savings and can variously be applied under different circumstances.

Appendix A

Material Thermophysical Properties

A.1 Thermophysical Properties of the Materials which are used in the Bookshop

Description	**Thermal Conductivity, λ (W/m K)**	**Density, ρ (Kg/m^3)**	**Specific Heat, c (J/Kg K)**	**Thermal diffusivity, a X 10^6 (m^2/s)**
Plaster[1]	0,72	1.860	840	0,460
Brick[1]	0,72	1.920	835	0,449
Concrete[2]	2,10	2.400	920	0,951
Expanded Polystyrene[2&3]	0,033	32	1.400	0,737
Glass Plate[1]	1,4	2.500	750	0,747
Tile[2]	0,5	-	-	-
Air[4]	-	1,177	718	-

[1]Reference [39]
[2]Reference [45]
[3]Reference [48]
[4]Reference [44]

A.2 U-Factors of the Materials which are used in the Bookshop

Description	Overall heat transfer coefficient, U ($W/m^2 K$)	Transmittance, τ %	Reflectance, ρ %	Absorptance, α %	τα, %
Door Single Glazing (10 mm glass)*	5,81	-	-	-	-
Window Double Glazing (12,7 mm air space)*	2,73[a]	-	-	-	-
Roof Double Glazing (15 cm air space)*	3,435[b]	-	-	-	-
North facing Window - Solar Film NG70 (Neutral Grey) on ¼ inch glass**	6,13*&**	59	12	29	67
Roof Glazing - Solar Film SDS S220X (Exterior Standard) on ¼ inch glass**	6,19*&**	12	60	28	20
Floor (Concrete & Tile)*	2,2	-	-	-	-

*Reference [45]

**Reference [43]

[a]This u-value for windows double glazing is used as the u-value for the north facing windows double glazing including the solar film NG70 and for east facing windows double glazing without any solar film.

[b]The u value of the roof double glazing is calculated by adding of the resistance of the solar film SDS S220X on ¼'' glass (R_{sf} = 1/UA value), with the resistance of the internal glass without solar film and the resistance by the convection and radiation heat transfer coefficient $\alpha_{in} = 8W/m^2K$ of the bookshop ($R_b = 1/\alpha_{in}A$). It is noted that in the air space of 15cm the lighting is mounted and its resistance is included in the u value of the solar film.

$$\frac{1}{U_{roof\_total}} = \frac{L_{glass}}{\lambda_{glass}} + \frac{1}{\alpha_{in}} + \frac{1}{U_{filter}} = \frac{0,0064m}{1,4W/mK} + \frac{1}{8W/m^2K} + \frac{1}{6,19W/m^2K} \Rightarrow U_{roof\_total} = 3,435W/m^2K \quad (A.1)$$

Appendix B

Finite Difference Calculation Equations of the Bookshop Walls

B.1 FDC Bookshop Thermal Model

Recalling Figure 4.2, it depicts the layout of the bookshop. Obviously, there are 5 different wall parts concerning the materials which consist of:

- Plaster-Brick-Expanded Polystyrene-Brick-Plaster (Green - Yellow Wall)
- Plaster-Expanded Polystyrene-Concrete-Plaster (Red Rectangular & Yellow line Wall)
- Plaster-Brick-Plaster (Red lines – Internal Wall)
- Plaster-Brick-Plaster (Green lines – External Wall)
- Plaster-Concrete-Plaster (Red Rectangular - Internal Wall)

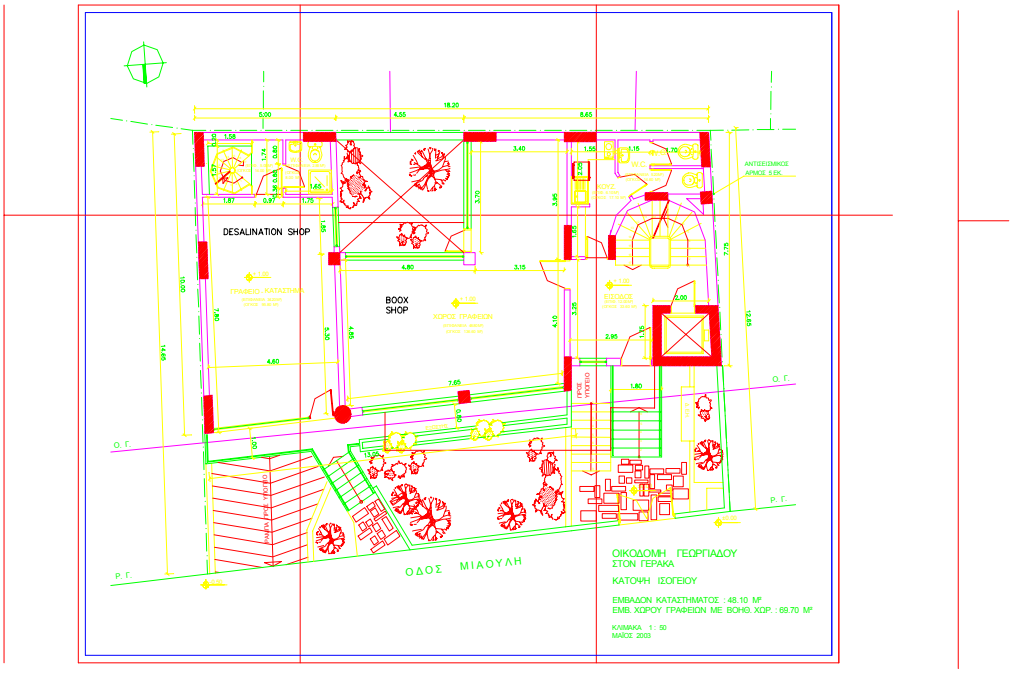

Figure 4.2: Layout of the Bookshop.

In general, each wall part consisting of any material can be represented by the following Figure 4.3. The explicit form of the finite-difference equations for any interior node of each wall are presented in this Appendix B.

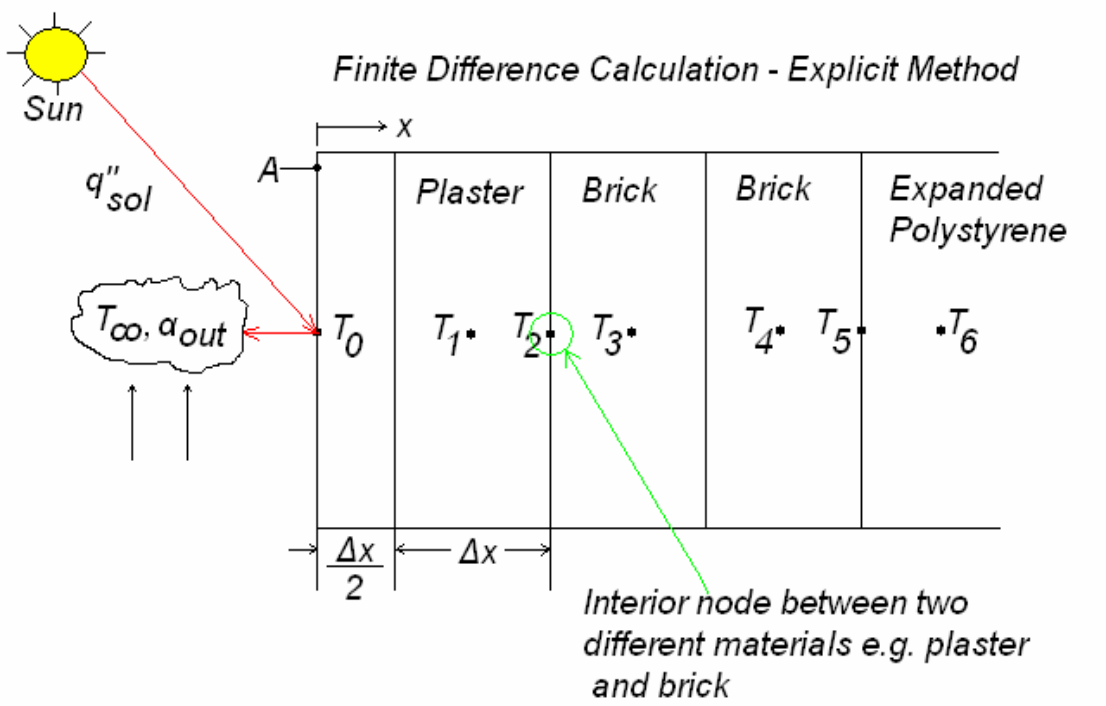

Figure 4.3: Surface node with convection, radiation and one-dimensional transient conduction.

B.2 FDC Equations of Plaster-Brick-Plaster of the North Wall (27 cm)

The dimensions of the materials of this part of the wall are: Plaster (2 cm), Brick (26 cm), Plaster (1 cm). The stability criterion is satisfied by using Δx = 1 cm and Δt = 47 sec.

The surface node of the outer wall follows from Equation (4.20) where

$$T_0^{p+1} = 0{,}4332\left[T_1^p + 0{,}3472T_{out} + 0{,}0139q''_{sol}\right] + 0{,}4164T_0^p \tag{B.1a}$$

The finite-difference solutions to the interior nodes are obtained by using Equations (4.14) and (4.28). Note that the nodes 1 to 27 are the nodes from surfaces of the outer to the inner wall.

$$T_1^{p+1} = 0{,}2166[T_0^p + T_2^p] + 0{,}5668T_1^p \tag{B.1b}$$

$$T_2^{p+1} = 0{,}2138[T_1^p + T_3^p] + 0{,}5724T_2^p \tag{B.1c}$$

$$T_3^{p+1} = 0{,}2111[T_2^p + T_4^p] + 0{,}5778T_3^p \tag{B.1d}$$

T_4^{p+1} up to T_{25}^{p+1} are of the same function as the T_3^{p+1}

$$T_{26}^{p+1} = 0{,}2138[T_{25}^p + T_{27}^p] + 0{,}5724T_{26}^p \tag{B.1e}$$

$$T_{27}^{p+1} = 0{,}4332\left[T_{26}^p + 0{,}1111T_{in}^p \pm 0{,}0139q''_{aux}\right] + 0{,}5187T_{27}^p \tag{B.1f}$$

B.3 FDC Equations of Plaster-Expanded Polystyrene-Concrete-Plaster of the North Wall (37 cm)

The dimensions of the materials of this part of the wall are: Plaster (2 cm), Expanded Polystyrene (3 cm), Concrete (30 cm), Plaster (2 cm). The stability criterion is satisfied by using $\Delta x = 1$ cm and $\Delta t = 48$ sec.

The surface node of the outer wall follows from Equation (4.20) where

$$T_0^{p+1} = 0{,}4424\left[T_1^p + 0{,}3472T_{out} + 0{,}0139q''_{sol}\right] + 0{,}404T_0^p \tag{B.2a}$$

The finite-difference solutions to the interior nodes are obtained by using Equations (4.14) and (4.28). Note that the nodes 1 to 37 are the nodes from surfaces of the outer to the inner wall.

$$T_1^{p+1} = 0{,}2212[T_0^p + T_2^p] + 0{,}5576T_1^p \tag{B.2b}$$

$$T_2^{p+1} = 0{,}4301T_1^p + 0{,}0197T_3^p + 0{,}5502T_2^p \tag{B.2c}$$

$$T_3^{p+1} = 0{,}3536[T_2^p + T_4^p] + 0{,}2929T_3^p \tag{B.2d}$$

T_3^{p+1} and T_4^{p+1} are of the same function

$$T_5^{p+1} = 0{,}0141T_4^p + 0{,}8949T_6^p + 0{,}0911T_5^p \tag{B.2e}$$

$$T_6^{p+1} = 0{,}4565[T_5^p + T_7^p] + 0{,}087T_6^p \tag{B.2f}$$

T_7^{p+1} up to T_{34}^{p+1} are of the same function as the T_6^{p+1}

$$T_{35}^{p+1} = 0{,}5347T_{34}^p + 0{,}1833T_{36}^p + 0{,}282T_{35}^p \tag{B.2g}$$

$$T_{36}^{p+1} = 0{,}2212[T_{35}^p + T_{37}^p] + 0{,}5576T_{36}^p \tag{B.2h}$$

$$T_{37}^{p+1} = 0{,}4424\left[T_{36}^p + 0{,}1111T_{in} \pm 0{,}0139q''_{aux}\right] + 0{,}5084T_{37}^p \tag{B.2i}$$

B.4 FDC Equations of Plaster-Expanded Polystyrene-Concrete-Plaster of the North Wall (44 cm)

The dimensions of the materials of this part of the wall are: Plaster (2 cm), Expanded Polystyrene (3 cm), Concrete (37 cm), Plaster (2 cm). The stability criterion is satisfied by using $\Delta x = 1$ cm and $\Delta t = 48$ sec.

The surface node of the outer wall follows from Equation (4.20) where

$$T_0^{p+1} = 0{,}4424\left[T_1^p + 0{,}3472T_{out} + 0{,}0139q''_{sol}\right] + 0{,}404T_0^p \quad \text{(B.3a)}$$

The finite-difference solutions to the interior nodes are obtained by using Equations (4.14) and (4.28). Note that the nodes 1 to 44 are the nodes from surfaces of the outer to the inner wall.

$$T_1^{p+1} = 0{,}2212[T_0^p + T_2^p] + 0{,}5576T_1^p \quad \text{(B.3b)}$$

$$T_2^{p+1} = 0{,}4301T_1^p + 0{,}0197T_3^p + 0{,}5502T_2^p \quad \text{(B.3c)}$$

$$T_3^{p+1} = 0{,}3536[T_2^p + T_4^p] + 0{,}2929T_3^p \quad \text{(B.3d)}$$

T_3^{p+1} and T_4^{p+1} are of the same function

$$T_5^{p+1} = 0{,}0141T_4^p + 0{,}8949T_6^p + 0{,}0911T_5^p \quad \text{(B.3e)}$$

$$T_6^{p+1} = 0{,}4565[T_5^p + T_7^p] + 0{,}087T_6^p \quad \text{(B.3f)}$$

T_7^{p+1} up to T_{41}^{p+1} are of the same function as the T_6^{p+1}

$$T_{42}^{p+1} = 0{,}5347T_{41}^p + 0{,}1833T_{43}^p + 0{,}282T_{42}^p \quad \text{(B.3g)}$$

$$T_{43}^{p+1} = 0{,}2212[T_{42}^p + T_{44}^p] + 0{,}5576T_{43}^p \quad \text{(B.3h)}$$

$$T_{44}^{p+1} = 0{,}4424\left[T_{43}^p + 0{,}1111T_{in} \pm 0{,}0139q''_{aux}\right] + 0{,}5084T_{44}^p \quad \text{(B.3i)}$$

B.5 FDC Equations of Plaster-Concrete-Plaster of the West Internal Wall (30 cm)

The dimensions of the materials of this part of the wall are: Plaster (2 cm), Concrete (26 cm), Plaster (2 cm). The stability criterion is satisfied by using $\Delta x = 1$ cm and $\Delta t =$ 47 sec.

The surface node of the outer wall (entrance wall) follows from Equation (4.20) where

$$T_0^{p+1} = 0{,}4332\left[T_1^p + 0{,}1111T_{ent}^p \pm 0{,}0139q''_{aux}\right] + 0{,}5187T_0^p \quad \text{(B.4a)}$$

The finite-difference solutions to the interior nodes are obtained by using Equations (4.14) and (4.28). Note that the nodes 1 to 30 are the nodes from surfaces of the entrance to the inner bookshop wall.

$$T_1^{p+1} = 0{,}2166[T_0^p + T_2^p] + 0{,}5668T_1^p \quad \text{(B.4b)}$$

$$T_2^{p+1} = 0{,}1795T_1^p + 0{,}5236T_3^p + 0{,}2969T_2^p \quad \text{(B.4c)}$$

$$T_3^{p+1} = 0{,}447[T_2^p + T_4^p] + 0{,}106T_3^p \quad \text{(B.4d)}$$

T_4^{p+1} up to T_{27}^{p+1} are of the same function as the T_3^{p+1}

$$T_{28}^{p+1} = 0{,}5236T_{27}^p + 0{,}1795T_{29}^p + 0{,}2969T_{28}^p \quad \text{(B.4e)}$$

$$T_{29}^{p+1} = 0{,}2166[T_{28}^p + T_{30}^p] + 0{,}5668T_{29}^p \quad \text{(B.4f)}$$

$$T_{30}^{p+1} = 0{,}4332\left[T_{29}^p + 0{,}1111T_{in}^p \pm 0{,}0139q''_{aux}\right] + 0{,}5187T_{30}^p \quad \text{(B.4g)}$$

B.6 FDC Equations of Plaster-Concrete-Plaster of the East Internal Wall (44 cm)

The dimensions of the materials of this part of the wall are: Plaster (2 cm), Concrete (40 cm), Plaster (2 cm). The stability criterion is satisfied by using $\Delta x = 1$ cm and $\Delta t =$ 47 sec.

The surface node of the outer wall (desalination shop wall) follows from Equation (4.20) where

$$T_0^{p+1} = 0{,}4332\left[T_1^p + 0{,}1111T_{des}^p \pm 0{,}0139q''_{aux}\right] + 0{,}5187T_0^p \tag{B.5a}$$

The finite-difference solutions to the interior nodes are obtained by using Equations (4.14) and (4.28). Note that the nodes 1 to 44 are the nodes from surfaces of the desalination shop to the inner bookshop wall.

$$T_1^{p+1} = 0{,}2166[T_0^p + T_2^p] + 0{,}5668T_1^p \tag{B.5b}$$

$$T_2^{p+1} = 0{,}1795T_1^p + 0{,}5236T_3^p + 0{,}2969T_2^p \tag{B.5c}$$

$$T_3^{p+1} = 0{,}447[T_2^p + T_4^p] + 0{,}106T_3^p \tag{B.5d}$$

T_4^{p+1} up to T_{41}^{p+1} are of the same function as the T_3^{p+1}

$$T_{42}^{p+1} = 0{,}5236T_{41}^p + 0{,}1795T_{43}^p + 0{,}2969T_{42}^p \tag{B.5e}$$

$$T_{43}^{p+1} = 0{,}2166[T_{42}^p + T_{44}^p] + 0{,}5668T_{43}^p \tag{B.5f}$$

$$T_{44}^{p+1} = 0{,}4332\left[T_{43}^p + 0{,}1111T_{in}^p \pm 0{,}0139q''_{aux}\right] + 0{,}5187T_{44}^p \tag{B.5g}$$

B.7 FDC Equations of Plaster-Brick-Plaster of the Internal Walls (26 cm)

The dimensions of the materials of this part of the wall are: Plaster (1 cm), Brick (24 cm), Plaster (1 cm). The stability criterion is satisfied by using Δx = 1 cm and Δt = 47 sec.

The surface node of the outer bookshop wall follows from Equation (4.20) where

$$T_0^{p+1} = 0{,}4332\left[T_1^p + 0{,}1111T_{ent\_or\_des}^p \pm 0{,}0139q''_{aux}\right] + 0{,}5187T_0^p \qquad \text{(B.6a)}$$

The finite-difference solutions to the interior nodes are obtained by using Equations (4.14) and (4.28). Note that the nodes 1 to 26 are the nodes from surfaces of the outer to the inner wall.

$$T_1^{p+1} = 0{,}2138[T_0^p + T_2^p] + 0{,}5724T_1^p \qquad \text{(B.6b)}$$

$$T_2^{p+1} = 0{,}2111[T_1^p + T_3^p] + 0{,}5778T_2^p \qquad \text{(B.6c)}$$

T_3^{p+1} up to T_{24}^{p+1} are of the same function as the T_2^{p+1}

$$T_{25}^{p+1} = 0{,}2138[T_{24}^p + T_{26}^p] + 0{,}5724T_{25}^p \qquad \text{(B.6d)}$$

$$T_{26}^{p+1} = 0{,}4332\left[T_{25}^p + 0{,}1111T_{in}^p \pm 0{,}0139q''_{aux}\right] + 0{,}5187T_{26}^p \qquad \text{(B.6e)}$$

B.8 FDC Equations of the Adiabatic Surfaces

It is mentioned in Chapter 4 that because of the fact that we cannot be aware of the temperature conditions of the building which is adjacent to the one we examine, we assume that its outer south wall is an adiabatic surface as it is shown in the following Figure B.1. Using the energy balance method, Equation (4.17), an explicit finite-difference equation may be derived to this surface node. Recalling Equation (4.14)

$$T_m^{p+1} = Fo\left(T_{m+1}^p + T_{m-1}^p\right) + (1-2Fo)T_m^p \tag{4.14}$$

and using for node 0 $T_{m+1}^p = T_{m-1}^p$ we obtain

$$T_0^{p+1} = 2FoT_1^p + (1-2Fo)T_0^p \tag{B.7a}$$

Taking into account that the walls, which are described by Equations (4.29) and (B.1), are also adjacent to the next building as it is depicted in Figure 4.2, Equations (4.29.a) and (B.1.a) are substituted by Equation (B.7b) in this case.

$$T_0^{p+1} = 0{,}4332T_1^p + 0{,}5668T_0^p \tag{B.7b}$$

Respectively, the wall which is described by Equations (B.2) and is also adjacent to the next building, Equation (B2.a) is substituted by the following Equation (B.7c).

$$T_0^{p+1} = 0{,}4424T_1^p + 0{,}5576T_0^p \tag{B.7c}$$

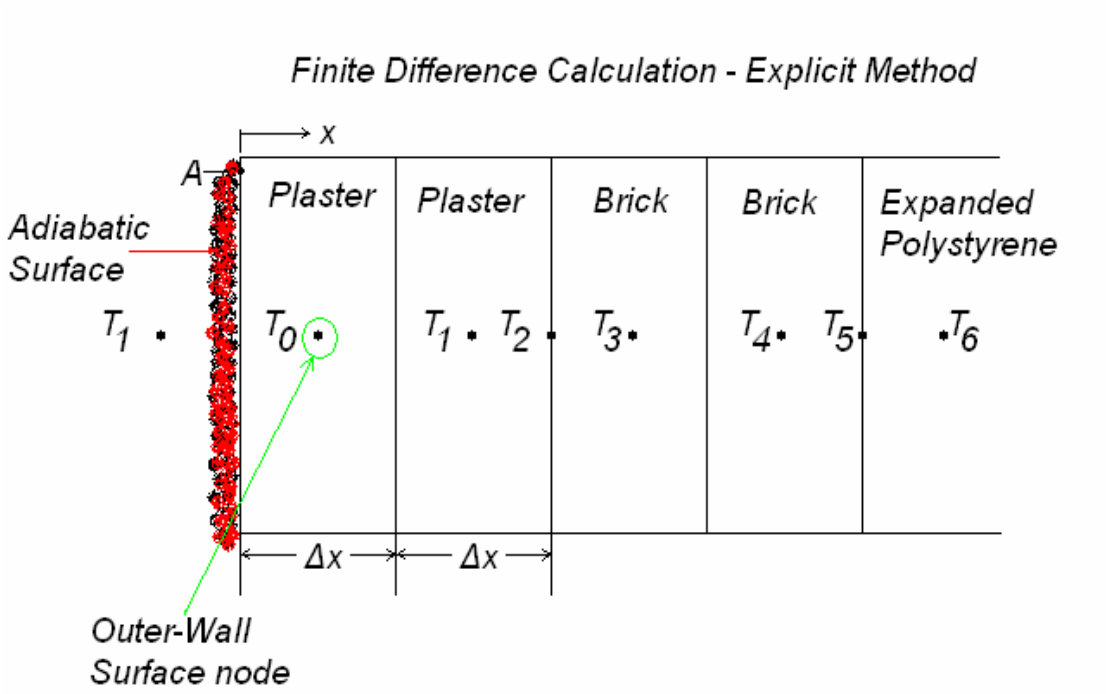

Figure B.1: Adiabatic surface node of the outer south wall.

Bibliography

[1] IEA Demand-Side Management working group: The power to choose Demand Response in liberalised energy markets. Energy Market Reform. OECD/IEA 2003.

[2] Stadler, I.: Dialogfähige Energiemanagementsysteme im Kontext von Energieverbrauch und Nutzerverhalten. PhD Dissertation. Universität Kassel. 2001.

[3] Rose, M.: Gebäude Systemtechnik in Wohn und Zweckbau mit dem EIB. 2. Auflage. Hüthig Verlag. Heidelberg. 1995.

[4] Matinal, C.: Standardization yes, but sameness no! EIB Journal. October 1999.

[5] KNX/EIB: Training Documentation for Combined and Upgrade Courses - Home and Building Systems Engineering. KNX/EIB. Brussels. 2005.

[6] Schnell, G.: Bussysteme in der Automatisierungstechnik. Vieweg Verlag. 1999.

[7] Leidenroth, H.: EIB-Anwender Handbuch. Verlag Technik. Berlin. 1999.

[8] Goosens, M., De Bruyne, S.: The fast lane to EIB technology. EIBA. Brussels. 1994.

[9] Romanos, P., Stadler, I., Hahn, I., Bukvic, A., et. all.: Supervisory control of road traffic and energy management of street lighting using EIB – KONNEX technology. Proceedings of the 1st International Conference on Traffic-Recent Developments-Transport Telematics. Patras. Greece. 2004.

[10] www.argoclima.it

[11] www.abb.com

[12] www.konnex.org

[13] National Instruments: LabVIEW Bookshelf – User Manual. U.S.A. 2001.

[14] Soeterboek, R.: Predictive Control. A Unified Approach. Prentice Hall International. U.K. 1992.

[15] Åström, K. J., Wittenmark, B.: Adaptive Control. Addison-Wesley. Reading. Mass. 1989.

[16] Harris, C. J., Billings, S. A. (Eds): Self–tuning and Adaptive Control: Theory and Applications. Peter Peregrinus Ltd. London. 1981.

[17] Wellstead, P. E. Zarrop, M. B.: Self-Tuning Systems. Control and Signal Processing. John Wiley & Sons. England. 1991.

[18] Garcia, C. E., Morari, M.: Internal Model Control. 1. A Unifying Review and Some New Results. Ind. Eng. Chem. Process. Des. Dev. 21. pp. 308-323. 1982.

[19] Garcia, C. E., Morari, M.: Internal Model Control. 2. Design Procedure for Multivariable Systems. Ind. Eng. Chem. Process. Des. Dev. 24. pp. 484-494. 1985.

[20] Garcia, C. E., Morari, M.: Internal Model Control. 3. Multivariable Control Law Computation and Tuning Guidelines. Ind. Eng. Chem. Process. Des. Dev. 24. pp. 484-494. 1985.

[21] Kinnaert, M.: Adaptive generalised predictive controller for MIMO systems. Int. J. Control. Vol. 50. No. 1. pp. 161-172. 1989.

[22] Mehra, R. K., Rouhani, R., Praly, L.: New Theoretical Developments in Multivariable Predictive Algorithmic Control. Proceedings of the Joint Automatic Control Conference. San Fransisco. Paper FA9-B. 1980.

[23] Abu el Ata-Doss, S., Fliess, M.: Nonlinear predictive control by inversion. Proceedings IFAC Symposium on Nonlinear Control Systems Design. Capri. Italy. 1989.

[24] Isermann, R., Lachmann, K.-H., Matko, D.: Adaptive Control Systems. Prentice Hall International. U.K. 1992.

[25] Soeterboek, A. R. M., Verbruggen, H. B., van den Bosch, P. P. J.: Predictive control of nonlinear processes. Proceedings of the IFAC Symposium on Intelligent Tuning and Adaptive Control ITAC 91. Singapore. 1991.

[26] Clarke, D. W., Mohtadi, C., Tuffs, P. S.: Generalised predictive control – Part I. The basic algorithm. Automatica. Vol. 23. No. 2. pp. 137-148. 1987.

[27] Clarke, D. W., Mohtadi, C., Tuffs, P. S.: Generalised predictive control – Part II. Extensions and interpretations. Automatica. Vol. 23. No. 2. pp. 149-160. 1987.

[28] Cutler, C. R., Ramaker, B. L.: Dynamic matrix control – A computer control algorithm. Proceedings JACC. San Fransisco. U.S.A. 1980.

[29] De Keyser, R. M. C., van Gauwenberghe, A.R.: Extended prediction self-adaptive control. Proceedings 7th IFAC Symposium on Identification and System Parameter Estimation. York. U.K. pp.1255-1260. 1985.

[30] Richalet, J., Abu el Ata-Doss, S., Arber, Ch., Kuntze, H. B., Jacubasch, A., Schill, W.: Predictive functional control: Application to fast and accurate robots. Proceedings 10th IFAC World Congress. Munich. F.R.G. 1987.

[31] Ydstie, B. E.: Extended horizon adaptive control. Proceedings 9th IFAC World Congress. Budapest. Hungary. 1984.

[32] Soeterboek, A. R. M., Verbruggen, H. B., van den Bosch, P. P. J., Butler, H.: Adaptive predictive control – a unified approach. Proceedings Sixth Yale Workshop on Applications of Adaptive Systems Theory. New Haven. U.S.A. 1990.

[33] Soeterboek, A. R. M., Verbruggen, H. B., van den Bosch, P. P. J., Butler, H.: On the unification of predictive control algorithms. Proceedings 29th IEEE Conference on Decision and Control. Honolulu. U.S.A. 1990.

[34] De Keyser, R. M. C.: Principles of model based predictive control. Proceedings First European Control Conference. Grenoble. France. pp.1753-1758. 1991.

[35] Åström, K. J., Eykhoff, P.: System identification - a survey. Automatica. Vol. 7. pp. 123-167. 1971.

[36] Ljung, L.: System Identification: Theory for the User. Prentice Hall International. Englewood Cliffs. N. J. 1987.

[37] Söderström, T., Stoica, P.: System Identification. Prentice Hall International. U.K. 1989.

[38] Schmid, J.: Transparente Wärmedämmung in der Architektur. C. F. Müller. Heidelberg. 1995.

[39] Incropera, F. P., DeWitt, D. P.: Fundamentals of Heat and Mass Transfer. John Wiley & Sons. U.S.A. 2002.

[40] Jaluria, Y., Torrance, K. E.: Computational Heat Transfer. Springer-Verlag. U.S.A. 1986.

[41] www.iset.uni-kassel.de

[42] Duffie, J. A., Beckman, W. A.: Solar Engineering of Thermal Processes. John Wiley & Sons. U.S.A. 1991.

[43] www.madico.com/arch_specs.asp

[44] Moran, M. J., Shapiro, H. N.: Fundamentals of Engineering Thermodynamics. John Wiley & Sons. U.S.A. 1999.

[45] ASHRAE (American Society of Heating, Refrigerating and Air-Conditioning Engineers, Inc.): Fundamentals. ASHRAE HANDBOOK. 2001.

[46] Bazaraa, M. S., Sherali, H. D., Shetty, C. M.: Nonlinear Programming – Theory and Algorithms. John Wiley & Sons. U.S.A. 1993.

[47] www.eex.de

[48] www.dow.com/styrofoam/europe/uk/proddata/styrofoam/